Level Density Studies in ^{45}Sc

Bart Wayne Smith

Triangle Universities Nuclear Laboratory

Department of Physics

Duke University

1989

LEVEL DENSITY STUDIES IN ^{45}Sc

by

Bart Wayne Smith

Department of Physics
Duke University

Date: August 28, 1989

Approved:

Edward G. Bilpuch
E. G. Bilpuch, Supervisor

Laurence Weiss

Alfred T. Gordon

Richard L. Walter

Warren Tornow

Dissertation submitted in partial fulfillment of the requirements
for the degree of Doctor of Philosophy in the
Department of Physics in the Graduate
School of Duke University

1989

ABSTRACT

(Physics-Nuclear)

LEVEL DENSITY STUDIES IN ^{45}Sc

by

Bart Wayne Smith

Department of Physics
Duke University

Date: August 28, 1989

Approved:

Edward G. Bilpuch
E. G. Bilpuch, Supervisor

Laurence Cram

Alfred T. Gorham

Richard L. Walter

Werner Tornow

An abstract of a dissertation submitted in partial fulfillment of the requirements for the degree of Doctor of Philosophy in the Department of Physics in the Graduate School of Duke University

1989

ABSTRACT

The s-wave resonance average level densities for eleven nuclides with A = 41 to 67 were determined from existing proton resonance data. These average level densities were consistent with values from s-wave neutron data. Both sets of s-wave level densities were then compared with two phenomenological level density models, the IST and KRK models. The level density parameter 'a' displays a linear dependence on the mass.

Following these promising results a detailed study of ^{45}Sc was performed at the High Resolution Laboratory of the Triangle Universities Nuclear Laboratory. The goal of these measurements was the determination of the parity and angular momentum dependence of the average level density. Resonance parameters for 585 resonances were extracted from the measured reaction data on ^{44}Ca(p,p) for incident proton energies of 2.95 to 3.72 MeV. Two $1/2^-$ analog states were observed at energies of 3.0 and 3.2 MeV, with the analog state at 3.2 MeV fragmented into six resonances.

The resonances observed in ^{45}Sc were used to determine the level densities for the various level sequences. Excellent results were obtained for the $1/2^+$ sequence, but the $1/2^-$, $3/2^-$, $3/2^+$ and $5/2^+$ sequences were not pure and were incomplete. The purity problems arose from the ambiguity in the J assignment for p- and d-wave resonances. Because of this ambiguity accurate evaluation of the angular momentum and parity dependence of the level density is not possible with these data. Additional study of the ^{44}Ca(p,p´) reaction could eliminate the ambiguity in the J assignments, and make possible more extensive analysis of the parity and angular momentum dependence of the average level density.

Acknowledgements

I would like to thank my advisor, Dr. E. G. Bilpuch, for his support and encouragement during my graduate studies. I am also very grateful to Dr. G. E. Mitchell for many helpful discussions and guidance in the preparation of this dissertation.

I also wish to thank Dr. W. K. Brooks, Dr. J. R. Vanhoy, Dr. B. J. Warthen, Dr. J. F. Shriner Jr., Dr. D. Fang, and especially Dr. J. S. Bull for their helpful discussions and assistance in completing this experiment. Many thanks also go to L. James, K. Keeter, C. Fowler, J. Li, S. Frankle, C. Frankle, and C. Jackson for their help in the various stages of this experiment.

The assistance and instruction of C. R. Westerfeldt, S. E. Edwards, R. Rummel, P. Carter, and P. Mulkey in the maintenance of the electronics and accelerator systems is gratefully acknowledged. The excellent work of the machine shop, headed by A. W. Lovette, is also greatly appreciated.

This work was supported in part by the United States Department of Energy.

On a personal note I wish to thank my sister Sally, and my parents Pat and Paul for their unfailing support and encouragement throughout my life. I wish to thank Daniel and Carol for getting me started in physics and supporting me through the years. Also I would like to thank Allan for his guidance and wisdom. Finally I want to thank my wife, Paige, who has endured and supported me throughout my studies--Thanks.

To God be the Glory.

Table of Contents

List of Figures

List of Tables

LEVEL DENSITY STUDIES IN ^{45}Sc

Chapter One

Introduction

It has been more than fifty years since the publication of Bethe's classic articles on level densities in nuclear systems (Bethe 1936,1937). Since that time a large amount of work has been undertaken both to measure and to model nuclear level densities. Nuclear level densities are of great importance in many areas of pure and applied nuclear physics. Recent interest in nuclear level densities has increased: key reasons include studies of symmetry breaking in compound nuclear systems and analysis of the fluctuation properties of nuclear level spacings. The predicted enhancement of fundamental symmetry violation in a complex system is critically dependent on the value of the level density. The fluctuation properties are crucial to the most successful statistical theory of nuclear states--Random Matrix Theory. The proposed connection between the fluctuation properties and the degree of chaoticity has led to increased interest in these topics.

However, for most purposes the greatest need is for a reliable estimate of the average level density; an estimate which can be obtained with phenomenological models--not requiring a first principle theory. Therefore much effort has been expended on the development of phenomenological models. Some of these models are rather successful in describing the available data. However, since these models are phenomenological, it is not clear how reliably they can be extended to different excitation energies, mass or

angular momentum. Extension of the present data base of neutron resonance data should provide interesting tests for the present models. Historically there were major problems with the quality of the proton resonance data, including poor overall experimental resolution and resonance analysis complications arising from Coulomb interference effects, contributions from several orbital angular momenta, and the requirement of a multilevel, multichannel analysis.

These experimental difficulties were addressed at the Triangle Universities Nuclear Laboratory (TUNL) with the development of the High Resolution Laboratory (HRL) in the 1960's. The HRL utilizes a feedback system with two beams (one for the experiment, one for control). This system, which is described in chapter three, yields an overall experimental resolution of 350-400 eV for an incident proton beam of 1-4 MeV. This resolution has provided the HRL with the ability to obtain high quality proton resonance data; these data include weaker energy levels that are typically not observed. The HRL has accumulated a significant amount of proton resonance data that is useful in a variety of nuclear studies. In parallel with this development data analysis techniques have also been significantly improved. Interactive resonance analysis computer codes have been developed to analyze the extensive resonance data. These codes coupled with increased computing power have greatly increased the speed with which data can be analyzed, allowing higher density nuclei to be studied.

The present study has two main purposes. The first is to establish the viability of the inclusion of proton resonance data in the nuclear data base for average level densities. The second is to obtain new data for the ^{45}Sc nuclear system in order to permit more detailed level density studies. To achieve the first objective level densities were determined for s-wave resonances in nuclei that had been previously studied at the HRL. These level densities were compared with experimental neutron level densities. The proton data was then analyzed with two current phenomenological level density

models and compared with results obtained using neutron data in the models. There is general agreement between the results for the neutron and proton data, suggesting that the proton data can be confidently included in the nuclear data base for average level densities.

The second part of this study is the determination of the level densities for all the observed level sequences in the ^{45}Sc system. A level sequence is a set of energy levels which all have the same good quantum numbers J, the angular momentum, and π, the parity. The objective was to obtain high quality (and high density) proton resonance data for higher angular momentum level sequences, that is, p- and d-wave level sequences. Such data would permit examination of the dependence of the level density on J and π. The study of the J and π dependence is much more difficult with neutron resonance data, since in most cases only s-wave resonances are observed and analyzed reliably.

In this study of the ^{45}Sc system a total of 585 resonances were observed in the incident proton energy range 2.95 - 3.72 MeV. Resonances with orbital angular momentum of ℓ = 0, 1 and 2 were observed; there were difficulties establishing J for the ℓ = 1 and 2 resonances. As a result the comparison between the $1/2^+$ and $1/2^-$ states to test for parity dependence of the level density was inconclusive. However, excellent s-wave data were obtained, and the present results for the ℓ=1 and ℓ=2 resonances provide the major first step toward the goal of obtaining pure and complete sets of data for large p- and d-wave sequences.

Chapter Two

Average Level Densities

This study is concerned with the average nuclear level density. A discussion of the background of average level density measurements and analysis will be presented. Although in principle the nuclear level density is a simple concept, many complications make both the determination and the prediction of level densities difficult. This chapter reviews some of the high points of phenomenological level density studies in order to provide a general picture of these complications.

In 1936-37 Bethe (Bethe 1936, 1937) published landmark papers on level densities which have been the starting point for most subsequent level density studies. The calculation of level densities requires the use of statistical physics methods. This statistical approach is useful because of the intimate connection between the entropy of a system (the nucleus) and the number of states contained in that system.

Bethe derived a general expression for the spacing of levels that involved only two parameters. The resulting expression is

$$D(U) = \sqrt{(2\pi n)\left(\frac{U^{n+1}}{a}\right)^{n}}\ \exp\left(-\frac{n}{n-1}\sqrt[n]{aU^{n-1}}\right)$$

where 'a' is called the level density parameter, and the parameter 'n' is related to the excitation energy U by

$$U = a\tau^{n}$$

where τ is the nuclear temperature.

Proceeding from this expression for D(U) requires a specific model: both a and n are model dependent. In Bethe's work two phenomenological models were considered. The first was based on a Fermi gas model, where the nucleons were considered free particles and the total energy of the nucleus was equal to the sum of the individual particle energies. The second model is based on the liquid drop model, where the total energy of the system is the sum of the interaction potential energy and the kinetic energy of the particles.

These two models treat the magnitude of the interaction between particles very differently. In the Fermi gas model the interactions are very small: internucleon distances change rapidly within the nucleus, just as the intermolecular distance does in a gas. In the liquid drop model the interactions between nucleons are very large and internucleon distances remain fairly constant. In this study the model of interest is the Fermi gas model. Bethe's development of this model will be followed.

Bethe established that for the Fermi gas model a value of n = 2 is appropriate. This yields for the spacing relation

$$D(U) = 2\frac{U^{3}}{a}\sqrt{\pi}\exp\left(-2\sqrt{aU}\right).$$

Bethe noted that the spacing would be dependent on the angular momentum of the nucleus and introduced J-dependence in the form

$$D(J) \propto \left[\frac{2\sigma^{3}}{2J+1}\right]\exp\left[\frac{\left(J+\frac{1}{2}\right)^{2}}{2\sigma^{2}}\right].$$

The parameter σ is known as the spin cutoff parameter. Under these assumptions the general level density formula based on the Fermi gas model is

$$D(U,J) \propto \frac{U^3}{a}\sqrt{\pi}\,\exp\left(-2\sqrt{aU}\right)\left[\frac{2\sigma^3}{2J+1}\right]\exp\left[\frac{\left(J+\frac{1}{2}\right)^2}{2\sigma^2}\right].$$

Details of the derivation of this expression are given in Bethe's papers. This expression can be used to calculate spacings based on parameters determined from existing data. Although this result was a major development, it is a phenomenological model -- the parameters are dependent on (and limited by) the available data.

The next major development in average level density studies occurred when the nuclear data base had been enlarged to the point that allowed the determination of more detailed phenomenological parameters. This data base indicated that the level density depended not only upon the excitation energy and angular momentum of the levels, but also on shell effects, and on the atomic mass A. In these analysis semiempirical relations were derived which could be used to model level densities and to predict level densities in systems which could not be measured empirically.

The major work of this type was performed by Gilbert and Cameron in 1965 (Gilbert, 1965). Their analysis was based on the same level density relation that Bethe had developed. However, they developed parameterizations which corrected for other effects. The main corrections were for atomic mass A dependency, odd-even pairing effects, and shell effects. In developing the correction for the pairing effects Gilbert and Cameron followed the approach of Newton (1956). Newton introduced a 'solution' to the pairing energy problem by subtracting a pairing energy from the actual excitation energy. The pairing correction was achieved with two energy functions P(N) and P(Z), where the excitation energy was

$$U = E - P(Z) - P(N).$$

The shell corrections, S(N) and S(Z), were used in correcting for the dependence of the level density parameter a on the atomic mass A. For spherical nuclei

$$a/A = 0.00917\ S + 0.142,$$

and for deformed nuclei

$$a/A = 0.00917\ S + 0.120,$$

where S is the total shell correction,

$$S = S(N) + S(Z).$$

The results of Gilbert and Cameron were (and still are) extremely useful. However, since the corrections and parameters used in their level density relation are based on empirical data, the validity of the calculations is restricted to limited excitation energy ranges. With more experimental data additional shell effects have been observed; the Gilbert and Cameron formulation fails to account accurately for these new results. The main problem is the excitation energy dependence of the shell effects, especially the 'washing' out of the shell effects at higher excitation energies.

Due to this problem other methods for calculating level densities have been proposed. One approach has developed with the advent of greatly increased computational power. This method generally involves the computation of level densities starting from a set of shell model single-particle energy levels. However there are normalization problems with this method. The shell-independent part of the calculation must be normalized to the liquid drop model estimate and the shell-dependent part normalized to experimental shell correction energies. A more detailed discussion of this approach is found in Huizenga (1972, 1973).

Further improvements in level density calculations have been made recently by determining new phenomenological relations which account for all of the observed effects. Very successful results have been obtained with models developed by Ignatyuk et al. (1975) and Kataria et al. (1978). Both of these models allow reliable and accurate estimates of level densities at higher excitation energies.

Ignatyuk's level density relation is based on Bethe's Fermi gas model relation

with additional parameters that account for the observed energy and mass dependence and is formulated as follows

$$\rho(U,J) = \frac{2J+1}{24\sqrt{2}\sqrt[4]{a(U-\delta)^5}\sigma^3}\exp\left\{2\sqrt{a(U-\delta)} - \frac{\left(J+\frac{1}{2}\right)^2}{2\sigma^2}\right\}$$

where

$$\sigma^2 = \left(\frac{6\overline{m}^2}{\pi^2}\right)\sqrt{a(U-\delta)}.$$

This formulation involves only three parameters: a, the level density parameter; $\overline{m^2}$, the mean square value of the projection of the single-particle angular momentum; and δ, the correction for the odd-even difference in the level density. Ignatyuk developed a new phenomenological relation for the level density parameter a

$$a(U) = \tilde{a}\left(1 - \frac{f(U)\,\delta W}{U}\right).$$

In this relation ã is a parameter that describes the asymptotic behavior of a at high excitation energies and is dependent on the atomic mass A according to the relation

$$\tilde{a}/A = \alpha + \beta A$$

The best (in a least squares fitting sense) values for the parameters α and β were found to be 0.154 and 6.3×10^{-5}, respectively. The dimensionless function f(U) determines the energy dependence of a at lower excitation energies and has the form

$$f(U) = 1 - \exp(-\gamma U).$$

The best value for the parameter γ was found to be 0.054. The term δW is the shell correction to the mass formula given as,

$$\delta W = M_{\text{experimental}} - M_{\text{liquid drop}}.$$

In Kataria's model the approach to the level density calculation is slightly different from that of Ignatyuk, but also yields excellent results. The basic relation, again similar to Bethe's, is

$$\rho(U,J) = \frac{(2J+1)W(U)}{2\sqrt{2}\sigma^3(U)} \exp\left(-\frac{J(J+1)}{2\sigma^2(U)}\right)$$

where

$$W(U) = C\ \exp[S(U)].$$

Kataria developed a temperature dependent entropy S and excitation energy U with the following forms

$$S = 2a\tau + \frac{\Delta_s}{\tau}\left(\frac{\pi^2\omega^2\tau^2\cosh(\pi\omega\tau)}{\sinh^2(\pi\omega\tau)} - \frac{\pi\omega\tau}{\sinh(\pi\omega\tau)}\right)$$

and

$$U = a\tau^2 + \Delta_s\left(\frac{\pi^2\omega^2\tau^2\cosh(\pi\omega\tau)}{\sinh^2(\pi\omega\tau)} - 1\right).$$

The other parameters are defined as

$$a = \left(\frac{\pi^2}{6}\right)g_o,\ C = \frac{\sqrt{\pi}}{12\sqrt[4]{aU^5}} \text{ and } \sigma^2 = \frac{J_{rigid}}{\hbar^2}\left(\frac{2S}{a}\right)$$

where g_o is the density of equidistant single particle states.

Although both of these models have been very successful, there is increased complexity in the phenomenological relations for the parameters. This complexity is evidence of the competing nuclear effects which lead to wide variations in nuclear level densities. Because of the phenomenological basis for the above models it is desirable to increase the data base used in determining the parameters. One of the goals of this study is to determine whether current proton data is of sufficiently high quality to include in the data base. In addition this study will attempt to determine level densities for higher angular momentum states.

Chapter Three

Proton Resonance Data Acquisition and Analysis

The proton resonance data discussed in this thesis was obtained at the High Resolution Laboratory (HRL) at the Triangle Universities Nuclear Laboratory (TUNL). This chapter describes the facilities used for the acquisition of proton reaction data and the theory and method used in the analysis of these data.

§3.1 TUNL High Resolution Laboratory and Experimental Setup

The TUNL High Resolution Laboratory has been in operation for many years. During that time a considerable amount of proton reaction data has been collected. The quality of these data is very high due to the excellent energy resolution capabilities of the laboratory; typical overall resolution is approximately 350-400 eV. This resolution has permitted the observation of very weak nuclear levels. As a result of these observations fairly complete sequences of proton resonances have been compiled, which have greatly expanded the use of proton reaction data in tests of statistical nuclear theory.

§3.1.1 KN Van de Graaff Accelerator, Control Systems and Electrostatic Analyzer System

A schematic of the High Resolution Laboratory and control systems is presented in figure 3.1. Originally the KN Van de Graaff accelerator was designed for operation up to 3MV on terminal, limited mainly by sputtering effects due to an aluminum electrode accelerator tube. In 1982 the accelerator was upgraded with a stainless steel tube allowing operation up to 4MV on terminal. The electrostatic analyzer system used was originally developed by Parks et al. in 1958, and in recent years has been upgraded to allow computer control (Westerfeldt, 1988).

Since the KN Van de Graaff accelerator is single ended, the ion source producing the protons is contained inside the terminal of the accelerator. The ion source consists of a 100 Mhz radio frequency oscillator which excites hydrogen gas within the source bottle. This source dissociates the H_2 molecules into HH^+ and H^+ ions; both species are extracted from the source bottle by the use of a high voltage positive probe at the back of the bottle and a high voltage negative focus electrode at the front of the bottle. After extraction both ion species are accelerated through the tube and enter an analyzing magnet which separates them due to their mass difference. The HH^+ ions are bent through an angle of 17° and the H^+ ions are bent through 25°; the two beam lines are shown in figure 3.1. After the analyzing magnet the proton beam is focussed and steered by a series of magnetic steerers and quadrupole lenses resulting in a sharp focus on the target in the scattering chamber. After leaving the magnet, the HH^+ beam first passes between the corona slits. These slits monitor the low frequency (< 20 Hz) energy fluctuations of the beam; a feedback is sent to the terminal through the corona control circuit, reducing the voltage fluctuations at the terminal.

After passing through the corona slits the HH^+ beam then passes through a set of limiting slits and enters the electrostatic analyzer where the beam is bent through 90°. The analyzer is the central component in the high resolution system, consisting of two stainless steel plates curved in a 90° arc and separated by 4.5 mm. The plates are biased

Figure 3.1: Schematic of the High Resolution Laboratory

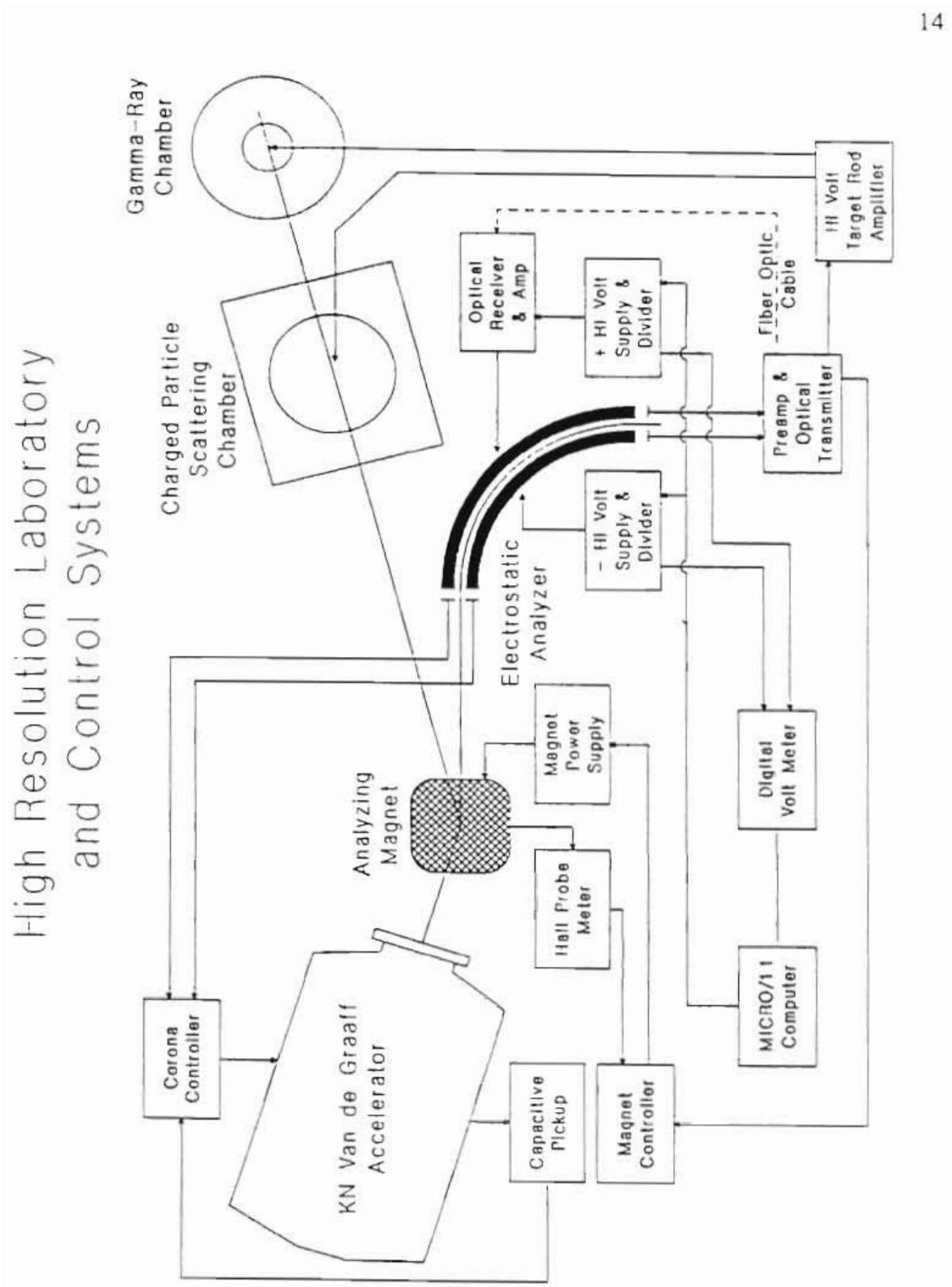
High Resolution Laboratory
and Control Systems
Gamma-Ray Chamber
Charged Particle Scattering Chamber
Optical Receiver & Amp
+ HI Volt Supply & Divider
Fiber Optic Cable
HI Volt Target Rod Amplifier
Preamp & Optical Transmitter
- HI Volt Supply & Divider
Electrostatic Analyzer
Magnet Power Supply
Digital Volt Meter
Analyzing Magnet
Hall Probe Meter
MICRO/11 Computer
Corona Controller
KN Van de Graaff Accelerator
Capacitive Pickup
Magnet Controller

with equal and opposite voltages. By controlling the voltages on the two plates a beam with energy proportional to the plate voltage is allowed to pass completely through the analyzer. The proportionality constant is determined by the geometry and for this analyzer has a 1 volt to 111 eV ratio. The voltages on the plates are controlled by a PDP-11 microprocessor which monitors the voltages through a Fluke DVM. The microprocessor in turn controls two programmable Bertan power supplies that are connected to the plates.

As the beam passes through the analyzer it impinges on the exit slits of the analyzer. If the energy of the beam is higher than the corresponding voltage on the plate, then the beam will have a larger radius of curvature than the plates and will strike the left (or high energy) exit slit. Conversely, if the beam is lower in energy it will strike the right (or low energy) exit slit. Thus monitoring the difference signal from the exit slits provides a very accurate measurement of the energy fluctuations of the beam. This signal is used to help stabilize the beam in the analyzer in a feedback loop to the outer plate of the analyzer, as well as in a feedback loop that passes through a low pass filter and then to the analyzing magnet power supply. The main use of this energy fluctuation signal, however, is to homogenize the energy of the proton beam on target. The target rod is floated at about 3kV and is modulated by the exit slit difference signal, correcting for the energy fluctuation by increasing the voltage of the target rod (decelerating the protons as they approach the target) or decreasing the voltage (accelerating the protons as they approach the target). This system produces a very monoenergetic proton beam on target. For thin film targets the system is capable of an overall resolution of 300-400 eV.

§3.1.2 Scattering Chamber and Detectors

A top view of the scattering chamber is shown in figure 3.2 indicating the path of the beam and the location of the target and detectors. The targets were held in a target rod which was lowered from above and typically contained four targets and a tuning ring. The proton beam entered the chamber after being focussed to a diameter of approximately 0.125 inch by a combination of collimators and steering and focussing elements in the beam line. For the thin solid targets studied the majority of protons pass through the target without interacting. These protons are the collected in a Faraday cup at the back of the chamber. Typical beam currents were 4-5μA with 30 nA on the tuning ring.

The charged particle detectors used in the experiments were surface barrier silicon detectors placed at 90°, 108°, 135°, 150° and 165° relative to the beam direction. Each detector was collimated to eliminate as much secondary scattering as possible. The collimation and location of each detector was determined by measuring Rutherford scattering. Each detector was adjusted to receive approximately the same number of particles during data collection. The solid angles for the detectors were as follows: 90° - 1.16 msr, 108° - 2.00 msr, 135° - 3.39 msr, 150° - 4.05 msr and 165° - 4.50 msr.

Due to the location of the detectors, in particular the 90° detector, the target rod was rotated 25° with respect to the beam to allow all of the detectors a view of the interaction area of the proton beam and target. During experiments a liquid nitrogen trap was used in conjunction with a diffusion pump and freon baffle to maintain a chamber vacuum of 1μtorr.

§3.1.3 Target Preparation

The targets used in these experiments were thin film targets which were prepared with the vapor deposition method using a high current evaporator system. An in depth

Figure 3.2: Top view of the HRL charged particle scattering chamber.

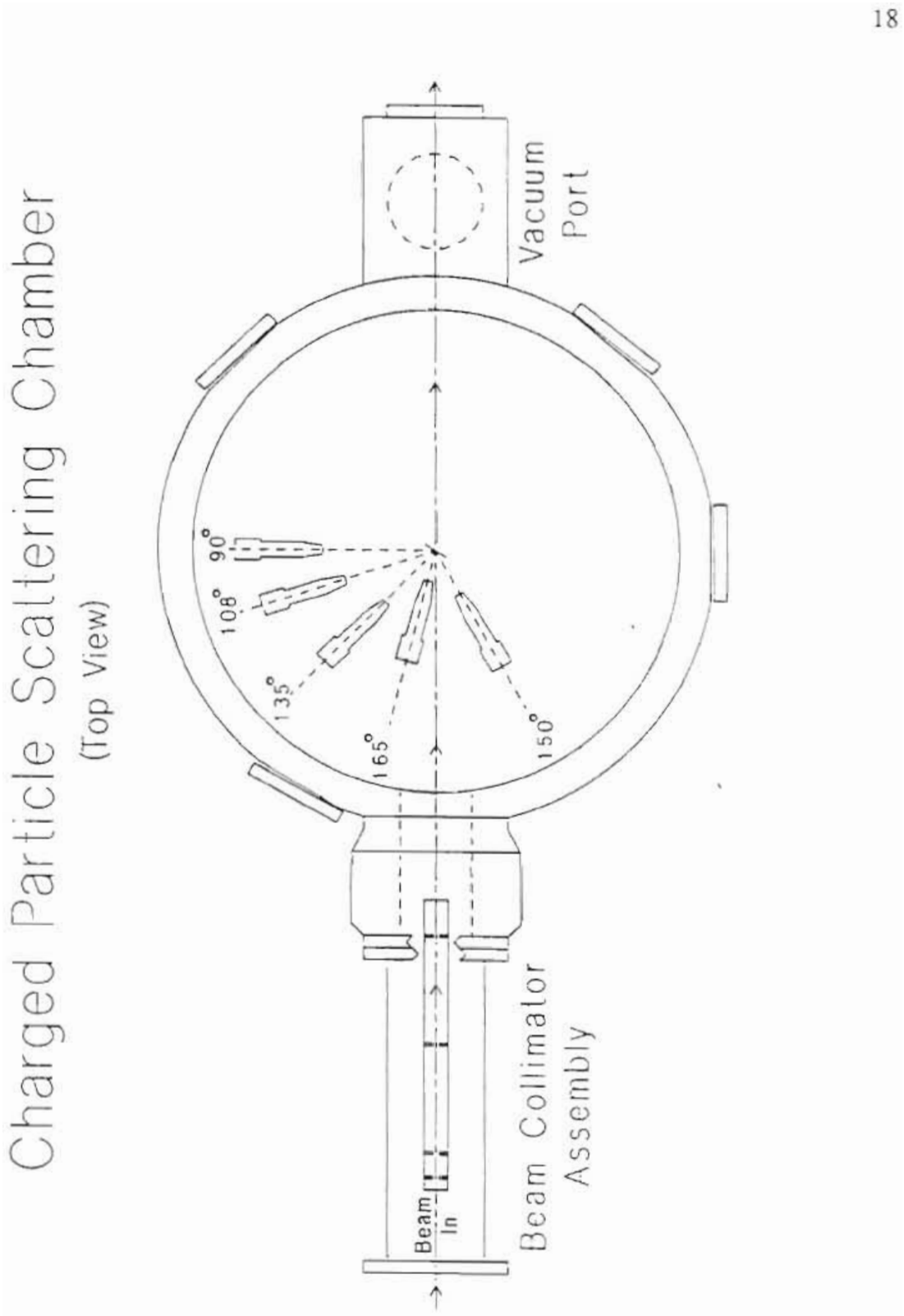
Charged Particle Scattering Chamber
(Top View)
Vacuum Port
90°
108°
135°
165°
150°
Beam In
Beam Collimator Assembly

discussion of techniques used in this method is given by Brooks (1988).

Typically the element of interest is obtained in an oxide compound. The compound is then either reduced to the element of interest, using a reducing agent such as tantalum, or simply mixed with the reducing agent in preparation for evaporation. Then either the element of interest or the mixture is placed in a tantalum boat through which high currents (100-250 A) are passed and the material evaporates onto target rings placed above the boat. The target rings were already prepared by placing a 5 $\mu g/cm^2$ carbon thin film on them. Typical thicknesses of the element of interest were 1-3 $\mu g/cm^2$. To confirm this thickness two methods were utilized: a thickness monitor was used during the evaporation procedure to provide an estimate of the thickness, and elastic scattering tests at relatively low energies (2 MeV) were conducted comparing the number of scattered protons observed with the number expected due to Coulomb scattering from a known thickness of material.

§3.1.4 Electronics, Data Acquisition, and XSYS

A schematic of the electronic data acquisition system is shown in figure 3.3. After a scattering event has occurred the scattered particle deposits all of its energy in the depletion zone of a charged particle detector. This generates a pulse which is first amplified in a preamplifier and then by a linear amplifier. The outputs from the linear amplifier are a bipolar and unipolar signal. The bipolar signal is used to discriminate against carbon scattering events and the unipolar signal is converted by the ADC unless the event is determined to be a carbon scattering event.

The unipolar signal is sent to a multiplexer and then to the ADC. Before arriving at the multiplexer the unipolar signal is delayed 900 ns in order to allow the processing of the bipolar signal. If the bipolar signal indicates a carbon event then the multiplexer

Figure 3.3: Block diagram of HRL data acquisition electronics.

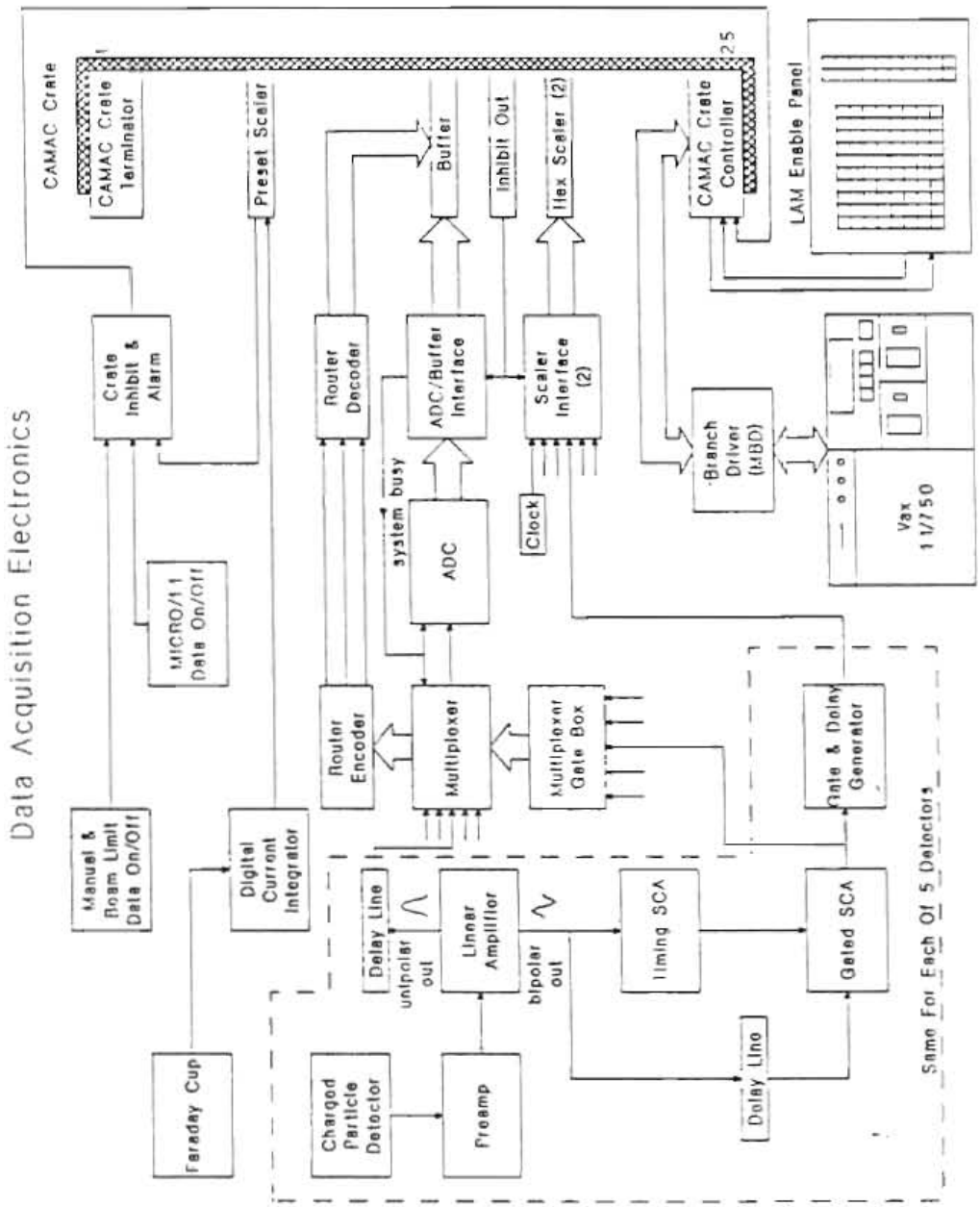
Data Acquisition Electronics
CAMAC Crate
CAMAC Crate Terminator
Preset Scaler
Buffer
Inhibit Out
Ilex Scaler (2)
CAMAC Crate Controller
LAM Enable Panel
Crate Inhibit & Alarm
Router Decoder
ADC/Buffer Interface
Scaler Interface (2)
Branch Driver (MBD)
Vax 11/750
MICRO/11 Data On/Off
system busy
ADC
Clock
Manual & Beam Limit Data On/Off
Digital Current Integrator
Router Encoder
Multiplexer
Multiplexer Gate Box
Gate & Delay Generator
Delay Line
unipolar out
Linear Amplifier
bipolar out
Timing SCA
Gated SCA
Faraday Cup
Charged Particle Detector
Preamp
Delay Line
Same For Each Of 5 Detectors

is inhibited and does not allow the unipolar signal through to the ADC. The discrimination for carbon events is accomplished by splitting the bipolar signal , sending one line through a TSCA, the output of which is connected to the control of a gated SCA, and sending the other line through a delay and then to the input of the gated SCA. The TSCA is set to determine if a particular event has a scattering energy corresponding to a carbon event. If a carbon event is determined to have taken place then the TSCA inhibits the gated SCA, no signal is sent to the multiplexer, and the unipolar signal is not processed. If the event is determined to be a non-carbon event then the gated SCA sends signals to both the multiplexer (allowing the processing of the unipolar signal) and a gate and delay generator (which sends a short logic pulse to a scaler interface to register that a scattering event has occurred). When the multiplexer receives the command to process the unipolar signal the routing address (this indicates which detector observed the event) is encoded into a 3-bit signal. This 3-bit signal is sent along with the output from the multiplexer. When the ADC completes its conversion the output is tagged as originating in the corresponding detector.

After the conversion by the ADC the routing bits and the converted signal are accumulated in a buffer in the CAMAC crate to await transfer to the MBD and finally to the VAX. Note that the scaler interface registers scattering events in the Hex scaler in the CAMAC crate as well, and that by comparing the number of counts for a given detector with the number of scattering events processed by the ADC for that detector, the dead time for the detector can be calculated.

Data are collected until a specified amount of charge has passed through the target. The charge is measured by collecting the beam in a Faraday cup which is connected to a current integrator. When a specified amount of charge has been collected the preset scaler in the CAMAC crate notifies the VAX that the data run is finished, and inhibits the acquisition of further data.

To insure that the beam position on target and the beam energy are steady there are inhibiter circuits that stop data taking during unacceptable conditions. The energy of the beam is monitored by the microprocessor using a DVM which is connected to the analyzer plates. If the voltage on the plates indicates an energy variation greater than 10 eV from the selected energy then the microprocessor sends a signal inhibiting data collection. (The energy corrections are less effective when the beam energy deviates significantly from the desired energy.) In addition limits are set on the proton beam current in the Faraday cup; if the beam intensity increases or decreases beyond a specified range then a signal is sent to inhibit the data collection.

To control the CAMAC crate and the Multi Branch Driver (MBD), which connects the CAMAC crate to the VAX, the XSYS data acquisition software package is used. XSYS was developed at TUNL (King, 1981), and discussed in depth by Roberson and Gould (1985). In its application in the HRL, XSYS completely controls the data acquisition via the following process. Initially an energy for the incident proton beam is specified through the VAX , the corresponding voltage for the analyzer plates is determined by the microprocessor and sent through DACs to the two power supplies for the plates. Once the voltage on the plates and the beam through the analyzer has stabilized, the inhibit signal is canceled and data collection begins. Data is collected, generating a spectrum for each detector, until the preset amount of charge has been collected in the Faraday cup, after which data collection is again inhibited. A typical spectrum collected from a detector is shown in figure 3.4 After the charge preset is reached several subprocesses are enabled which: record the spectra that have been collected on magnetic tape, sum selected peaks in the spectra to generate yield curves, increment the energy of the proton beam and restart the process. A typical yield curve fora series of data points is presented in figure 3.5. The yield curves are the basis for all further analysis since they represent the relative probability for the nuclear reactions.

Figure 3.4: Charged particle spectrum from ^{44}Ca targets at 165°. The carbon scattering peak has been electronically removed.

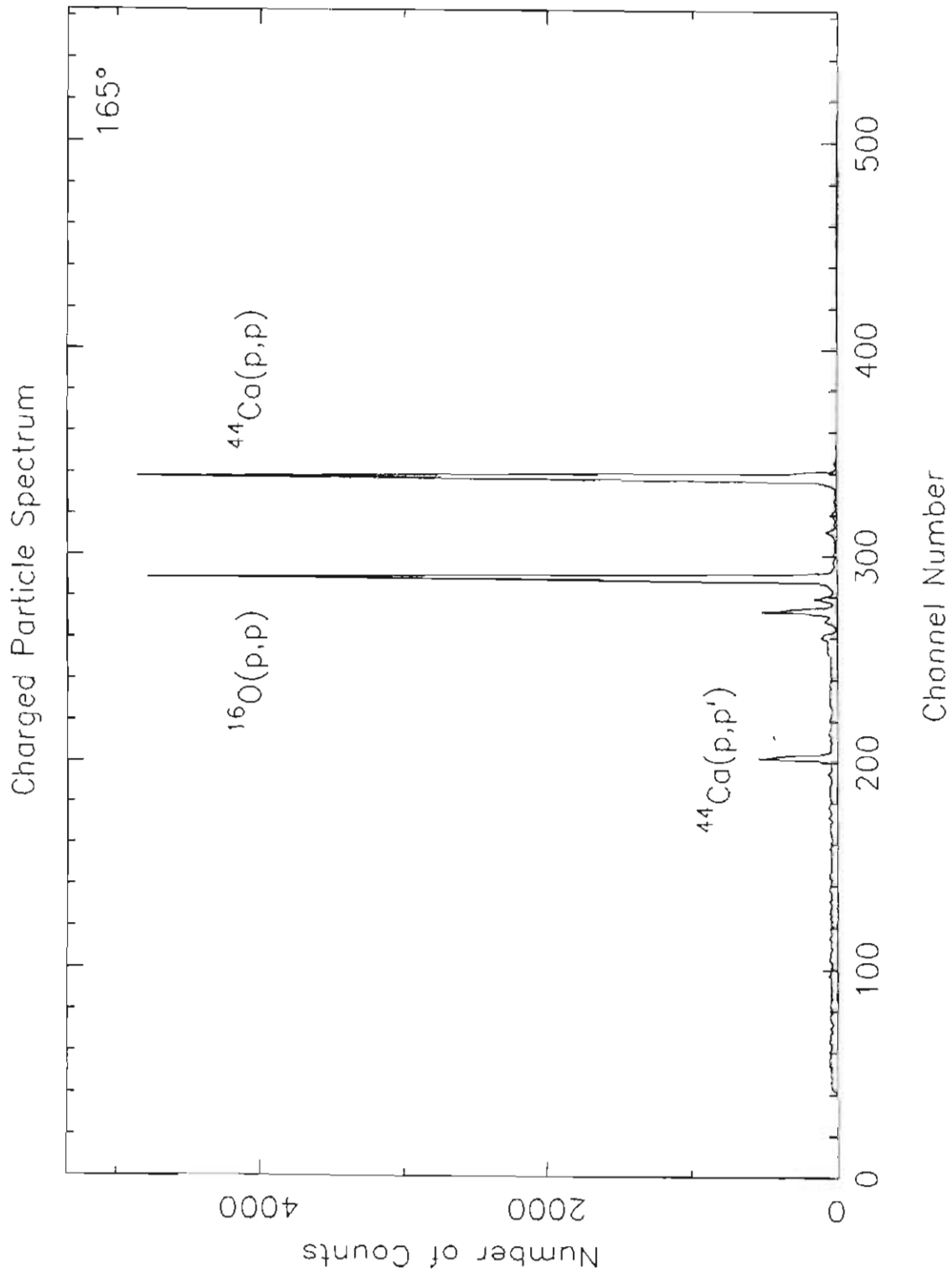
Charged Particle Spectrum
165°
^{44}Ca(p,p)
^{16}O(p,p)
^{44}Ca(p,p')
Number of Counts
0
2000
4000
0
100
200
300
400
500
Channel Number

Figure 3.5: Yield curve generated from the $^{44}Ca(p,p)$ reaction peak at 165°.

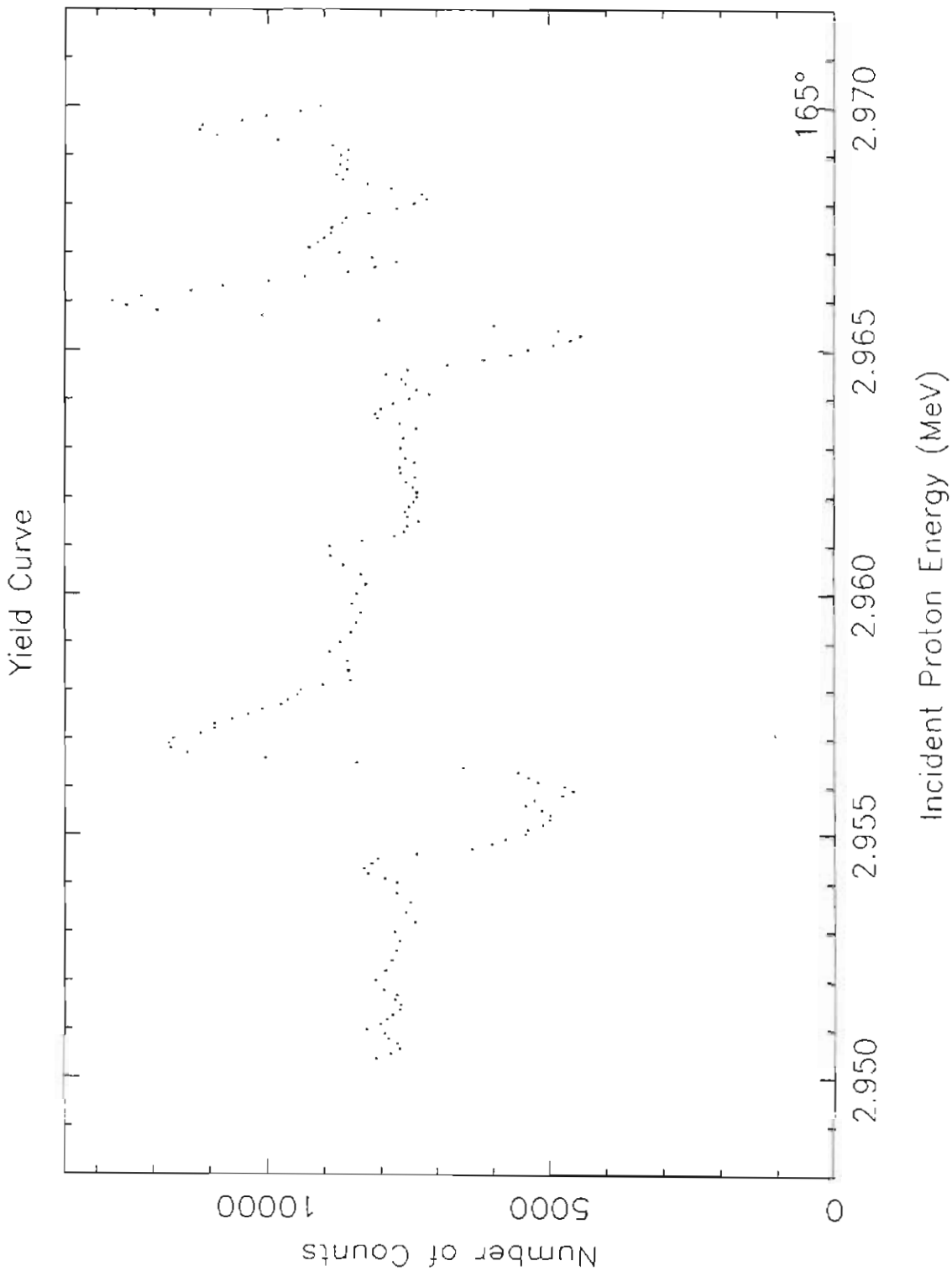
Yield Curve
Number of Counts
0
5000
10000
2.950
2.955
2.960
2.965
2.970
Incident Proton Energy (MeV)
165°

§3.2 Discussion of Analysis of Experimental Data.

Once the yield curves have been generated the next step is to extract the nuclear reaction information. Variations in the yield curves are indications of resonances or nuclear levels. The information of interest for each level includes the following: the angular momentum J, the parity π, the energy location E_0, the laboratory width Γ and the corresponding nuclear reduced width γ^2. This information is obtained by generating a theoretical differential cross section and comparing the calculation with the data. Due to the complexity of compound nuclear reactions this cross-section calculation must include multilevel and multichannel considerations; the yield curves in general will involve many resonances and several reaction channels, (p,p), (p,p´) (p,p´´), (p,α), etc.

The most successful approach to such resonance analyses is the R-matrix theory developed by Wigner and Eisenbud (1947). The R-matrix theory allows the formulation of the scattering cross-section without knowledge of either the nuclear potential or the nuclear wave function. To accomplish this the R-matrix theory utilizes two key ideas: references to the internal region are replaced with adjustable parameters and a boundary condition at the nuclear interaction surface is specified to allow the complete determination of the external wave function.

In the following section the R-matrix theory will be developed using the same conventions and definitions adopted by Lane and Thomas (1958). Not all of the details of the derivations will be provided. More detailed information is found in Lane and Thomas's comprehensive review or in Erich Vogt's article (1962). Vogt's article provides excellent physical background information concerning the basis and development of the R-matrix theory.

§3.2.1 R-Matrix Analysis

In determination of the scattering cross-section there are three effective regions of interest, the internal nuclear region, the nuclear interaction surface and the external region. The forms of the wave functions in the internal and external regions are as follows:

$$\Psi_{internal} = \sum_{\lambda} A_{\lambda} X_{\lambda} \text{ , with } A_{\lambda} = \int \Psi X_{\lambda}^{*} dV$$

$$\Psi_{external} = \frac{u_{\alpha sl}(r_{\alpha})}{r_{\alpha}} \left[i^{l} Y_{m}^{l}(\Omega_{\alpha}) \right] \psi_{\alpha sv}$$

Since the internal wave functions must be determined through the use of the nuclear potential which is not explicitly known, all references to the internal wave function need to be eliminated by replacing them with adjustable parameters. Since to calculate the cross-section the external wave function must be completely determined at all points and energies, a boundary condition is needed which contains the value and derivative of the external wave function. Both of these needs are satisfied in the derivation of the R-matrix.

To start the derivation it is necessary to solve for A_{λ}. To do this consider the Schrodinger wave equation for both the total wave function Ψ and resonant states X_{λ}. These wave equations are,

$$-\frac{\hbar^2}{2m}\nabla^2\Psi + V\Psi = E\Psi \text{ ,and } -\frac{\hbar^2}{2m}\nabla^2 X_{\lambda} + VX_{\lambda} = E_{\lambda} X_{\lambda} .$$

Multiply the first equation by X^{*}_{λ} and take the complex conjugate of the second equation while also multiplying by Ψ giving

$$-\frac{\hbar^2}{2m}\Psi\nabla^2 X_{\lambda}^{*} + \Psi V X_{\lambda}^{*} = \Psi E_{\lambda} X_{\lambda}^{*}$$

and

$$-\frac{\hbar^2}{2m}X_\lambda^*\nabla^2\Psi + X_\lambda^*V\Psi = X_\lambda^*E\Psi$$

Subtract the first equation from the second obtaining

$$-\frac{\hbar^2}{2m}\left[X_\lambda^*\nabla^2\Psi - \Psi\nabla^2X_\lambda^*\right] + \left[X_\lambda^*V\ \Psi - \Psi V\ X_\lambda^*\right] = (E - E_\lambda)X_\lambda^*\Psi$$

Note that the second term will be zero if V is hermitian. Next integrate over the nuclear volume on both sides of the equation

$$-\frac{\hbar^2}{2m}\int_v\left[X_\lambda^*\nabla^2\Psi - \Psi\nabla^2X_\lambda^*\right]dV = (E - E_\lambda)\int_v X_\lambda^*\Psi dV$$

Using Green's theorem the left hand side can be reduced to a surface integral. The right hand side can be replaced by A_λ.

$$-\frac{\hbar^2}{2m}\int_S\left[X_\lambda^*\vec{\nabla}\Psi - \vec{\nabla}X_\lambda^*\Psi\right]\cdot\hat{n}\,dS = (E - E_\lambda)A_\lambda$$

Now carrying out the dot product of the del operator and the channel unit vector

$$-\frac{\hbar^2}{2m_c}\int_S\left[X_\lambda^*\,grad_n(\Psi) - grad_n\left(X_\lambda^*\right)\Psi\right]dS = (E - E_\lambda)A_\lambda$$

On the nuclear interaction surface define for convenience the following, utilizing the form of the external wave function,

$$\Psi = \sum_c\sqrt{\frac{2m_c\,a_c}{\hbar^2}}\,V_c\phi_c\ ,$$

where

$$V_c = \sqrt{\frac{\hbar^2}{2m_c\,a_c}}\,u_c(a_c)\quad \text{, and } \phi_c = \psi_{asv}\left(i^l Y_m^l\right)\frac{1}{r_\alpha}$$

Similarly,

$$grad_n(r_c\,\Psi) = \sum_c\sqrt{\frac{2m_c a_c}{\hbar^2}}D_c\,\phi_c\ \text{, where } D_c = \sqrt{\frac{\hbar^2 a_c}{2m_c}}\left(\frac{du_c}{dr_c}\right)_{r_c=a_c}$$

and for just the gradient of Ψ,

$$grad_n(\Psi) = \sum_c \sqrt{\frac{2m_c}{\hbar^2 a_c}}(D_c - V_c)\phi_c .$$

Substituting these definitions into the earlier equation and rearranging gives

$$\sum_c \left[\sqrt{\frac{\hbar^2}{2m_c a_c}}(D_c - V_c)\int_S X_\lambda^* \phi_c \, dS - \sqrt{\frac{\hbar^2 a_c}{2m_c}} V_c \int_S \phi_c \, grad_n\left(X_\lambda^*\right) dS \right] = (E_\lambda - E)A_\lambda .$$

Now define parameters that contain all the internal region information,

$$\gamma_{\lambda c} = \sqrt{\frac{\hbar^2}{2m_c a_c}} \int_S \phi_c^* X_\lambda \, dS$$

and

$$\delta_{\lambda c} = \gamma_{\lambda c} + \sqrt{\frac{\hbar^2 a_c}{2m_c}} \int_S \phi_c^* \, grad\left(X_\lambda\right) dS$$

and note the boundary condition at the nuclear interaction surface

$$\delta_{\lambda c} = B_c \gamma_{\lambda c} .$$

The quantity $\gamma_{\lambda c}$ is known as the reduced width amplitude and has importance not only in the R-matrix theory but also in nuclear reaction theory. Using these relations gives

$$\sum_c \left[(D_c - V_c)\gamma_{\lambda c} - V_c\left(B_c \gamma_{\lambda c} - \gamma_{\lambda c}\right) \right] = (E_\lambda - E)A_\lambda .$$

Solving for A gives

$$A_\lambda = \frac{1}{(E_\lambda - E)} \sum_c (D_c - V_c B_c)\gamma_{\lambda c}$$

and for Ψ

$$\Psi = \sum_\lambda A_\lambda X_\lambda = \sum_c \left[\sum_\lambda \frac{\gamma_{\lambda c} X_\lambda}{(E_\lambda - E)} \right] (D_c - V_c B_c) .$$

The reference to X_λ can be eliminated, by multiplying both sides by $\phi^*_{c'}$ and integrating over the nuclear interaction surface

$$\int_S \phi^*_{c'} \Psi dS = \sum_c \left[\sum_\lambda \frac{\left(\int_S \phi^*_{c'} X_\lambda dS \right) \gamma_{\lambda c}}{(E_\lambda - E)} \right] (D_c - V_c B_c) .$$

Substitute for the integral on the left and the right giving

$$V_{c'} = \sum_c \left[\sum_\lambda \frac{\gamma_{\lambda c'} \gamma_{\lambda c}}{(E_\lambda - E)} \right] (D_c - V_c B_c)$$

and finally

$$V_{c'} = \sum_c R_{c'c} (D_c - V_c B_c) \text{ , where } R_{c'c} = \sum_\lambda \frac{\gamma_{\lambda c'} \gamma_{\lambda c}}{(E_\lambda - E)} .$$

The relation on the left is the boundary condition needed to allow the complete determination of the external wave function. The relation on the right is the definition of the R-matrix, which contains references to the internal region in the form of the parameters $\gamma_{\lambda c'}$.

The next step is to determine the external wave function. Recall the form of the external wave function

$$\Psi = \frac{u_{a s l}(r_a)}{r_a} \left[i^l Y^l_m (\Omega_a) \right] \Psi_{\alpha \nu} ,$$

where $u_{a s l}(r_a)$ is a solution to the radial Schrodinger equation

$$\left[\frac{d^2}{dr_a^2} - \frac{l(l+1)}{r_a^2} - \frac{2M_a}{\hbar^2} (V_{a s l} - E_a) \right] u_{a s l}(r_a) = 0 .$$

Considering only a Coulomb interaction in the region external to the nuclear interaction region, corresponds to a potential of the form

$$V_{a s l} = \frac{Z_{a1} Z_{a2} e^2}{r_a} .$$

Using the notation of Lane and Thomas, define new parameters to aid in the solution of

this equation,

$$k_c \equiv k_\alpha = \sqrt{\frac{2M_\alpha |E_\alpha|}{\hbar^2}}, \text{the wave number}$$

$$\upsilon_c \equiv \upsilon_\alpha = \frac{\hbar k_\alpha}{M_\alpha}, \text{the relative velocity}$$

$$\eta_c \equiv \eta_{\alpha l} = \frac{Z_{\alpha 1} Z_{\alpha 2} e^2}{\hbar \upsilon_\alpha}, \text{the Coulomb field parameter}$$

$$\sigma_c \equiv \sigma_{\alpha l} = \arg \Gamma(1 + l_c + i\eta_c), \text{the Coulomb phase shift}$$

$$\text{and } \rho_c \equiv \rho_\alpha = k_\alpha r_\alpha .$$

Using these definitions rewrite the Schrodinger equation in the dimensionless form,

$$\left[\frac{d^2}{d\rho_\alpha^2} - \frac{l(l+1)}{\rho_\alpha^2} - \frac{2\eta_\alpha}{\rho_\alpha} \pm 1\right] u_{\alpha sl}(\rho_\alpha) = 0 .$$

The top sign indicates positive energies and the bottom sign indicates negative energies. Due to the energy region of the data only the positive energy solution will be considered.

The solutions of interest need to correspond to incoming and outgoing waves. Writing the radial function u in terms of these waves has the form

$$u_{\alpha l}(\rho_\alpha) = C_{\alpha l} I_{\alpha l} + D_{\alpha l} O_{\alpha l} ,$$

where C and D are amplitude coefficients of the incoming and outgoing waves. The incoming and outgoing waves for the dimensionless Schrodinger equation are,

$$I_c \equiv I_{\alpha l} \propto \exp\left[-i\left(\rho_\alpha - \eta_\alpha \log 2\rho_\alpha - \tfrac{1}{2} l\pi + \sigma_{\alpha 0}\right)\right]$$
$$O_c \equiv O_{\alpha l} \propto \exp\left[i\left(\rho_\alpha - \eta_\alpha \log 2\rho_\alpha - \tfrac{1}{2} l\pi + \sigma_{\alpha 0}\right)\right] .$$

These functions can be expressed in terms of regular (zero at the origin) and irregular (singularity at the origin) functions,

$$I_c = (G_c - iF_c)\exp(i\omega_c) \quad \text{and} \quad O_c = (G_c + iF_c)\exp(-i\omega_c)$$

where,

$$\omega_c \equiv \omega_{\alpha l} = \sigma_{\alpha l} - \sigma_{\alpha 0} = \sum_{n=1}^{l} \tan^{-1}\left(\frac{\eta_\alpha}{n}\right)$$

F and G are called the Coulomb functions and are related to the spherical Bessel and Neumann functions

$$F_{\alpha l}(r_\alpha) = k_\alpha r_\alpha j_l(k_\alpha r_\alpha) \quad \text{and} \quad G_{\alpha l}(r_\alpha) = -k_\alpha r_\alpha n_l(k_\alpha r_\alpha)$$

and have the asymptotic forms,

$$F_c \equiv F_{\alpha l} \propto \sin\left(\rho_\alpha - \eta_\alpha \log 2\rho_\alpha - \frac{1}{2} l\pi + \sigma_{\alpha 0}\right)$$
$$G_c \equiv G_{\alpha l} \propto \cos\left(\rho_\alpha - \eta_\alpha \log 2\rho_\alpha - \frac{1}{2} l\pi + \sigma_{\alpha 0}\right).$$

Using the new form for u gives for the general wave function

$$\Psi = \sum_{\alpha s l v m} C_{\alpha l}\left(i^l Y_m^{\ l}\right)\frac{I_{\alpha l}}{r_\alpha}\psi_{\alpha s v} + D_{\alpha l}\left(i^l Y_m^{\ l}\right)\frac{O_{\alpha l}}{r_\alpha}\psi_{\alpha s v}$$

or in a more convenient form,

$$\Psi = \sum_c y_c \mathcal{I}_c + x_c O_c .$$

Where $\mathcal{I}$ and O are the incoming and outgoing waves, respectively, having unit flux and crossing a sphere centered at the origin, and are defined as follows

$$\mathcal{I}_c \equiv \mathcal{I}_{\alpha s l v m} = \left(i^l Y_m^{(l)}\right)\frac{I_{\alpha l}}{\sqrt{v_\alpha}\, r_\alpha}\psi_{\alpha s v}$$

and

$$O_c \equiv O_{\alpha s l v m} = \left(i^l Y_m^{(l)}\right)\frac{O_{\alpha l}}{\sqrt{v_\alpha}\, r_\alpha}\psi_{\alpha s v}$$

To obtain the scattering amplitude and eventually the cross section it is necessary to express the outgoing wave amplitudes x in terms of the incoming wave amplitudes y, which is possible through the use of a collision matrix U. The relationship is given as

$$x_{c'} = -\sum_c U_{cc'} y_c .$$

Substituting this into the earlier form for Ψ gives,

$$\Psi = \sum_c \left(y_c \mathcal{I}_c - \sum_{c'} U_{cc'} y_{c'} \mathcal{O}_c \right)$$

rearranging and assuming only one entrance channel gives

$$\Psi = \sum_{cc'} \left(\delta_{cc'} \mathcal{I}_c - U_{cc'} \mathcal{O}_{c'} \right) y_c$$

Due to the need for a term in the wave function that represents the incident proton beam the introduction of the wave function Ψ' which is proportional to the spherical Bessel function is needed. The spherical Bessel function is chosen because of the form of a plane wave shown below.

$$e^{ikz} = \sum_{l=0}^{\infty} (2l + 1) i^l j_l(kr) P_l(\cos\theta)$$

Therefore

$$\begin{aligned} \Psi' &\propto \sum_c F_c \\ &\propto \sum_c (G_c - iF_c) - (G_c + iF_c) \\ &\propto \sum_c I_c - O_c \exp(2i\omega_c) \\ &= \sum_{cc'} \left(\delta_{cc'} \mathcal{I}_c - \delta_{cc'} \mathcal{O}_c e^{2i\omega_c} \right) y_c \end{aligned}$$

Now incorporate this wave function into the form for Ψ by subtracting Ψ' from both sides of the previous relation for Ψ giving

$$\Psi = \Psi' + \sum_{cc'} \left(e^{2i\omega_c} \delta_{cc'} - U_{cc'} \right) \mathcal{O}_{c'} y_c$$

Before proceeding determine what value of y_C is needed in order to make Ψ' correspond to the form of an incident plane wave. Rewriting Ψ' in a form that includes the spherical Bessel function

$$\Psi' = \sum_c \left(\mathcal{I}_c - O_c e^{2i\omega_c} \right) y_c$$

$$= \sum_c i^l Y_m^{(l)} \frac{\psi_c}{\sqrt{\upsilon_c}\, r_c} \left(I_c - O_c e^{2i\omega_c} \right) y_c$$

$$= \sum_c i^l Y_m^{(l)} \frac{\psi_c e^{i\omega_c}}{\sqrt{\upsilon_c}\, r_c} [(G_c - iF_c) - (G_c + iF_c)] y_c$$

$$= \sum_c i^l Y_m^{(l)} \frac{\psi_c e^{i\omega_c}}{\sqrt{\upsilon_c}} \left(\frac{-2iF_c}{r_c} \right) y_c$$

$$= \sum_c i^l Y_m^{(l)} (j_l k_c) \frac{-2i\psi_c e^{i\omega_c}}{\sqrt{\upsilon_c}} y_c$$

Note that for the incident plane wave m = 0, which reduces the spherical harmonic to the form.

$$Y_0^{(l)}(\Omega) = \sqrt{\frac{2l+1}{4\pi}}\, P_l(\cos\theta)$$

giving

$$\Psi' = \sum_c i^l \sqrt{\frac{2l+1}{\pi}} \frac{P_l \cos(\theta)}{2} (j_l k_c) \frac{-2i\psi_c e^{i\omega_c}}{\sqrt{\upsilon_c}} y_c$$

Choose the following y_c to give the form of an incident plane wave

$$y_c \equiv y_{a\,sl\,v0} = \frac{i\sqrt{\pi}}{k_a} \sqrt{2l+1}$$

finally for Ψ'

$$\Psi' = \sum_c i^l (2l+1) j_l P_l \cos(\theta) \frac{\psi_c e^{i\omega_c}}{\sqrt{\upsilon_c}}$$

From Schiff (1968) the asymptotic form of this relation is

$$\Psi'_{a\,s\,v} \propto \frac{\Psi_{a\,s\,v}}{\sqrt{\upsilon_a}} \left[\left(1 - \frac{\eta_a^2}{ik_a(r_a - z_a)} \right) \exp i\{ k_a z_a - \eta_a \log k_a(r_a - z_a) - \sigma_{a0} \} \right.$$

$$\left. - \frac{\sqrt{\pi}}{k_a r_a} C_a(\theta_a) \exp i\{ \rho_a - \eta_a \log 2\rho_a + \sigma_{a0} \} \right]$$

where,

$$C_\alpha(\theta_\alpha) = \frac{\eta_\alpha}{\sqrt{4\pi}} \csc^2\left(\frac{\theta_\alpha}{2}\right) \exp\left\{-2i\,\eta_\alpha \log \sin\left(\frac{\theta_\alpha}{2}\right)\right\}$$

Note that in the above relation the first term in the bracket corresponds to an incident plane wave in the z direction , and the second term corresponds to a Coulomb scattered wave with the coefficients $C_{\alpha'}$. Evaluating Ψ using all pertinent relations (and the equivalent notations c and $\alpha s l v m$) gives

$$\Psi = \Psi' + \sum_{cc'}\left(e^{2i\omega_c}\delta_{cc'} - U_{cc}\right)\left[\left(i^{l'}Y_{m'}^{(l')}\right)\frac{O_{\alpha l}}{\sqrt{v_{\alpha'}}\,r_{\alpha'}}\psi_{\alpha' s' v'}\right]\left(\frac{i\sqrt{\pi}}{k_\alpha}\sqrt{2l+1}\right)$$

Note

$$\exp\left(-\frac{1}{2}l\pi\right) = (-i)^l$$

Rewriting the outgoing wave

$$O_{\alpha l'} = (-i)^{l'}\exp\left[i\left(\rho_{\alpha'} - \eta_{\alpha'}\log 2\rho_{\alpha'} + \sigma_{\alpha' 0}\right)\right]$$

Using this relation and rearranging gives,

$$\Psi \propto \Psi'_{\alpha s v} + \sum_{\alpha' s' l' v' m' l} \frac{i\sqrt{\pi(2l+1)}}{k_\alpha}\left[e^{2i\omega_{\alpha' l'}}\delta_{\alpha' s l' v' m', \alpha s l v 0} - U_{\alpha' s l' v' m', \alpha s l v 0}\right]$$
$$\times \frac{\psi_{\alpha' s' v'}}{\sqrt{v_{\alpha'}}\,r_{\alpha'}}Y_{m'}^{(l')}(\Omega_{\alpha'})\exp i\left\{\rho_{\alpha'} - \eta_{\alpha'}\log 2\rho_{\alpha'} + \sigma_{\alpha' 0}\right\}$$

Rewrite Ψ' so it is of similar form to the above equation

$$\Psi'_{\alpha s v} \propto \frac{\psi_{\alpha s v}}{\sqrt{v_\alpha}}\left(1 - \frac{\eta_\alpha^2}{ik_\alpha(r_\alpha - z_\alpha)}\right)\exp i\left\{k_\alpha z_\alpha - \eta_\alpha \log k_\alpha(r_\alpha - z_\alpha) - \sigma_{\alpha 0}\right\}$$
$$- \frac{\sqrt{\pi}}{k_\alpha}C_{\alpha'}(\theta_{\alpha'})\frac{\psi_{\alpha' s' v'}}{\sqrt{v_{\alpha'}}\,r_{\alpha'}}\exp i\left\{\rho_{\alpha'} - \eta_{\alpha'}\log 2\rho_{\alpha'} + \sigma_{\alpha' 0}\right\}\delta_{\alpha' s' v', \alpha s v}\Big]$$

Now substituting and grouping terms

$$\Psi \sim \frac{\psi_{\alpha s v}}{\sqrt{v_\alpha}}\left(1 - \frac{\eta_\alpha^2}{ik_\alpha(r_\alpha - z_\alpha)}\right)\exp\, i\{k_\alpha z_\alpha - \eta_\alpha \log\, k_\alpha(r_\alpha - z_\alpha) - \sigma_{\alpha 0}\}$$
$$+ \frac{\sqrt{\pi}}{k_\alpha}\sum_{\alpha' s' l' v' m' l}\Big(i\sqrt{(2l+1)}\Big[e^{2i\omega_{\alpha' l'}}\delta_{\alpha' s' l' v' m', \alpha s l v 0}$$
$$- U_{\alpha' s' l' v' m', \alpha s l v 0}\Big]Y_{m'}^{(l')}(\Omega_{\alpha'}) - C_{\alpha'}(\theta_{\alpha'})\delta_{\alpha' s' v', \alpha s v}\Big)$$
$$\times \frac{\psi_{\alpha' s' v'}}{\sqrt{v_{\alpha'}}\, r_{\alpha'}}\exp\, i\{\rho_{\alpha'} - \eta_{\alpha'}\log 2\rho_{\alpha'} + \sigma_{\alpha' 0}\}$$

and finally

$$\Psi \sim \frac{\psi_{\alpha s v}}{\sqrt{v_\alpha}}\left(1 - \frac{\eta_\alpha^2}{ik_\alpha(r_\alpha - z_\alpha)}\right)\exp i\{k_\alpha z_\alpha - \eta_\alpha \log k_\alpha(r_\alpha - z_\alpha) - \sigma_{\alpha 0}\}$$
$$+ \sum_{\alpha' s' v'} A_{\alpha' s' v', \alpha s v}\frac{\psi_{\alpha' s' v'}}{\sqrt{v_{\alpha'}}\, r_{\alpha'}}\exp i\{\rho_{\alpha'} - \eta_{\alpha'}\log 2\rho_{\alpha'} + \sigma_{\alpha' 0}\}$$

where

$$A_{\alpha' s' v', \alpha s v} = \frac{\sqrt{\pi}}{k_\alpha}\Big\{-C_{\alpha'}(\theta_{\alpha'})\delta_{\alpha s v', \alpha s v} + i\sum_{l m l}\sqrt{2l+1}$$
$$\times\Big[e^{2i\omega_{\alpha l'}}\delta_{\alpha s l' v m', \alpha s l v 0} - U_{\alpha s l' v m', \alpha s l v 0}\Big]Y_{m'}^{(l')}(\Omega_{\alpha'})\Big\}$$

Note that the A coefficients are just the amplitudes of the outgoing waves, which correspond to the scattered and reaction wave amplitudes, and are related to the differential cross section as shown,

$$d\sigma_{\alpha' s' v', \alpha s v} = \left|A_{\alpha' s' v', \alpha s v}(\Omega_{\alpha'})\right|^2 d\Omega_{\alpha'}$$

Before calculating the cross section the R-matrix must be connected to the U-matrix to include the boundary condition found earlier. This defines everything that is needed for the cross-section calculation. Start with

$$\Psi = \sum_c x_c O_c + y_c \mathfrak{I}_c .$$

For ease of notation define V and D in terms of O and $\mathfrak{I}$. Recall

$$\mathfrak{I}_c(\rho_c) = \left(i^l Y_m^{(l)}\right)\frac{I_{\alpha l}^{+}(\rho_c)}{\sqrt{\upsilon_\alpha}\, r_\alpha}\psi_{\alpha s\nu} \text{ and } \mathfrak{O}_c(\rho_c) = \left(i^l Y_m^{(l)}\right)\frac{O_{\alpha l}^{+}(\rho_c)}{\sqrt{\upsilon_\alpha}\, r_\alpha}\psi_{\alpha s\nu}$$

Substituting into the relation for Ψ and rearranging gives,

$$\Psi = \sum_c \left[\frac{x_c O_{\alpha l}(\rho_c)}{\sqrt{\upsilon_\alpha}} + \frac{y_c I_{\alpha l}(\rho_c)}{\sqrt{\upsilon_\alpha}}\right]\left[\left(i^l Y_m^{(l)}\right)\frac{\psi_{\alpha s\nu}}{r_\alpha}\right].$$

Recalling the surface function

$$\phi_c(r_\alpha) = \left(i^l Y_m^{l}\right)\frac{\psi_{\alpha s\nu}}{r_\alpha}$$

allows Ψ to be written

$$\Psi = \sum_c \sqrt{\frac{2m_c a_c}{\hbar^2}} V_c\, \phi_c(r_c),$$

where

$$V_c = \sqrt{\frac{\hbar^2}{2m_c a_c}}\left[\frac{x_c O_\alpha(\rho_c)}{\sqrt{\upsilon_\alpha}} + \frac{y_c I_{\alpha l}(\rho_c)}{\sqrt{\upsilon_\alpha}}\right].$$

Similarly considering

$$\text{grad}_n(r\Psi) = \text{grad}_n\left(\sum_c r_c\left[\frac{x_c O_{\alpha l}(\rho_c)}{\sqrt{\upsilon_\alpha}} + \frac{y_c I_{\alpha l}(\rho_c)}{\sqrt{\upsilon_\alpha}}\right]\phi_c(r_c)\right)$$

and expanding gives,

$$\begin{aligned}\text{grad}_n(r\Psi) = &\left(\sum_c\left[\frac{x_c O_\alpha(\rho_c)}{\sqrt{\upsilon_\alpha}} + \frac{y_c I_{\alpha l}(\rho_c)}{\sqrt{\upsilon_\alpha}}\right]\phi_c(r_c)\right)\\ &+\left(\sum_c r_c\left[\frac{x_c\,\text{grad}_n\left[O_\alpha(\rho_c)\right]}{\sqrt{\upsilon_\alpha}} + \frac{y_c\,\text{grad}_n\left[I_{\alpha l}(\rho_c)\right]}{\sqrt{\upsilon_\alpha}}\right]\phi_c(r_c)\right)\\ &+\left(\sum_c r_c\left[\frac{x_c O_{\alpha l}(\rho_c)}{\sqrt{\upsilon_\alpha}} + \frac{y_c I_{\alpha l}(\rho_c)}{\sqrt{\upsilon_\alpha}}\right]\text{grad}_n\left[\phi_c(r_c)\right]\right)\end{aligned}$$

or

$$\text{grad}_n(r\Psi) = \left(\sum_c \sqrt{\frac{2m_c a_c}{h^2}} V_c \ \phi_c(r_c)\right)$$
$$+ \left(\sum_c r_c \left[\frac{x_c}{\sqrt{\upsilon_\alpha}}\left(\frac{d\rho_c}{dr_c}\right)\left(\frac{dO_{\alpha l}}{dr_c}\right) + \frac{y_c}{\sqrt{\upsilon_\alpha}}\left(\frac{d\rho_c}{dr_c}\right)\left(\frac{dI_{\alpha l}}{dr_c}\right)\right] \phi_c(r_c)\right)$$
$$+ \left(\sum_c r_c \left[\frac{x_c O_{\alpha l}(\rho_c)}{\sqrt{\upsilon_\alpha}} + \frac{y_c I_{\alpha l}(\rho_c)}{\sqrt{\upsilon_\alpha}}\right]\left(-\frac{1}{r_c}\right)\phi_c(r_c)\right)$$

and finally

$$\text{grad}_n(r\Psi) = \left(\sum_c \sqrt{\frac{2m_c a_c}{h^2}} V_c \ \phi_c(r_c)\right)$$
$$+ \left(\sum_c \left[\frac{x_c}{\sqrt{\upsilon_\alpha}}(k_c r_c)\left(\frac{dO_{\alpha l}}{dr_c}\right) + \frac{y_c}{\sqrt{\upsilon_\alpha}}(k_c r_c)\left(\frac{dI_{\alpha l}}{dr_c}\right)\right] \phi_c(r_c)\right)$$
$$- \left(\sum_c \sqrt{\frac{2m_c a_c}{h^2}} V_c \ \phi_c(r_c)\right) .$$

Using a new notation

$$\text{grad}_n(r\Psi) = \sum_c \sqrt{\frac{2m_c a_c}{h^2}} D_c \ \phi_c(r_c) ,$$

where

$$D_c = \sqrt{\frac{\hbar^2}{2m_c a_c}} \left[\frac{x_c \rho_c}{\sqrt{\upsilon_\alpha}}\left(\frac{dO_{\alpha l}}{dr_c}\right) + \frac{y_c \rho_c}{\sqrt{\upsilon_\alpha}}\left(\frac{dI_{\alpha l}}{dr_c}\right)\right].$$

Rewriting V and D in more convenient terms using

$$\upsilon_c = \frac{\hbar k_\alpha}{M_\alpha}$$

gives

$$V_c = \sqrt{\tfrac{1}{2}\hbar} \left[\rho_c^{-\frac{1}{2}} O_{\alpha l} x_c + \rho_c^{-\frac{1}{2}} I_{\alpha l} y_c\right]$$

and

$$D_c = \sqrt{\tfrac{1}{2}\hbar}\left[\rho_c^{\frac{1}{2}} O'_{\alpha l}\, x_c + \rho_c^{\frac{1}{2}} I'_{\alpha l}\, y_c\right]$$

and in matrix notation

$$V = \sqrt{\tfrac{1}{2}\hbar}\left[\rho^{-\frac{1}{2}} O\, x + \rho^{-\frac{1}{2}} I\, y\right]$$

and

$$D = \sqrt{\tfrac{1}{2}\hbar}\left[\rho^{\frac{1}{2}} O'\, x + \rho^{\frac{1}{2}} I'\, y\right].$$

Recalling the R-matrix relation and writing it in matrix notation gives

$$V = R(D - VB).$$

Substituting for V and D yields

$$\left[\rho^{-\frac{1}{2}} O\, x + \rho^{-\frac{1}{2}} I\, y\right] = R\left[\rho^{\frac{1}{2}} O'\, x + \rho^{\frac{1}{2}} I'\, y\right] - RB\left[\rho^{-\frac{1}{2}} O\, x + \rho^{-\frac{1}{2}} I\, y\right].$$

Now rearrange into the form

$$x = -U\, y$$

results in

$$\left[\rho^{-\frac{1}{2}} O - R\rho^{\frac{1}{2}} O' + RB\ \rho^{-\frac{1}{2}} O\right] x = -\left[-R\rho^{\frac{1}{2}} I' + RB\,\rho^{-\frac{1}{2}} I + \rho^{-\frac{1}{2}} I\right] y.$$

Solving for u gives the relation between the U and R matrices

$$U = \left[\rho^{-\frac{1}{2}} O - R\rho^{\frac{1}{2}} O' + RB\ \rho^{-\frac{1}{2}} O\right]^{-1}\left[-R\rho^{\frac{1}{2}} I' + RB\,\rho^{-\frac{1}{2}} I + \rho^{-\frac{1}{2}} I\right].$$

With this relation all needed information for the calculation of the cross section has been obtained. The calculation of the cross section has been coded for use in data analysis in the FORTRAN code MULTI6 first written by Sellin (1969). There have been major extensions and revisions to MULTI6 over the years; the latest version is described by Nelson (1983).

§3.2.2 Analysis Procedure Using MULTI6

The R-matrix theory has been coded in FORTRAN for computer usage in the analysis of the data at the HRL. An iterative trial and error method is used to determine the parameters for each of the energy levels These parameters are: resonance energy E_o , angular momentum of the compound state J, parity of the compound state π, exit channel spin s´, exit orbital angular momentum ℓ' and laboratory width Γ. In figure 3.6 the relations among the angular momentum parameters are shown. After each execution of a MULTI6 calculation the computed theoretical cross-sections are visually compared with the experimental yield curves (which have been normalized to the theoretical cross sections), adjustments are made in the parameters for the energy levels and then MULTI6 is then reexecuted until the fit and data compare well. The final resonance parameters are then used to construct level sequences.

§3.2.3 Results of Analysis: Level Sequences.

Once the analysis has been completed a table of resonance parameters is constructed. This table of parameters contains the following values: resonance energy E_o, angular momentum J, parity π, exit orbital angular momentum ℓ' and exit channel spin s´ , laboratory widths Γ and total and partial reduced widths γ^2. From this information a level sequence can be extracted for resonances with the same J^π value, yielding a sequence of levels or resonances that all have the same good quantum numbers.

An example of the level sequences obtained is shown in figure 3.7 using previously collected ^{45}Sc data (Wilson, 1975,1976). The levels have been sorted by J and π and are plotted versus energy. For each separate sequence a more detailed picture can be

Figure 3.6: Angular momentum coupling scheme for the ^{44}Ca(p,p) and ^{44}Ca(p,p´) reactions in the channel spin representation.

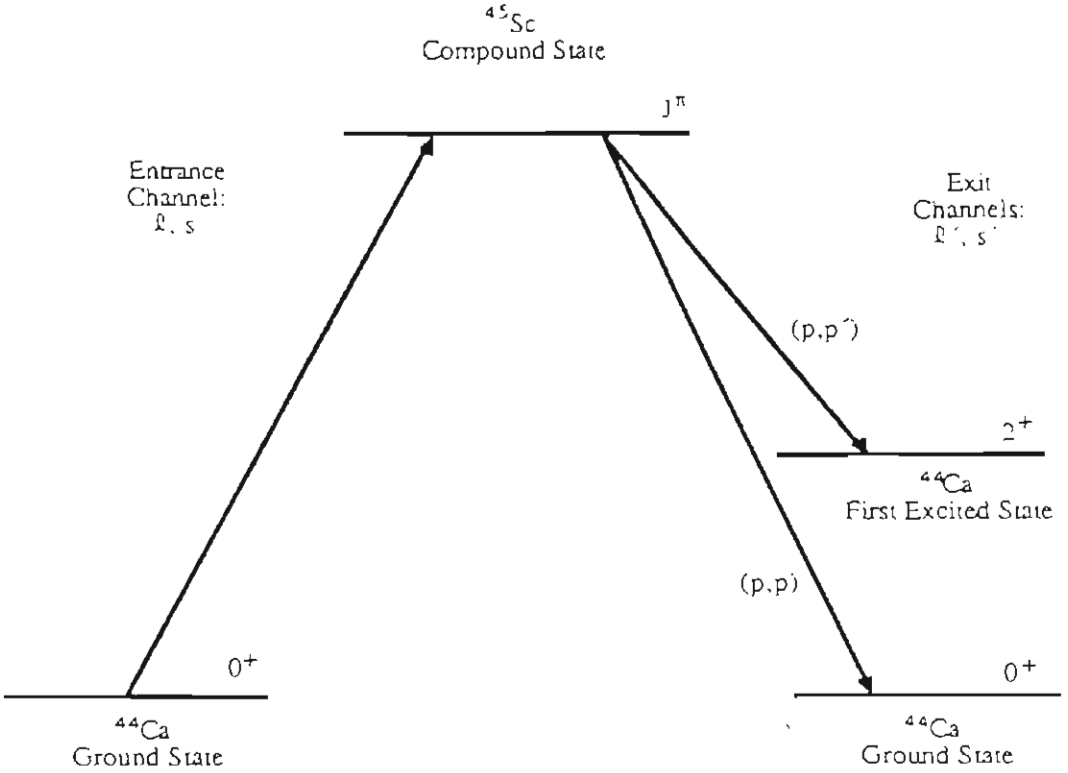

$$J = \ell' \oplus s'$$

$$\pi = (-1)^{\ell'}$$

Elastic Exit Channel Spin: $s_p' = 0 \oplus \frac{1}{2} = \frac{1}{2}$

Inelastic Exit Channel Spin: $s_p' = 2 \oplus \frac{1}{2} = \frac{3}{2}, \frac{5}{2}$

Exit Orbital Angular Momentum $\ell' = 0, 1, 2, \ldots$

Figure 3.7: Summary of level sequences observed in ^{45}Sc for incident proton energy ranges 1.5 to 3.0 MeV. Data from Wilson (1975, 1976).

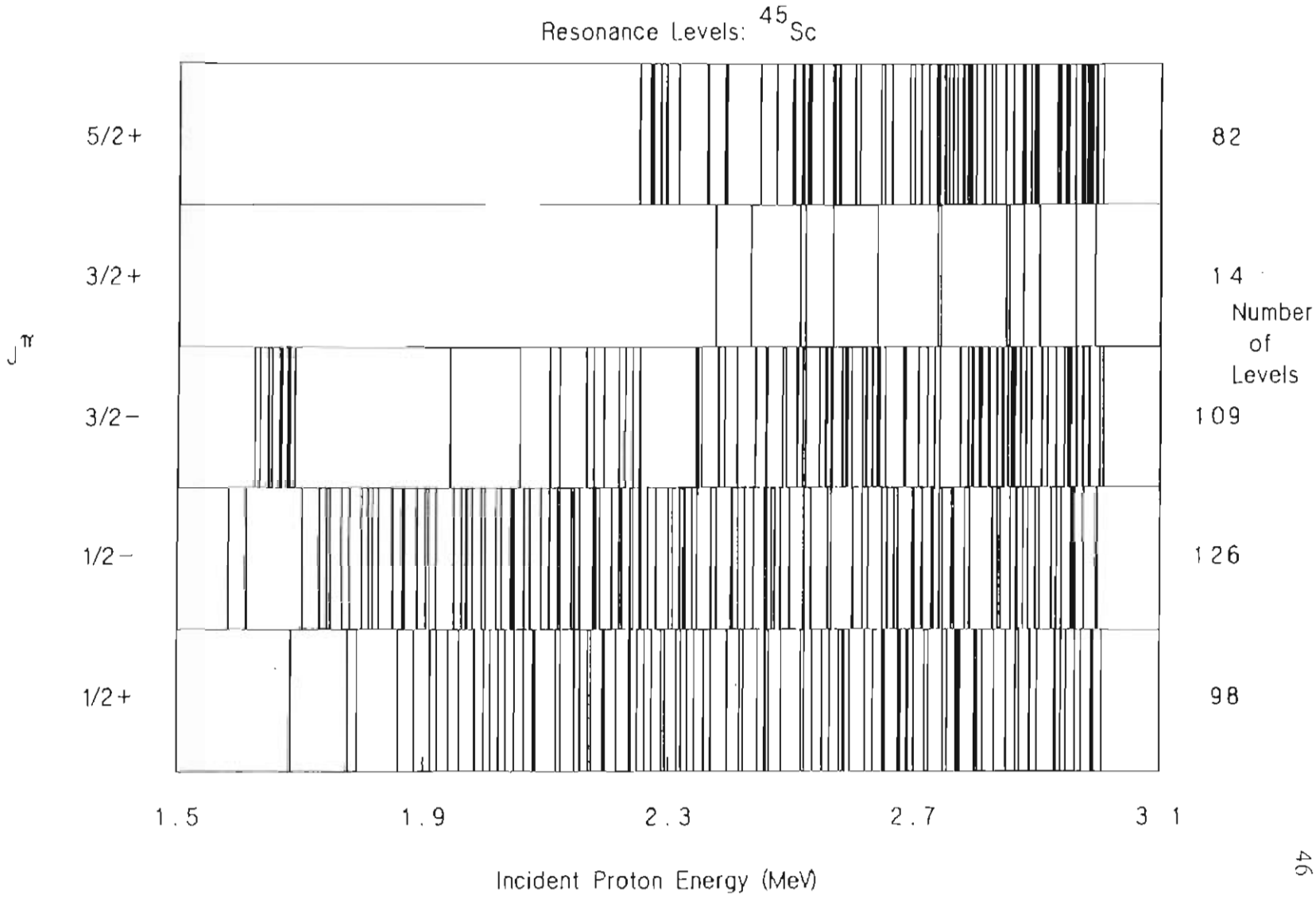
Resonance Levels: ^{45}Sc
5/2+
3/2+
3/2−
1/2−
1/2+
J^{π}
82
14
109
126
98
Number of Levels
1.5
1.9
2.3
2.7
3.1
Incident Proton Energy (MeV)

obtained by examining the number plot and the reduced width sum plot. An example of these plots for a given level sequence is shown in figure 3.8. Once the information required for these plots has been obtained more detailed analysis of the nuclear properties can be performed. These procedures will be discussed in the next chapter.

Figure 3.8: Sum of reduced widths and number plot for $1/2^+$ levels observed in ^{45}Sc. The analog state at 2.24 MeV has been removed. Data from Wilson (1975, 1976).

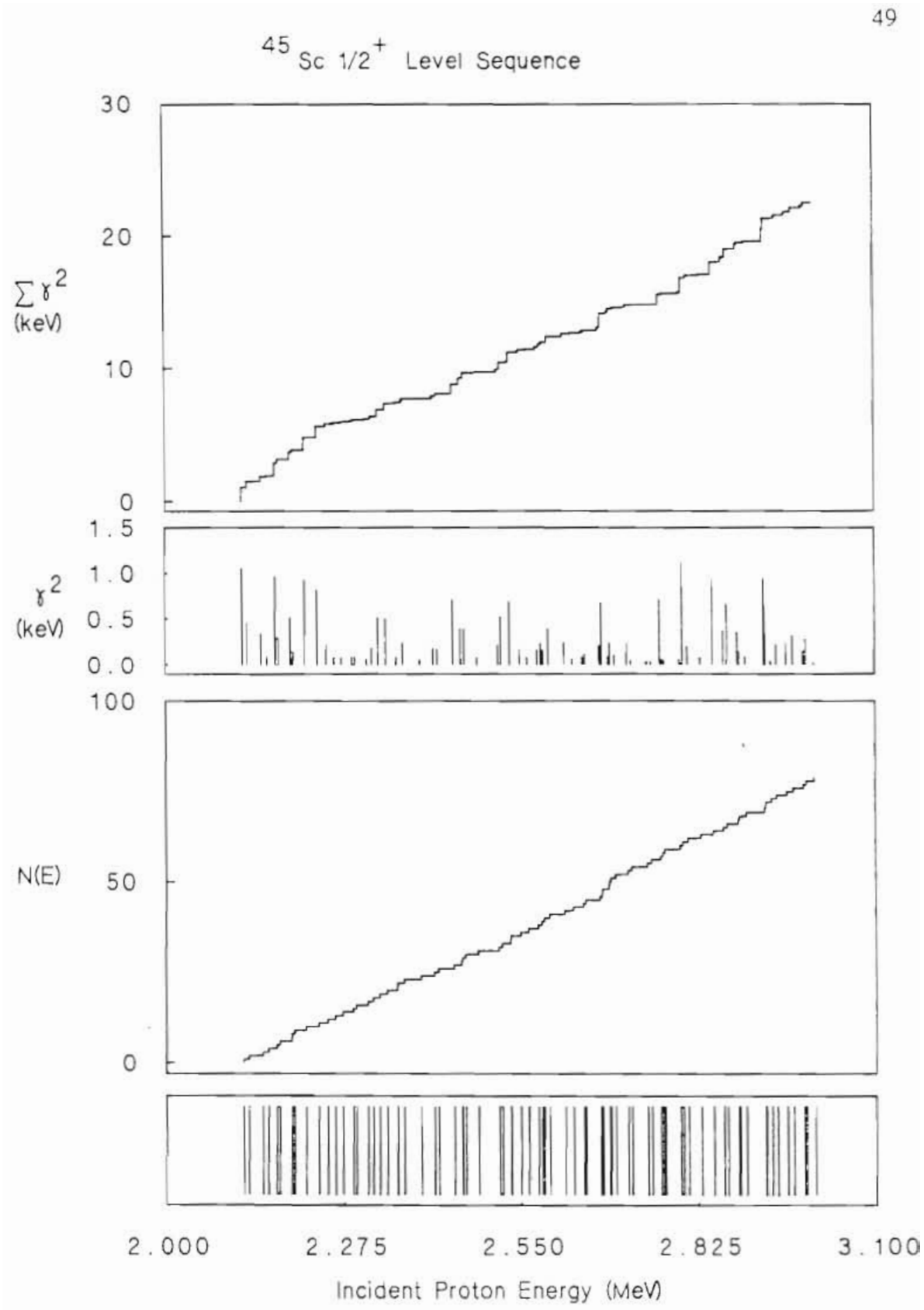
^{45}Sc 1/2^{+} Level Sequence
30
20
10
0
$\sum \gamma^2$ (keV)
1.5
1.0
0.5
0.0
γ^2 (keV)
100
50
0
N(E)
2.000
2.275
2.550
2.825
3.100
Incident Proton Energy (MeV)

Chapter Four

Level Densities:

Sequence Selection and Level Density Determination

In the study of level densities and other average nuclear properties there are several important considerations. These include both experimental limitations and the nuclear properties which make the determination of level densities difficult. In the following chapter these issues are addressed and the methods used for sequence selection and the determination of the level density discussed.

§4.1 Selection of Sequences

In the selection of a level sequence for determination of the level density there are many physical and experimental problems which must be considered to insure a meaningful and accurate level density determination.

One of the most basic is the requirement of a statistically significant number of levels in the sequence of interest. If the number of levels is too small then all average or statistical nuclear properties determined from the sequence will have a low confidence level. To determine an approximate lower limit for the number of levels a simple estimate is made, based on the value of $1/\sqrt{N}$. For a 20% fractional statistical

error level this gives a lower limit of approximately 25.

§4.1.1 Experimental and Systematic Concerns

One of the main experimental problems in determining level densities is the difficulty in observing levels whose widths are on the order of (or smaller than) the resolution of the experiment. In figure 4.1 ten resonances in a 20 keV region are shown in three plots with an overall experimental resolution of 350, 1000 and 5000 eV, respectively. The average laboratory width of the resonances is 50 eV. As the drawings illustrate, only with better resolution are the smaller levels observable. To obtain an accurate value of the nuclear level density one should use only level sequences that were collected with an experimental resolution no more than a factor of ten greater than the average width.

Another experimental problem in proton reaction measurements results from penetrability effects due to the Coulomb barrier. The penetrability affects not only the probability of a proton entering the nucleus but also exiting the nucleus after a reaction has taken place. In figure 4.2 the exit penetrability versus incident energy of elastic protons for a target nucleus of Z=20 with various exit orbital angular momenta ℓ' is presented. In general the limit of observability due to penetrability effects is approximately 0.01. From figure 4.2, for $\ell'=0$ (s-wave resonances) the viable incident energy range is above ~1.5 MeV, for $\ell'=1$ (p-wave resonances) above ~1.8 MeV and for $\ell'=2$ (d-wave resonances) above ~2.3 MeV. In selecting a sequence it is necessary to ensure that the data was collected at energies above those where penetrability effects seriously limit the states observed.

Another problem in the data analysis is the confidence in assigning the J^{π} of a resonance. Generally it is easy to determine the parity π of a resonance due to the effect

Figure 4.1: Overall experimental resolution effects on the observability of resonances. The top figure indicates the location and J^{π} of the resonances. The three lower plots show the resulting differential cross section for the indicated resolution. These calculations were performed for the ^{44}Ca(p,p) reaction with the resonance analysis code MULTI6. The average laboratory width of the resonances is 50 eV.

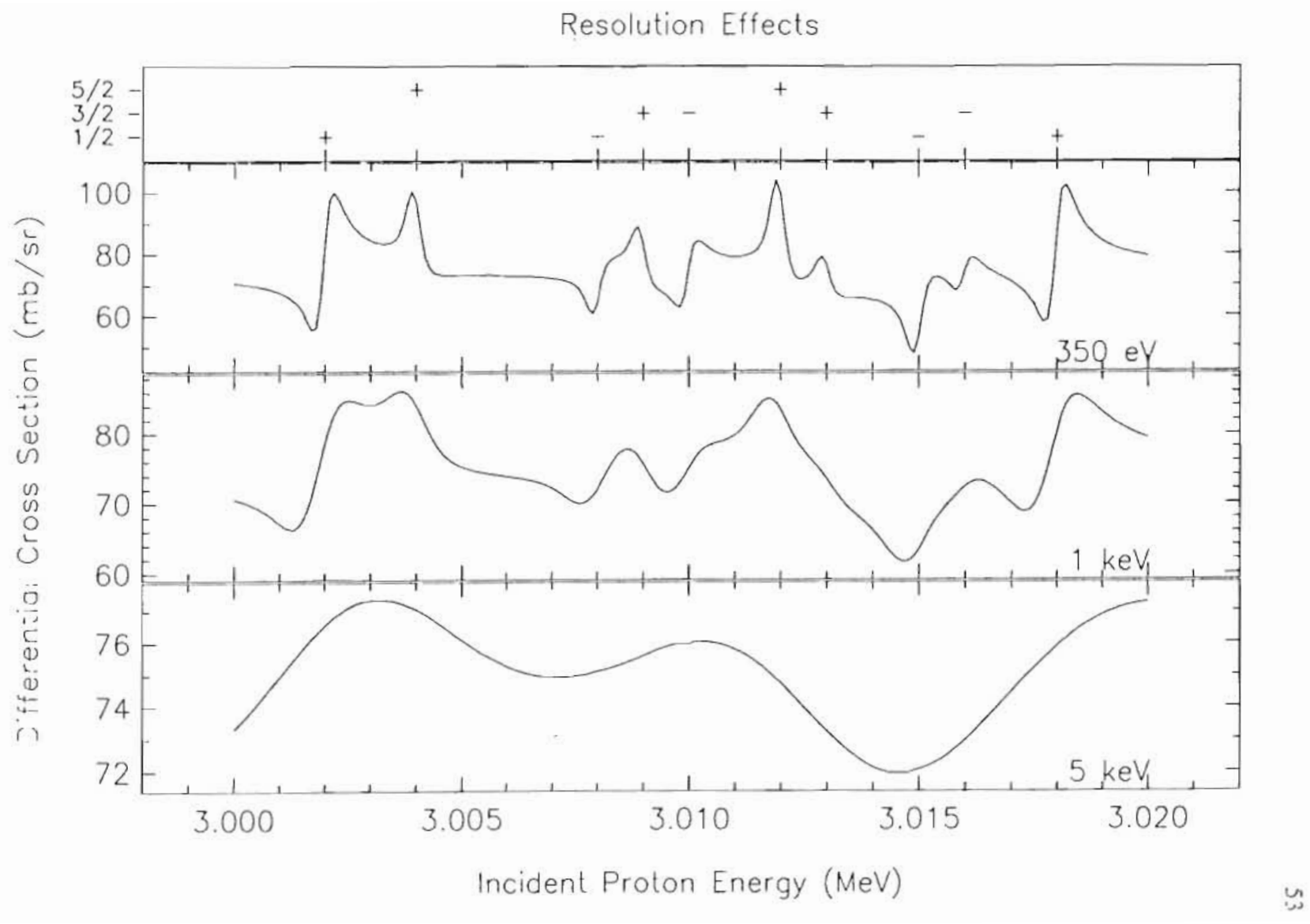
Resolution Effects
5/2
3/2
1/2
100
80
60
350 eV
80
70
60
1 keV
76
74
72
5 keV
3.000
3.005
3.010
3.015
3.020
Incident Proton Energy (MeV)
Differential Cross Section (mb/sr)

Figure 4.2: Exit penetrability versus energy for the ^{44}Ca(p,p) reaction.

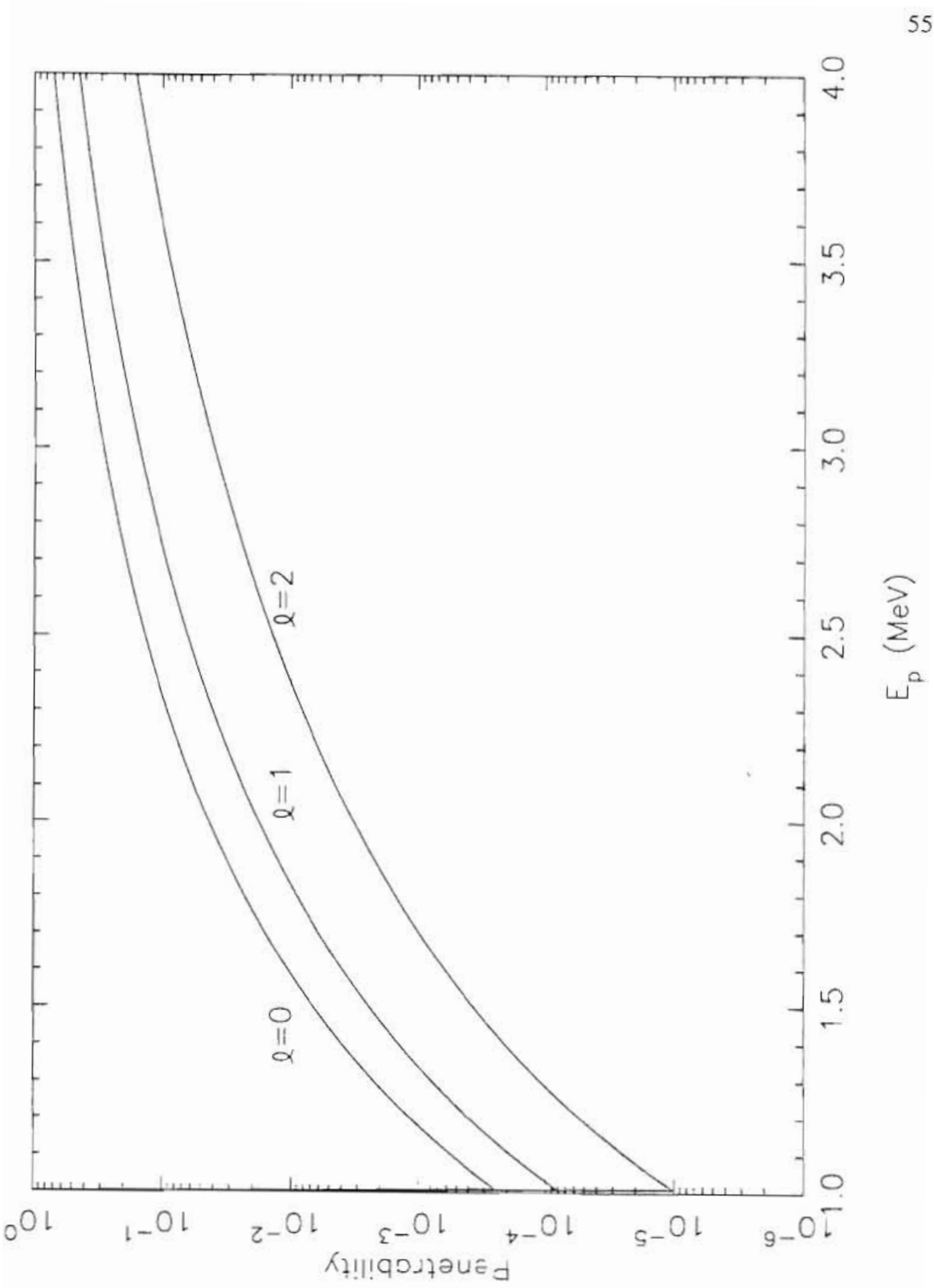
Penetrability
10^{0}
10^{-1}
10^{-2}
10^{-3}
10^{-4}
10^{-5}
10^{-6}
1.0
1.5
2.0
2.5
3.0
3.5
4.0
E_p (MeV)
$\ell=0$
$\ell=1$
$\ell=2$

that the parity has on the shape of a resonance at 90°. In figure 4.3 resonance shapes for different J^{π} are shown for various scattering angles. At 90° all positive parity states show a downward trend while all negative parity states show an upward trend. Once the parity has been determined a comparison of the resonance shape at other angles can determine the orbital angular momentum ℓ for the resonance. This can usually be done easily by visual inspection.

However, once the ℓ value has been determined it can be difficult to distinguish between the two p-wave or two d-wave species. If the individual resonance is large enough the distinction is possible, but for small resonances the experimental resolution or interference with other levels may prevent an accurate determination of J. Observation of the decay of the resonance into other reaction channels sometimes provides an accurate J assignment. An example is shown in figure 4.4. The two p-wave resonances appear similar in the (p,p) channel and are difficult to distinguish, but due to the anisotropy in the (p,p´) channel the resonance can be uniquely assigned J = 3/2. However, for some cases the J-value assignment is inconclusive even with standard reaction channel data. Then only more extensive experimental study can accurately determine J. There are uncertainties in a number of the J assignments for the p- and d-wave resonances. Although usually these ambiguities are limited to a few levels in a sequence, the J-value uncertainties increase the error in the average level densities determined from the sequence.

In addition to these experimental concerns there are nuclear properties (strength functions and analog states) that can affect the level density determination and thus should be considered in the sequence selection.

Figure 4.3: J^{π} resonance shapes for various scattering angles.

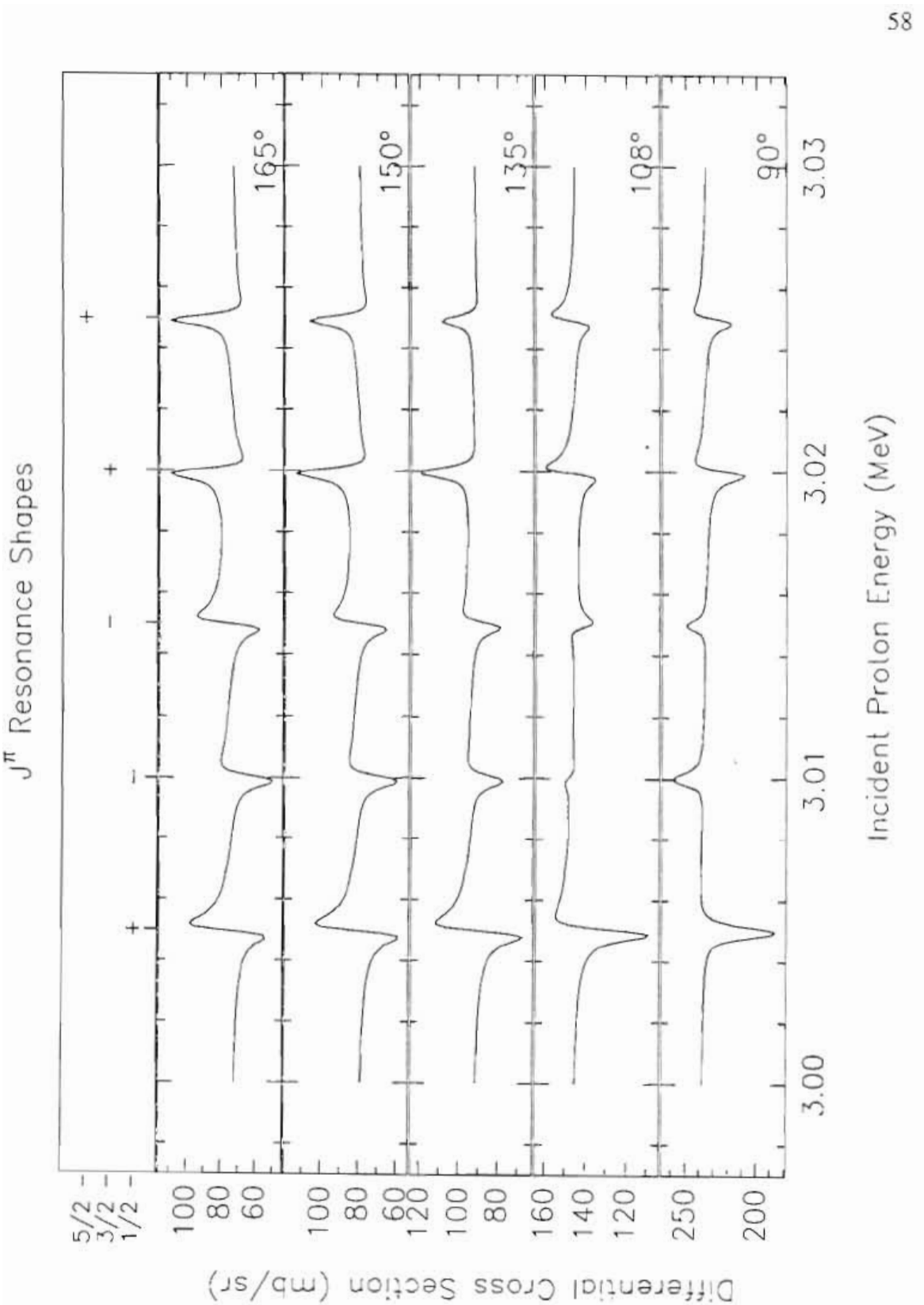
J^π Resonance Shapes
5/2 −
3/2 −
1/2 −
+
−
+
−
+
165°
150°
135°
108°
90°
100
80
60
100
80
60
120
100
80
160
140
120
250
200
3.00
3.01
3.02
3.03
Incident Prolon Energy (MeV)
Differential Cross Section (mb/sr)

Figure 4.4: Comparison of resonance shapes for $1/2^-$ and $3/2^-$ resonances in the $^{44}Ca(p,p)$ and $^{44}Ca(p,p')$ reactions.

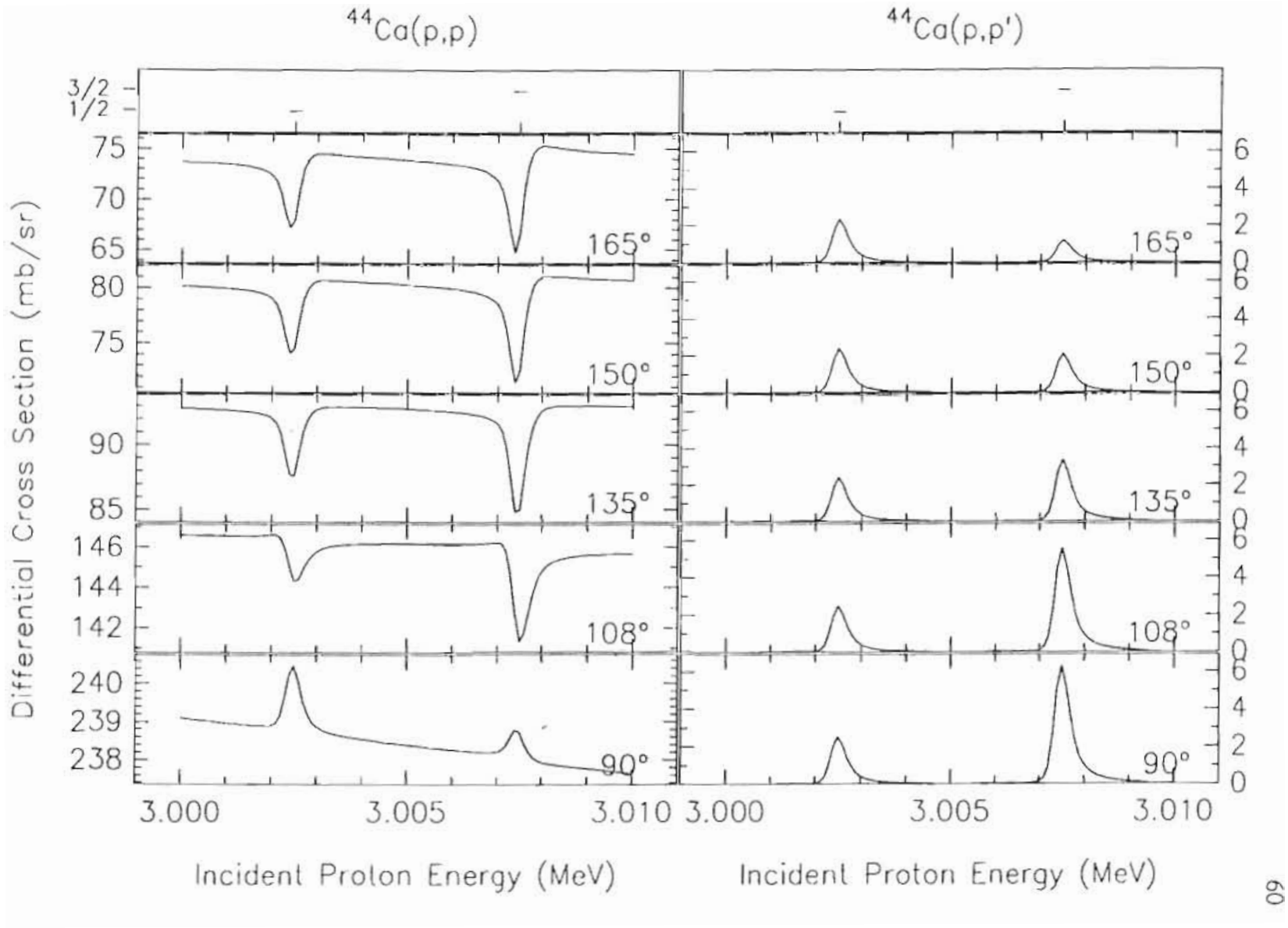
^{44}Ca(p,p)
^{44}Ca(p,p')
3/2
1/2
75
70
65
165°
80
75
150°
90
85
135°
146
144
142
108°
240
239
238
90°
6
4
2
0
3.000
3.005
3.010
Differential Cross Section (mb/sr)
Incident Proton Energy (MeV)
Incident Proton Energy (MeV)

§4.1.2 Strength Functions.

The definition of the strength function S is the average reduced width for a given sequence of resonances divided by the average spacing of the sequence.

$$S = \frac{\langle \gamma^2 \rangle}{\langle D \rangle}$$

This parameter is useful in the examination of average properties of nucleon-nucleus scattering and reactions, properties that are described by an optical model potential. Two of the more important properties of interest in this study are the dependence of the strength function on the atomic mass A and on the J^{π} of the sequence of interest. One can estimate likely candidates for level density considerations from the predicted strength function for a specific nucleus and J^{π}.

Studies of proton strength functions has been conducted over many years (Bilpuch et al., 1976). The dependence on A and J^{π}, as well as on the isospin of the target nucleus, have been approximately established in light and medium weight nuclei. For a specific case the value of the strength function will indicate the probability of obtaining an acceptable sequence. If the strength function is small, as is the $p_{3/2}$ proton strength function at A~44, then the resonances in the $3/2^-$ sequence may be difficult to observe. This is chiefly because the strength function is proportional to the average reduced width. If the average reduced width for a sequence is small relative to the resolution capabilities of an experiment, then fewer resonances will be observed and the resulting estimates for the level density will be inaccurate.

However if the proton strength function is large, as is the $p_{1/2}$ strength function at A~44, then results for the level densities should be more reliable. The value of the proton strength function value for the nucleus of interest thus provides an indication of the level of observability of the resonances in a given sequence.

§4.1.3 Analog State Considerations

The presence of analog states in a level sequence can cause difficulties in obtaining accurate and reliable values of strengths and widths. Thus it is important to compensate for the presence of analog states. In figure 4.5 a schematic diagram shows the energy relation between a parent and daughter analog state. In an analog parent-daughter system both nuclei have A nucleons but the daughter has one more proton than the parent. If the nuclear force is charge independent then the isospin quantum number T (= [N - Z]/2) is a good quantum number in an idealized nuclear system. If Coulomb interactions are small compared to nuclear interactions, then isospin is an approximately good quantum number in a real nuclear system. Analog states are defined as nuclear states that are multiplets of a given isospin T in nuclei that differ in the exchange of a neutron for a proton.

As shown in figure 4.5 a low-lying state in ^{45}Ca (the parent state) has an analog or daughter state in the region of interest in the ^{45}Sc system, data from Wilson (1975, 1976). For analogs of low-lying states the daughter state is typically very strong compared to the surrounding resonances and can dramatically dominate a sequence. An example of this domination by an analog states is shown in figure 4.6--the analog state is near E_p = 1.65 MeV.

When an analog state is present in a level sequence, one must compensate for its effects. Usually this is accomplished by excluding the analog state from the data. The reason for this exclusion is rooted in the method for determining the level density for a sequence. As will be described later the method for level density determination is sensitive to the average reduced width of a sequence, thus if the analog state dominates a sequence an accurate estimate of the average reduced width for the background states

Figure 4.5: Analog state energy schematic for ^{45}Ca and ^{45}Sc system.

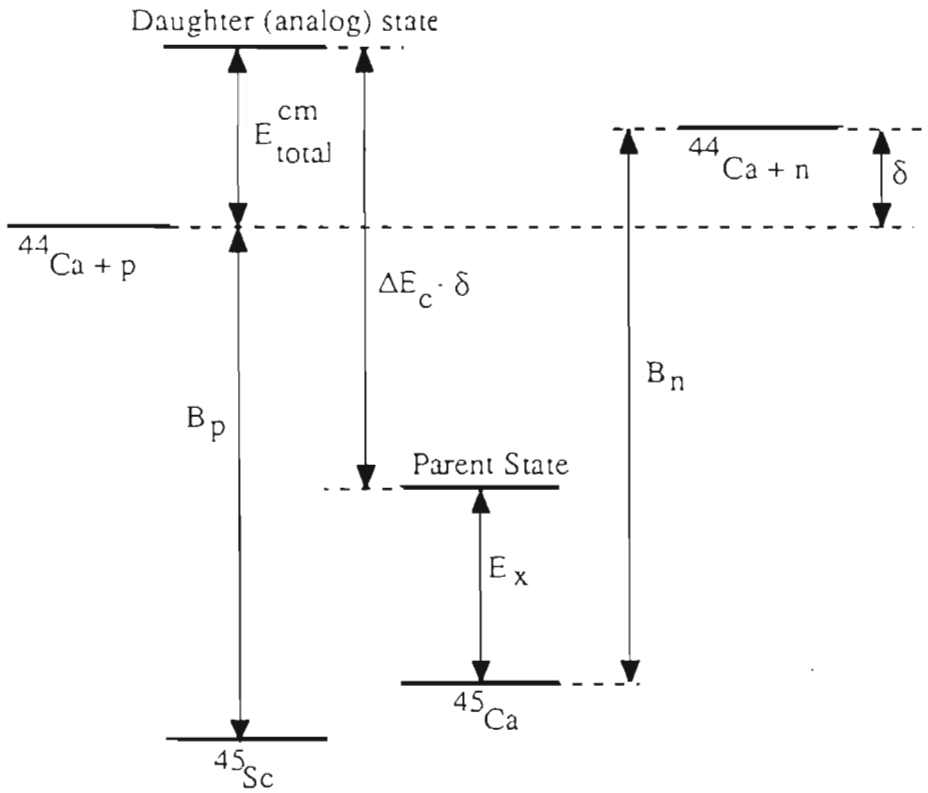

B_p = Binding energy of the proton = 6.8896 MeV (Nuclear Data Sheets, 1983)

B_n = Binding energy of the neutron = 7.4149 MeV (Nuclear Data Sheets, 1983)

δ = p-n mass difference = 1.2933 MeV

ΔE_c = Coulomb Energy = 7.229 MeV (Janecke, 1969)

Figure 4.6: Reduced widths for the $3/2^-$ level sequence in ^{45}Sc. Note that the analog state dominates the reduced width plots. Data from Wilson (1975, 1976).

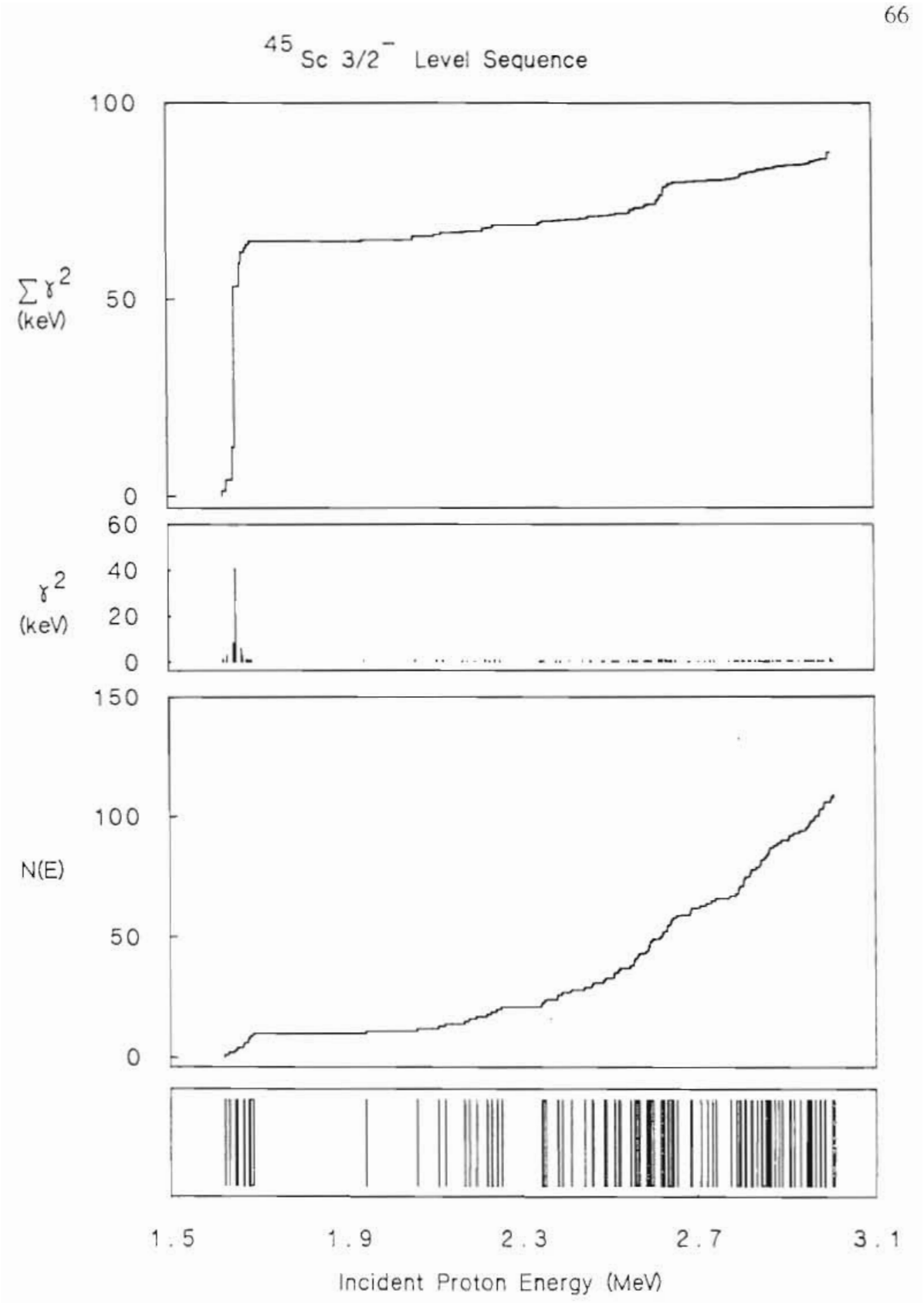
^{45}Sc 3/2$^-$ Level Sequence
100
50
0
$\sum\gamma^2$ (keV)
60
40
20
0
γ^2 (keV)
150
100
50
0
N(E)
1.5
1.9
2.3
2.7
3.1
Incident Proton Energy (MeV)

is impossible. In addition for some cases the analog state fragments into many smaller states, mixing 'strongly' with the background states. In these cases the exclusion process is more subjective. To determine which states must be eliminated it is helpful to use the spectroscopic factor, S_{dp}, of the parent state to estimate the analog width Γ_{pp} that should be observed in the proton channel. These factors are related by the following

$$S_{dp} = [2T + 1] \frac{\Gamma_{pp}}{\Gamma_{sp}} ,$$

where T is the z-component of the isospin and Γ_{sp} is the single particle width of the level. S_{dp} is measured by the appropriate (d,p) stripping reaction and Γ_{sp} is calculated from a specific model. With this estimate it is easier to determine the fragmented states that must be excluded from the sequence. An example of this exclusion process is given in Chapter 6 for an analog state found in the ^{44}Ca(p,p) experiment.

§4.1.4 Statistical Tests for Sequence Completeness and Purity

The statistical properties of a level sequence can be used in the determination of the purity and completeness of a sequence and often can provide an accurate estimate of the number of levels missed. The two most useful and common statistical tests involve the use of the Wigner distribution (level spacings) and the Porter-Thomas distribution (level widths).

§4.1.4.1 Wigner Distribution.

The nearest neighbor level spacings should obey a distribution of the type

$$P(x)dx = \frac{\pi}{2} x \exp\left(-\frac{\pi x^2}{4}\right)dx \text{ , where } x = \frac{D}{\langle D \rangle},$$

where D is the level spacing and ⟨D⟩ is the average spacing. This distribution is known as the Wigner distribution and represents the distribution of nuclear spacings very well. A detailed discussion of the Wigner distribution and its application is given by Lynn(1968). In the present study the Wigner distribution is compared with the experimental spacing distribution. In figure 4.7(a) a spacing distribution for ^{44}Ca(p,p) $1/2^+$ levels is compared with a Wigner distribution. The Wigner distribution predicts few small spacings-- level repulsion. There are also few large spacings, with an average spacing of x~1.

For the data in figure 4.7(a) there is an excess of small spacings relative to the Wigner distribution. This excess could be caused by experimental or analysis related effects. The most probable effect causing this excess is the inclusion of levels that have a different J or π. This would cause the observed spacings to be smaller, since these levels would occur between valid levels in the sequence. In this context a comparison between the Wigner distribution and the experimental data gives an indication of the 'purity' of a sequence. However, obtaining a quantitative estimate of how many extra levels were observed is not straightforward. An in depth study of this analysis was performed by Watson (1981). Here this comparison is used qualitatively.

As presented in figure 4.7(a) the comparison is between binned data and a smooth curve. There is an inherent problem in this type of comparison, since the binned data are based on an arbitrary selection of bin widths. By selecting appropriate bin widths it is possible to make the data compare more or less favorably with the Wigner distribution. This arbitrariness of bin width selection has been partially eliminated in this study by using bin widths which have equal probability. However, even then changing the number of equally probable bins leads to data which appears somewhat different. To

Figure 4.7: Wigner distribution overlay comparison for (a) binned experimental spacings with 8 bins of equal probability and (b) cumulative plot of experimental spacings. Data from Wilson (1975, 1976).

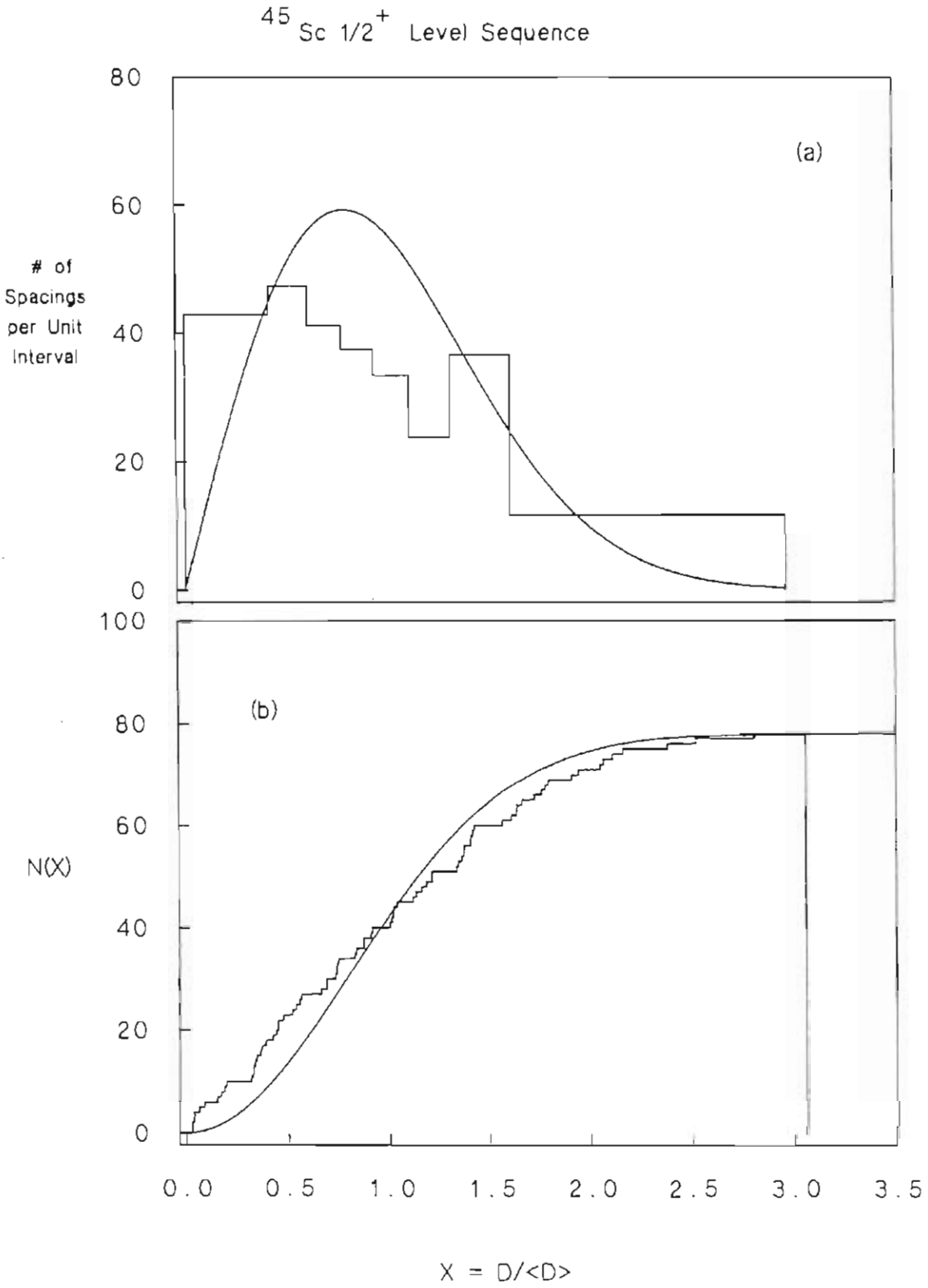
^{45}Sc 1/2^{+} Level Sequence
(a)
(b)
# of Spacings per Unit Interval
N(X)
X = D/<D>
0
20
40
60
80
100
0.0
0.5
1.0
1.5
2.0
2.5
3.0
3.5

remove this problem a cumulative Wigner distribution is used; an example is presented in figure 4.7(b). The cumulative number of levels N(x) is plotted versus x, with

$$N\left(x_i\right) = i \text{ , where } x_i = \frac{D_i}{\langle D \rangle},$$

with the theoretical distribution

$$N\left(x'\right) = \int_0^{x'} P\left(x\right) dx$$

where P(x) is the Wigner distribution.

The cumulative distribution approach removes any subjectivity in the data presentation and a comparison of this to the cumulative Wigner distribution yields the same information as for the differential plots. In figure 4.7(a) there are more small spacings than expected, as well as fewer levels than expected at larger spacings. The same data as in figure 4.7(a) are presented as a cumulative distribution in figure 4.7(b); again at smaller spacings too many levels are observed, indicating that 'extra' levels were included.

The Wigner distribution is valuable in obtaining a subjective estimate of the purity of a level sequence. This allows the sequence selection to be made more confidently by estimating the impurity of the sequence, and thus determining good candidates for further study.

§4.1.4.2 Porter-Thomas Distribution.

Another distribution which is of major value is the Porter-Thomas distribution. In 1956 Porter and Thomas (Porter, 1956) found that for a given sequence of nuclear levels the reduced widths associated with the sequence had a chi-square distribution with one degree of freedom, which in nuclear physics has since been called the Porter-

Thomas distribution. This distribution is usually written in terms of the parameter y,

$$P(y) = \sqrt{\frac{1}{2\pi y}} \exp\left(-\frac{y}{2}\right), \text{ where } y = \frac{\gamma^2}{\gamma^2_{\text{average}}}.$$

For a given sequence the percentage of missing resonances corresponds to the integral of the Porter-Thomas distribution from zero to y_{cutoff}, where y_{cutoff} is proportional to the minimum observed reduced width. That is,

$$\text{Fraction missing} = MF(E) = \int_0^{y_{min}(E)} P(y)\,dy$$

This allows the determination of the missing fraction of levels for a given sequence, and therefore a more accurate determination of the level density. However, this approach assumes that all levels with reduced widths larger than the reduced width used in the calculation are observed.

In using the Porter-Thomas distribution as a test for sequence selection the data are plotted in bins and compared to the theoretical distribution as shown in figure 4.8(a). It is clear that levels with widths below a minimum y value (or minimum γ^2 value) were not observed. It is also clear that anomalously strong levels were not observed in this sequence. The observation of levels with widths considerably larger than the other levels in the sequence usually indicates the presence of an analog state or some other non-statistical behavior.

Note that with the binned data the same problem is encountered as with the Wigner distribution, the selection of the bin width. Although equal probability bins were used again, a better solution of this problem is the use of a cumulative plot. An example of such a plot is shown in figure 4.8(b). The data are plotted according to

$$N(y_i) = i, \text{ where } y_i = \frac{\gamma_i^2}{\langle \gamma^2 \rangle}$$

Figure 4.8: Porter-Thomas distribution overlay comparison for (a) binned experimental widths with 8 bins of equal probability and (b) a cumulative distribution of the experimental widths. Data from Wilson (1975, 1976).

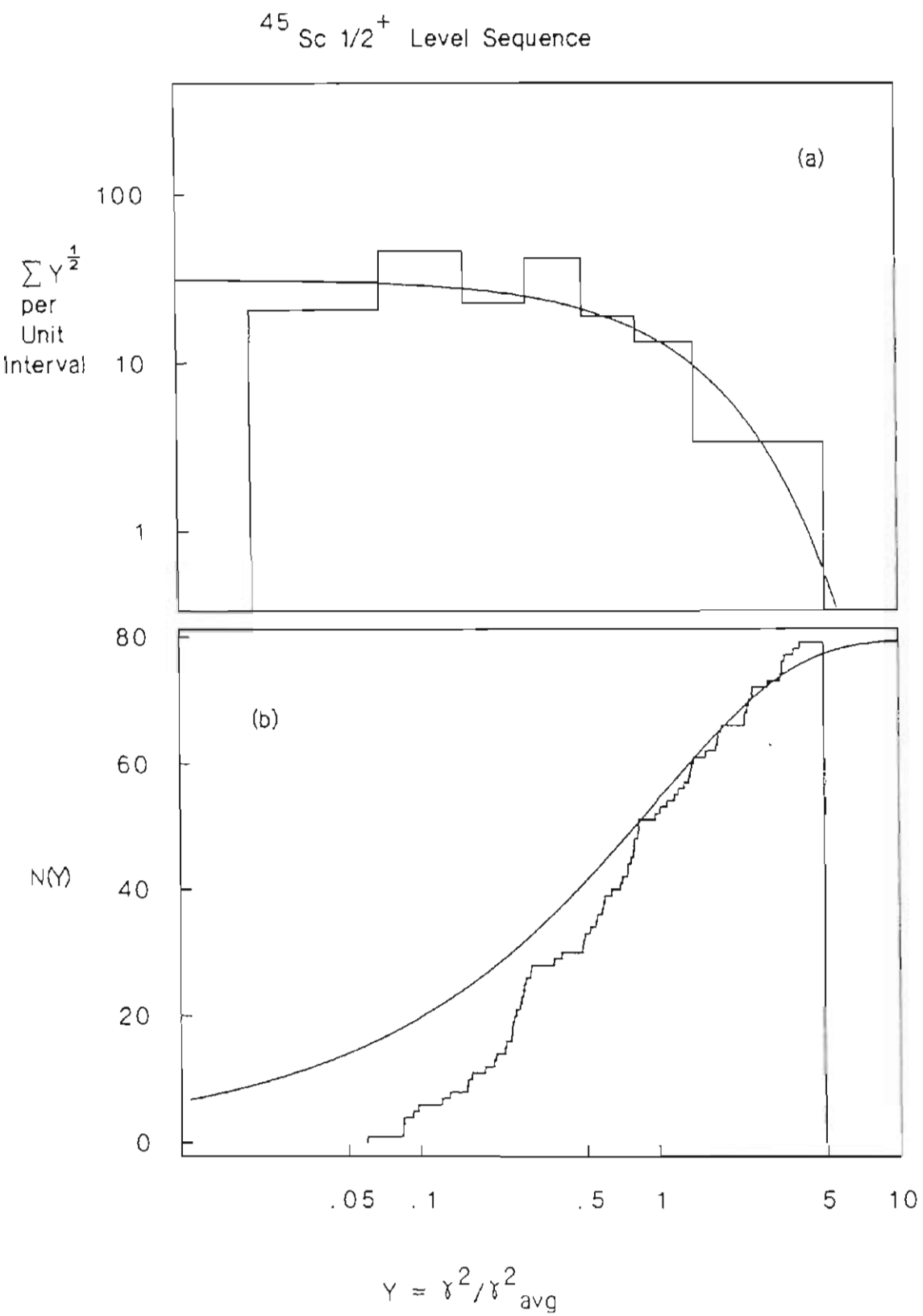
^{45}Sc 1/2^{+} Level Sequence
(a)
100
10
1
$\sum Y^{\frac{1}{2}}$ per Unit Interval
(b)
80
60
40
20
0
N(Y)
.05
.1
.5
1
5
10
$Y = \gamma^2/\gamma^2_{avg}$

with the theoretical distribution plotted as

$$N(y') = \int_0^{y'} P(y)\,dy$$

where P(y) is the Porter-Thomas distribution.

From the visual comparison between the data and the Porter-Thomas distribution it is clear that the smaller widths have been missed; with the Porter-Thomas distribution a quantitative estimate of the fraction missed can be obtained. This is accomplished by selecting the smallest width (and corresponding y value) for the sequence of interest and integrating the Porter-Thomas distribution from zero to this y value. This procedure seems the most reliable way to determine the missing fraction in a sequence.

The preceding physical, experimental and statistical concerns are important in the selection of the sequence to be examined. However, once the sequence has been selected an appropriate portion of the sequence must be chosen for the level density determination. This selection process is discussed next.

§4.1.5 Percentage of Missing Levels Limits.

The following method is used to select the portion of a sequence which is to be considered for analysis. An algorithm was devised to remove some of the subjectivity and allow a more standardized method of selection.

For a given sequence assume that above an energy E_0 all levels with laboratory width greater than some minimum laboratory width ($\Gamma > \Gamma_{min}$) are observed. With this assumption determine the largest minimum γ^2 value for the sequence (maximizing the missing fraction value), and calculate a maximum fraction of missing levels. This calculation is performed using the Porter-Thomas distribution as described in section 4.1.4.2. This γ^2 value corresponds to the maximum reduced width value of the Γ_{min}

level, which occurs at the lower energy bound E_0. From this a maximum fraction of missing levels for the section of the sequence where $E > E_0$ can be determined.

Next consider how this maximum fraction behaves versus energy (over the whole energy range of the sequence), using the minimum observed laboratory width Γ_{min}. Once this behavior is determined, select a missing fraction which seems to give the best sequence selection for all nuclei to be analyzed. For the cases in this study the fraction was found to be nominally 0.30 (30% missing levels). Selection of this fraction determines the energy range of the section to be analyzed.

The actual calculational procedure is as follows: First select a minimum laboratory width (Γ_{min}). Normally this was the minimum observed laboratory width for the sequence being analyzed. Second, determine the minimum reduced width (γ^2_{min}) as a function of energy using the Γ_{min}.

$$\gamma^2_{min}(E) = \frac{\Gamma_{min}}{2P(E)}$$

Third, determine the average reduced width for the sequence using the observed reduced widths.

$$\gamma^2_{avg} = \frac{1}{N}\sum_{i=1}^{N}\gamma_i^2$$

Fourth, calculate the minimum y values for the energy range,

$$y_{min}(E) = \frac{\gamma^2_{min}(E)}{\gamma^2_{avg}}$$

Fifth, calculate the maximum fraction of missing levels at a given energy and given minimum laboratory width, using the y values previously found. This is done by integrating the PT distribution from zero to $y_{min}(E)$,

$$\text{Fraction missing} = MF(E) = \int_0^{y_{min}(E)} P(y)\,dy$$

where,

$$P(y) = \sqrt{\frac{1}{2\pi y}} \exp\left(-\frac{y}{2}\right).$$

Finally plot MF(E) versus energy to examine the behavior of the fraction of missing levels over the energy range of the sequence in question. An example of such a plot is shown in figure 4.9. From this plot one can determine the portion of the sequence which seems suitable for further study. As mentioned earlier, in this analysis a lower limit of 30% was chosen.

§4.2 Level Density Determination

To first order the determination of the level density from a sequence of resonances is very simple, since the level density is equal to the number of levels observed divided by the energy range of the sequence. However, this result often can be very inaccurate, since only some fraction of the resonances is actually observed.

To correct for missing resonances (those with widths below a minimum reduced width) the Porter-Thomas distribution is used. Two improved methods for determining the missing fraction were used: an iterative method and a bootstrap method.

§4.2.1 Iterative Method

This method uses a cyclic algorithm that approaches a constant value for the fraction of missing levels in a given sequence. The method is as follows: First the minimum reduced width, γ^2_{min}, for the sequence is determined along with the average reduced width $\gamma^2_{average}$. From these values the first value of y_{cutoff} is calculated using

Figure 4.9: Percentage of missing levels versus energy for the ^{44}Ca(p,p) reaction assuming a minimum observable laboratory width of 5 eV.

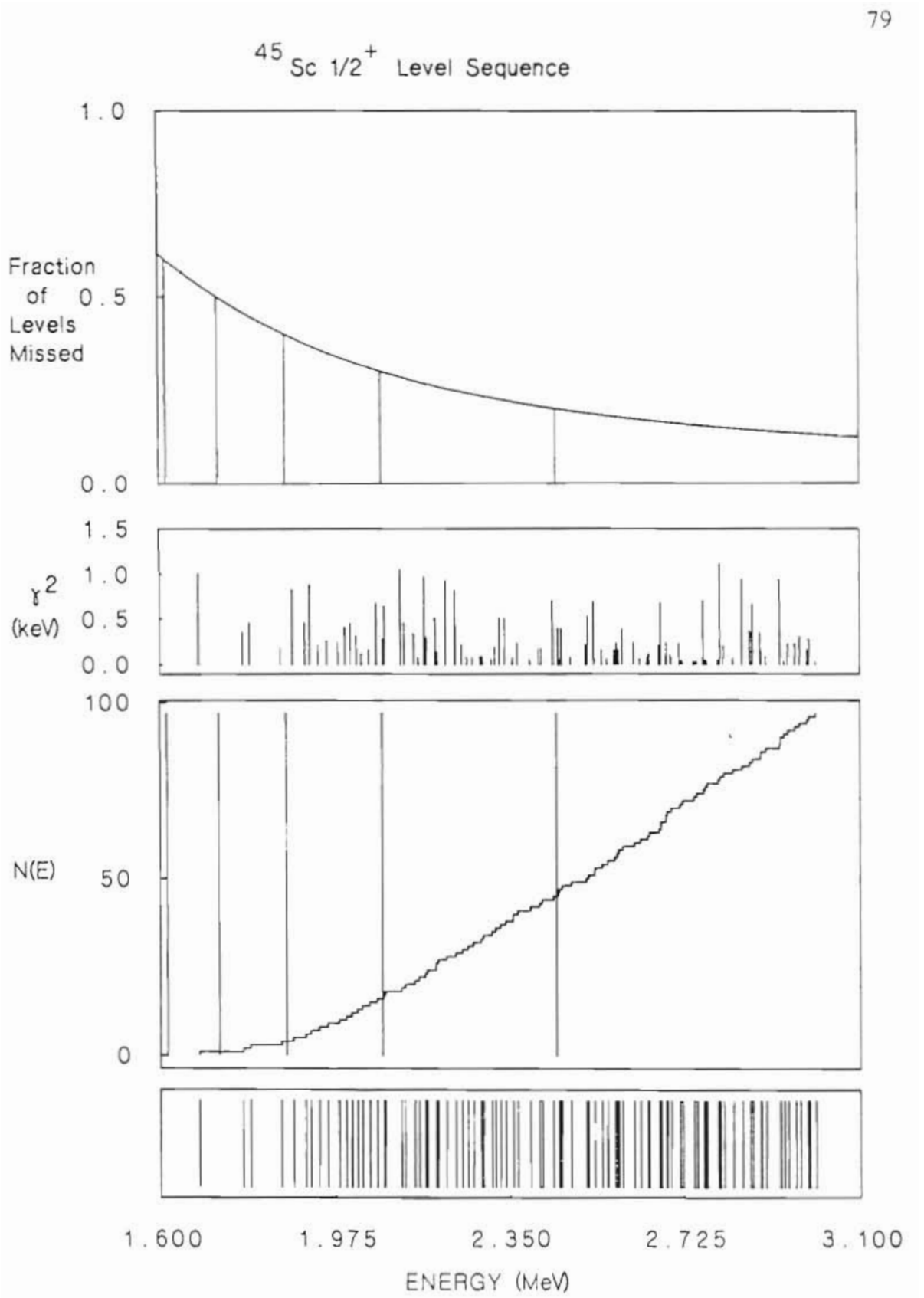
45 Sc 1/2+ Level Sequence
1.0
Fraction of Levels Missed
0.5
0.0
1.5
1.0
γ2 (keV)
0.5
0.0
100
N(E)
50
0
1.600
1.975
2.350
2.725
3.100
ENERGY (MeV)

$$y_{cutoff} = \frac{\gamma^2_{minimum}}{\gamma^2_{average}} .$$

From this the missing fraction M.F. is calculated by

$$\text{Missing Fraction (M.F.)} = \int_0^{y_{cutoff}} P(y)dy .$$

This in turn allows the determination of the theoretical number of levels in the sequence

$$N_{theoretical} = N_{observed}\left(\frac{1}{1 - M.F.}\right).$$

This value is used to determine a new average reduced width

$$\gamma^2_{average} = \frac{\Sigma\gamma_i^{\,2}}{N_{theoretical}} .$$

This new average reduced width can be used to give a new value for y_{cutoff}, thus starting the process over. After a few iterations (typically less than five) a constant value for the missing fraction is found. This value is used to determine the average level spacing $\langle D \rangle$, or level density ρ. The calculation is simply

$$\langle D \rangle = \frac{1}{\rho} = \frac{E_{max} - E_{min}}{N_{theoretical}} .$$

Although the iterative method works well, it depends completely on the value of the smallest width. Due to experimental problems and possible uncertainty in assigning the smaller levels another method is chosen, the bootstrap method.

§4.2.2 Bootstrap Method

The bootstrap method uses the whole sequence to determine the missing fraction and thus allows more confidence in the spacing or density determination. The procedure is quite straightforward. First randomly select, with replacement, $N_{observed}$ levels

from the sequence of $N_{observed}$ levels. Once this selection is performed the minimum width of this new sequence is determined along with the average width. A y_{cutoff} is calculated and the missing fraction is determined. The process of randomly selecting the levels in the sequence and determining the corresponding missing fraction is repeated many times, typically 1,000-10,000. The results are used to generate a missing fraction distribution. From this distribution the mean missing fraction is found and used as the representative missing fraction for the sequence. In figure 4.10 the missing fraction distribution for a $^{44}Ca(p,p)$ $1/2^+$ sequence is presented, with the mean value bin marked. In addition to the value of the missing fraction, the bootstrap method allows the determination of an estimate of the error in the missing fraction. The central 68% of the distribution is determined and used to provide error estimates. For a normal distribution this corresponds to one standard deviation. These limits are also shown in figure 4.10.

The bootstrap method has proven superior to the iterative method, since the whole sequence is used in the missing fraction determination. However, comparisons between the results of the two methods generally agree quite well. The use of both methods is made in this study, on various s-wave resonance sequences in chapter five and on the $^{44}Ca(p,p)$ results in chapter seven.

Figure 4.10: Missing fraction distribution for ^{45}Sc $1/2^+$ levels generated by the bootstrap method.

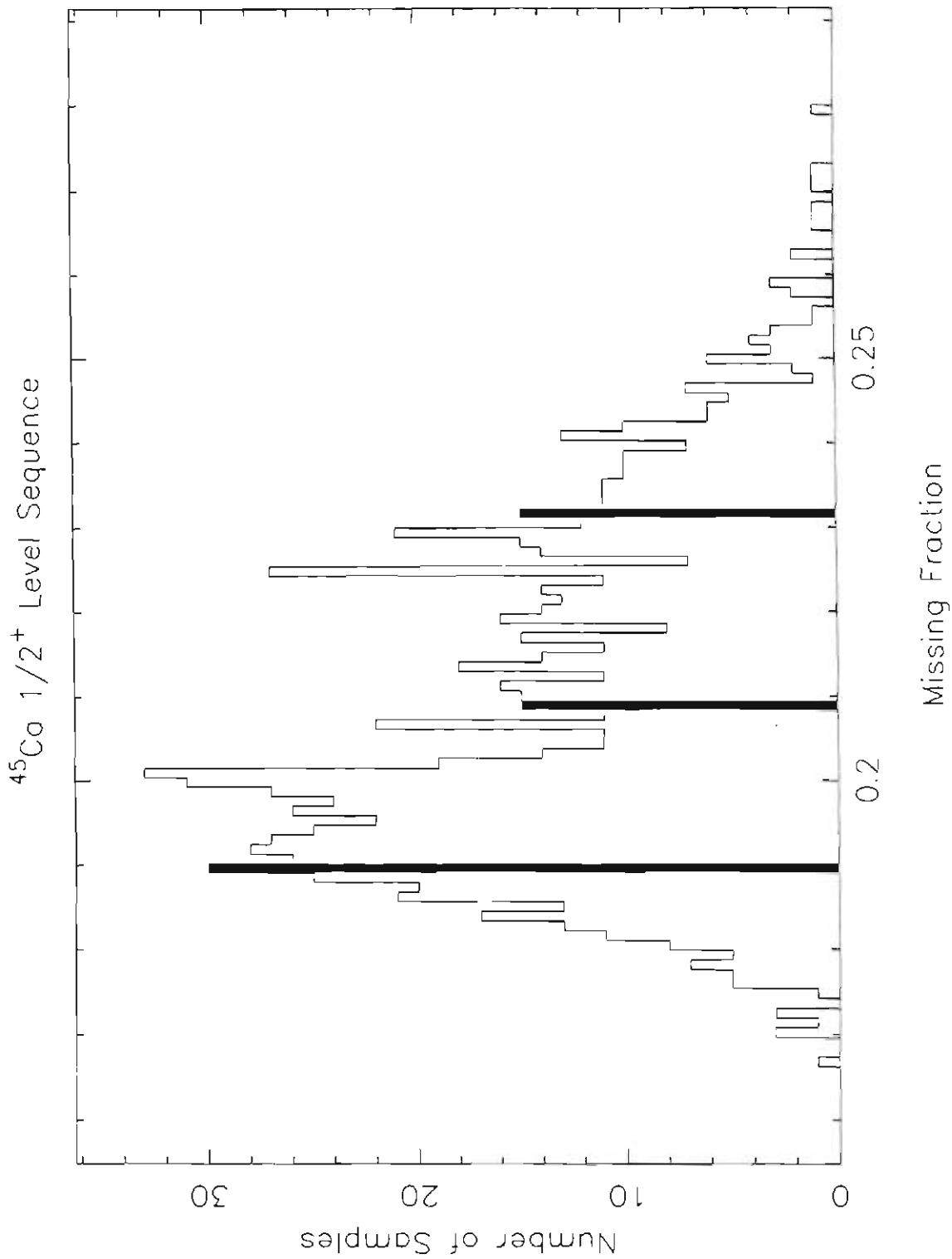
^{45}Ca 1/2^{+} Level Sequence
Number of Samples
0
10
20
30
0.2
0.25
Missing Fraction

Chapter Five

s-wave Level Densities

A part of the motivation for this study was to consider whether proton resonance data could be used to increase the nuclear data base for level density determinations. In the past almost all level density analyses have been based on neutron data. Recent work to answer this question was conducted in collaboration with Vonach and his group. The results have been published (Vonach,1988).

§5.1 Determination of Level Densities for s-wave Resonance Data.

Using the methods outlined in chapter four proton s-wave resonance spacings were determined for eleven nuclei. The results are presented in table 5.1. There is general agreement between the iterative and bootstrap results. However, due to greater confidence in the bootstrap method, the level densities determined by that method will be used for the comparisons to neutron data and to theoretical calculations.

To determine whether the proton data can be included in the data base, one of the first steps is the comparison of the atomic mass (A) dependence of the level densities of the proton data and appropriate neutron data. Ideally both proton and neutron data should exhibit the same behavior. The neutron data used in the comparison are presented in table 5.2.

Table 5.1: Proton s-wave Level Densities

Nucleus	Reference	E_p Range (MeV)	$N_{obs.}$	M. F.[a]	ρ_I[b] (MeV^{-1})	ρ_B[a] (MeV^{-1})
^{41}K	Keyworth,1966	2.2102-2.5975	25	.26	88.	87.
^{43}Sc	Wilson, 1976	2.1524-2.9809	26	.15	36.	37.
^{45}Sc	Wilson, 1975	2.1183-3.0055	79	.19	113.	110.
^{55}Mn	Moses, 1971	2.1666-2.6855	47	.36	156.	141.
^{57}Co	Lindstrom, 1971	2.4375-3.1404	28	.23	51.	52.
^{57}Co	Watson, 1981	3.1212-4.0005	56	.15	75.	75.
^{59}Co	Lindstrom, 1972	2.5888-3.1042	82	.31	243.	231.
^{63}Cu	Browne, 1970	2.7150-3.0970	44	.32	178.	170.
^{47}V	Prochnow, 1973	2.0878-3.0678	22	.19	28.	28.
^{49}V	Prochnow, 1972	2.4958-3.1020	46	.19	94.	94.
^{51}V	Prochnow, 1973	2.2421-2.9488	68	.24	132.	127.
^{67}Ga	Sales, 1981	3.0448-3.2548	52	.38	481.	397.

Notes:

a: Calculated using bootstrap method.

b: Calculated using iterative method.

Table 5.2: Neutron s-wave Level Densities

Nucleus	Reference	E_n Range (keV)	$N_{obs.}$	M.F.	ρ (MeV^{-1})
^{41}Ar	Mughabhab, 1981	0 - 630	7	.22	14.
^{41}Ca	Mughabhab, 1981	0 - 1400	31	.28	31.
^{43}Ca	Mughabhab, 1981	0 - 580	27	.25	63.
^{45}Ca	Mughabhab, 1981	0 - 570	21	.13	41.
^{47}Ti	Mughabhab, 1981	0 - 370	12	.19	40.
^{49}Ti	Mughabhab, 1981	0 - 360	16	.19	55.
^{51}Cr	Mughabhab, 1981	0 - 600	41	.11	75.
^{55}Cr	Agrawal, 1984	0 - 900	15	.09	18.
^{55}Fe	Mughabhab, 1981	0 - 500	23	.17	56.
^{57}Fe	Mughabhab, 1981	0 - 900	41	.14	52.
^{59}Fe	Mughabhab, 1981	0 - 350	11	.20	39.
^{59}Ni	Perey, 1986	0 - 650	52	.00	80.
^{61}Ni	Perey, 1983	0 - 450	30	.07	72.
^{63}Ni	Mughabhab, 1981	0 - 600	30	.25	67.
^{67}Zn	Garg, 1981	0 - 380	80	.16	250.

§5.2 Comparison of Proton and Neutron Level Densities

Due to the variation in excitation energies of the nuclei the level densities must be converted to an standard excitation energy. This is performed by using the model of Kataria and determining what the level density would be at an excitation energy of 8 MeV. This procedure yields a multiplicative factor R,

$$R = \frac{\rho\left(\frac{1}{2}^{+}, U = 8MeV\right)}{\rho\left(\frac{1}{2}^{+}, U = U_{exp}\right)}$$

which converts each level density.

The results of this conversion are presented in figure 5.1. The A dependence of the level density is similar for both proton and neutron data. This result suggests that the proton data are suitable for inclusion in the nuclear data base. The proton and neutron data are next compared with two theoretical models.

§5.3 Comparison to Theoretical Level Density Models

One of the most important parameters in level density calculations is the parameter a. Two recently developed models, discussed in chapter two,will be used: one by Ignatyuk et al. (known as the IST model) and the other by Kataria et al. (known as the KRK model). In examining the data the atomic mass A dependence of the level density parameter a was determined for both the proton and neutron data.

The dependence of this parameter on A is shown in figure 5.2, where three models are compared, the simple Fermi gas model, the IST model and the KRK model.

Figure 5.1: Comparison of experimental neutron and proton data. All level densities were converted to a standard excitation energy of 8 MeV.

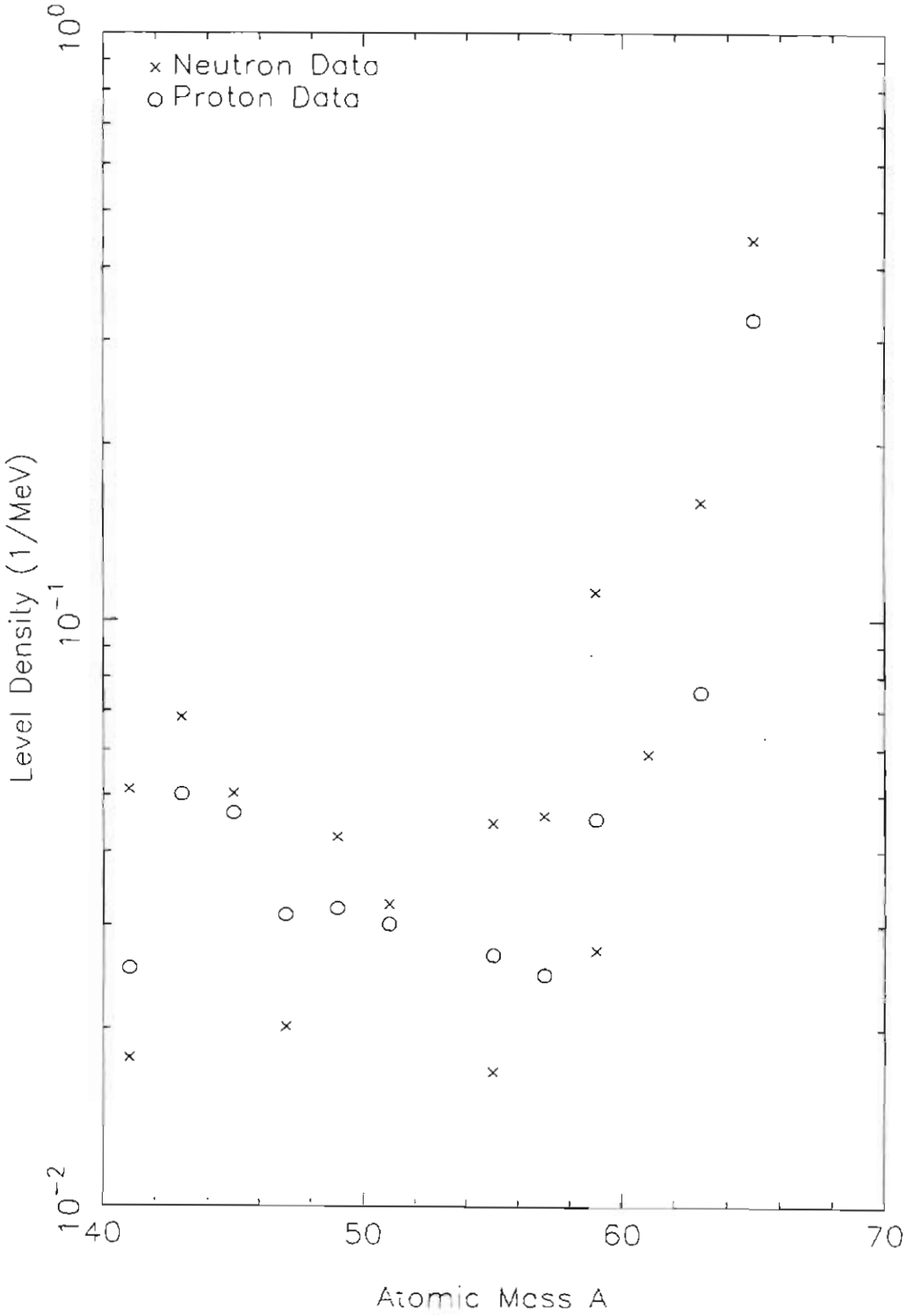
× Neutron Data
o Proton Data
Level Density (1/MeV)
10^{0}
10^{-1}
10^{-2}
40
50
60
70
Atomic Mass A

Figure 5.2: Comparison of dependence of the parameter a on A using neutron and proton data. The calculations were performed with three models: (a) Fermi Gas, (b) IST model and (c) KRK model.

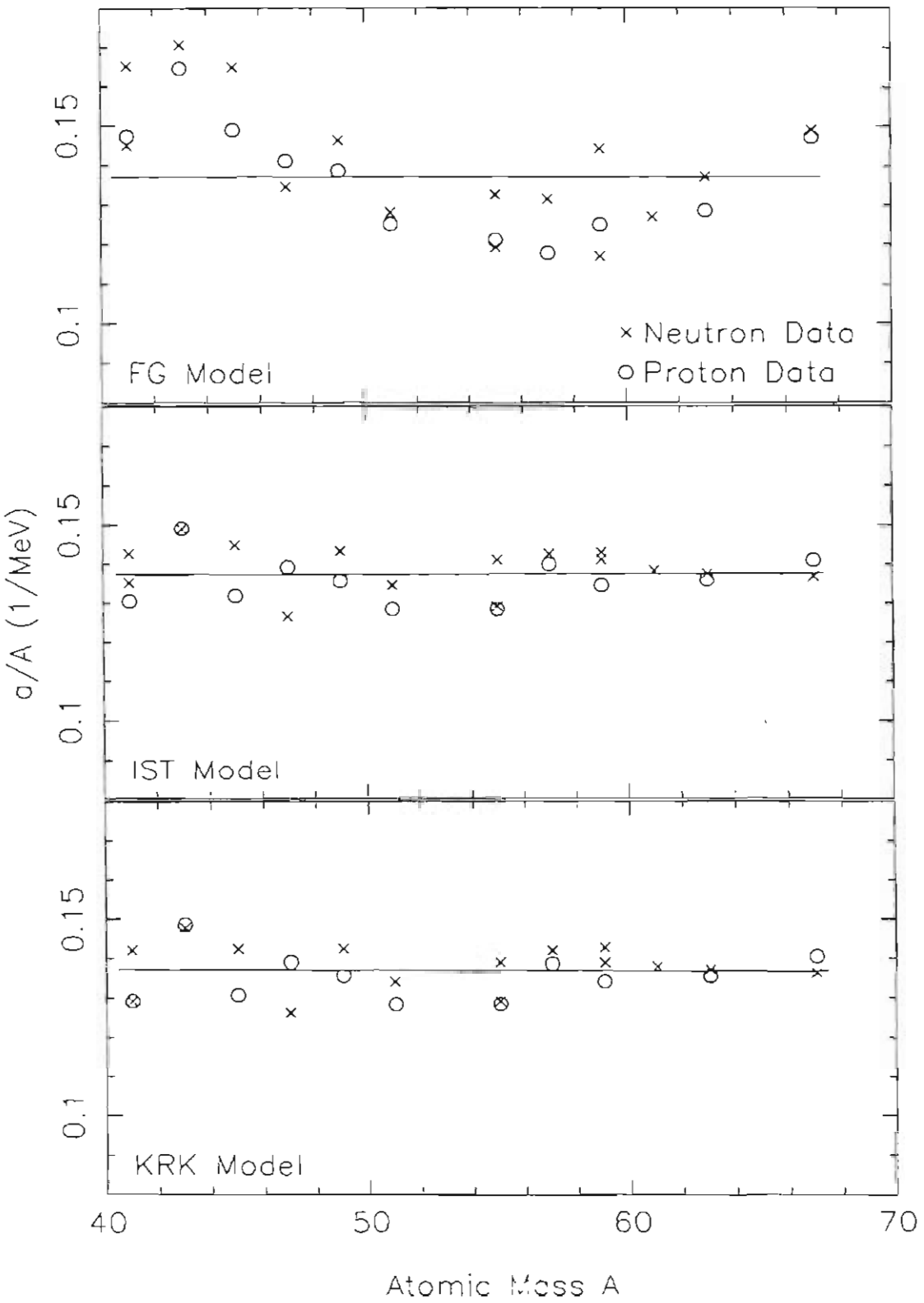
0.15
0.1
× Neutron Data
○ Proton Data
FG Model
0.15
0.1
IST Model
a/A (1/MeV)
0.15
0.1
KRK Model
40
50
60
70
Atomic Mass A

There is a linear dependence in the IST and KRK models, but a nonlinear dependence in the FG model. Note also the good agreement between the values found for the proton and neutron data.

Based on these results the conclusion is that high quality proton data can be used in the nuclear data base for level density calculations. Further, these results increased interest in obtaining more high quality high density level sequences to examine both the angular momentum dependence and the parity dependence of the level density. Because of these interests further work in the ^{45}Sc system has been performed. The following chapters discuss the data acquisition and analysis of the ^{45}Sc data.

Chapter Six

^{44}Ca (p,p) Experiment

The ^{45}Sc data was measured using the experimental setup and data analysis methods described in chapter three. This chapter will discuss the specific results for the ^{45}Sc system obtained by elastic and inelastic proton scattering. Data for the ^{45}Sc system had previously been obtained using incident protons for E_p = 1 - 3 MeV. The current experiment utilized the upgraded KN accelerator at TUNL to extend the data from E_p = 2.95 to 3.72 MeV.

§6.1 Data Acquisition

Using the experimental system at the HRL, data for the reactions ^{44}Ca(p,p) and ^{44}Ca(p,p´) were collected in 100 eV energy steps over the energy range given above. Five detectors were located at angles of 90°, 108°, 135°, 150° and 165° with solid angles corresponding to those listed in chapter three. The targets used were thin film targets with a ^{44}Ca layer approximately 1 $\mu g/cm^2$ thick. This layer was evaporated with a CaO and Ta mixture in a Tungsten closed boat.

The time to acquire one data point was approximately one minute with 4 to 5 μA of beam on target. A sample spectrum at 165° is shown in chapter three in figure 3.4. The yield curves generated by successive data points are created by summing the num-

ber of counts contained in the peaks of interest, i.e. the elastic and inelastic scattering peaks. Due to the frequent occurrence of small resonances the energy steps for the data acquisition were 100 eV. An example of a yield curve for the ^{44}Ca(p,p) and ^{44}Ca(p,p´) reactions is presented in figure 3.5. Yield curves were generated at all five angles for the entire energy range E_p = 2.95 - 3.72 MeV for both ^{44}Ca(p,p) and ^{44}Ca(p,p´).

The data were collected and stored on magnetic tape, and then processed and prepared for analysis using the R-Matrix code MULTI6.

§6.2 Data Analysis

The analysis of the reaction data was carried out using MULTI6 following an iterative process described in chapter three. For the energy range studied 585 resonances were observed with $J^\pi = 1/2^+$(s-wave), $1/2^-$ and $3/2^-$ (p-wave), and $3/2^+$ and $5/2^+$ (d-wave). Due to penetrability effects states with $\ell > 2$ were not expected to be observed. The resonances and their associated parameters are listed in appendix A. The resulting data and fit are presented in figures 6.1-6.5 for the ^{44}Ca(p,p) and ^{44}Ca(p,p´) reaction cross sections at 165°.

Certain practical problems arose in the data analysis, in particular interference and resolution limitation effects. The interference effects were most severe when a smaller level was close to a much larger level. In figure 6.6 an example of the shape differences for the cross section with a smaller (Γ_{lab} = 25 eV) $3/2^+$ resonance interfering with a larger (Γ_{lab} = 100 eV) $1/2^+$ resonance is shown as a function of energy separation. It is evident that this effect reduces the confidence in assigning the J^π of smaller levels in the presence of larger levels.

The resolution limits a definitive J assignment for p- and d-wave resonances. This was particularly evident for smaller levels with strong inelastic channels.

Figure 6.1: Data and fit for the ^{44}Ca(p,p) and ^{44}Ca(p,p') reactions at 165° for incident proton energies of 2.95 to 3.11 MeV.

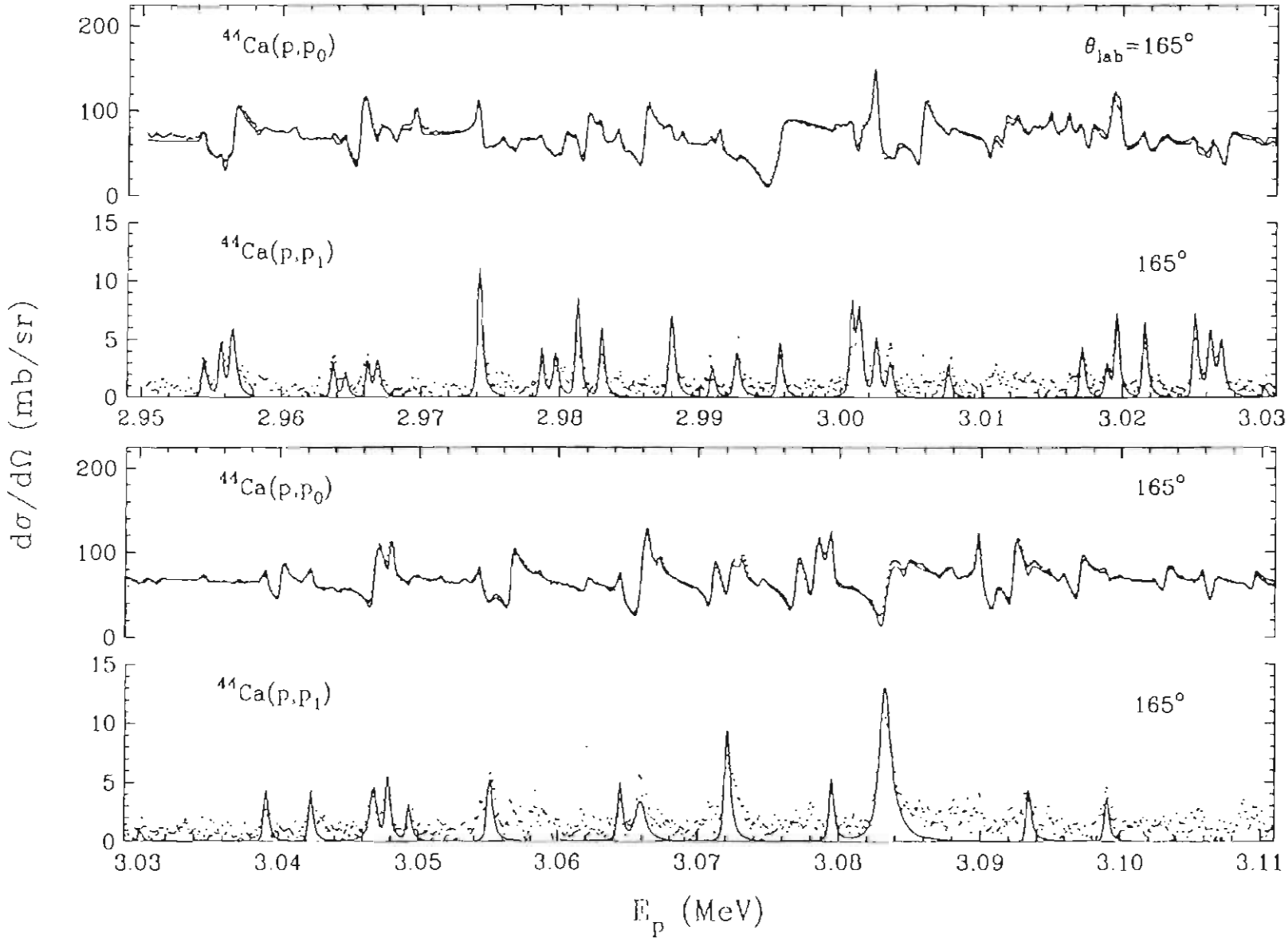
^{44}Ca(p,p$_0$)
θ_{lab}=165°
^{44}Ca(p,p$_1$)
165°
^{44}Ca(p,p$_0$)
165°
^{44}Ca(p,p$_1$)
165°
dσ/dΩ (mb/sr)
E$_p$ (MeV)

Figure 6.2: Data and fit for the ^{44}Ca(p,p) and ^{44}Ca(p,p$'$) reactions at 165° for incident proton energies of 3.11 to 3.27 MeV.

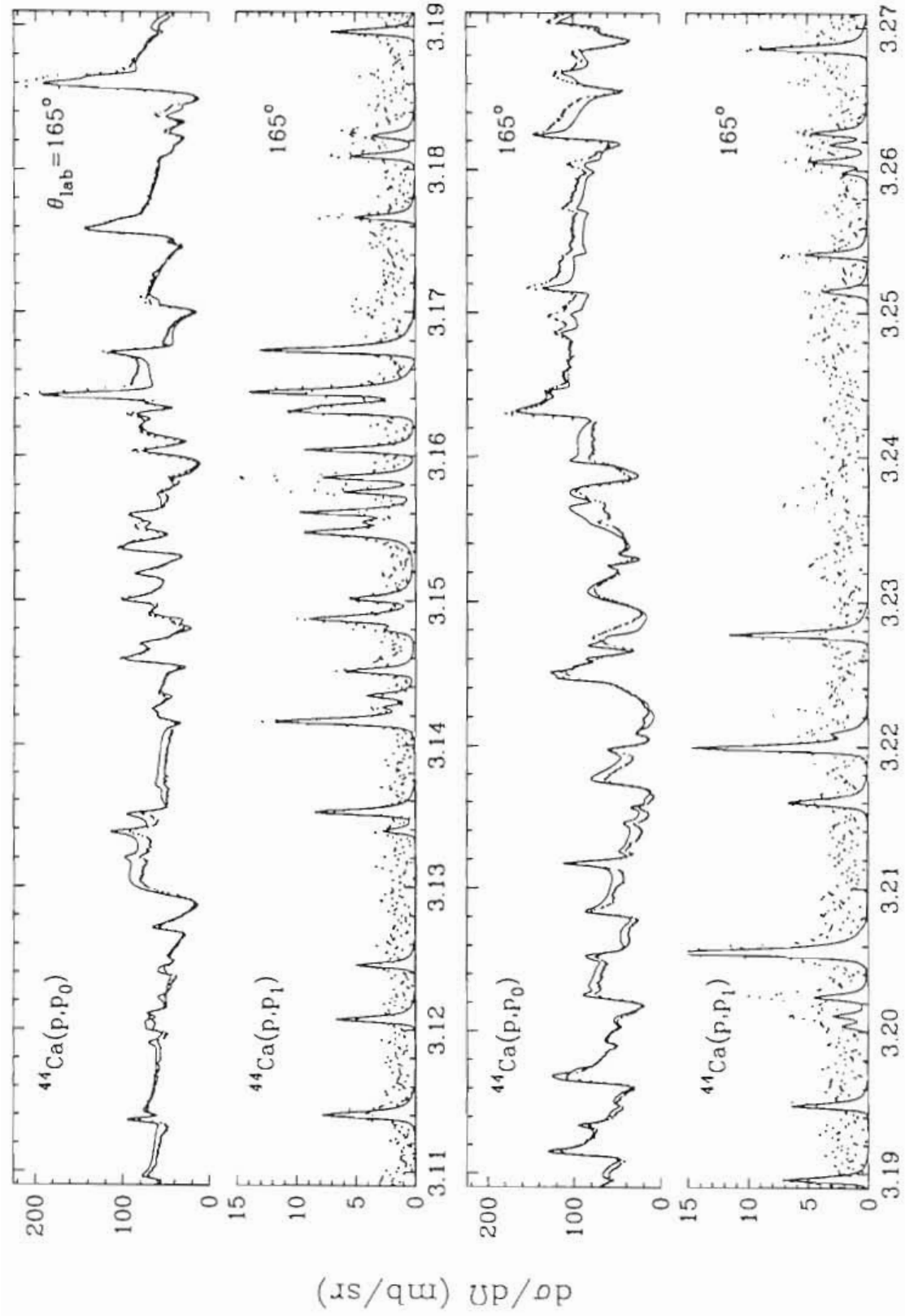
θ_{lab}=165°
^{44}Ca(p,p$_0$)
^{44}Ca(p,p$_1$)
165°
^{44}Ca(p,p$_0$)
^{44}Ca(p,p$_1$)
165°
200
100
0
15
10
5
0
3.11
3.12
3.13
3.14
3.15
3.16
3.17
3.18
3.19
3.20
3.21
3.22
3.23
3.24
3.25
3.26
3.27
dσ/dΩ (mb/sr)
E$_p$ (MeV)

Figure 6.3: Data and fit for the ^{44}Ca(p,p) and ^{44}Ca(p,p') reactions at 165° for incident proton energies of 3.27 to 3.43 MeV.

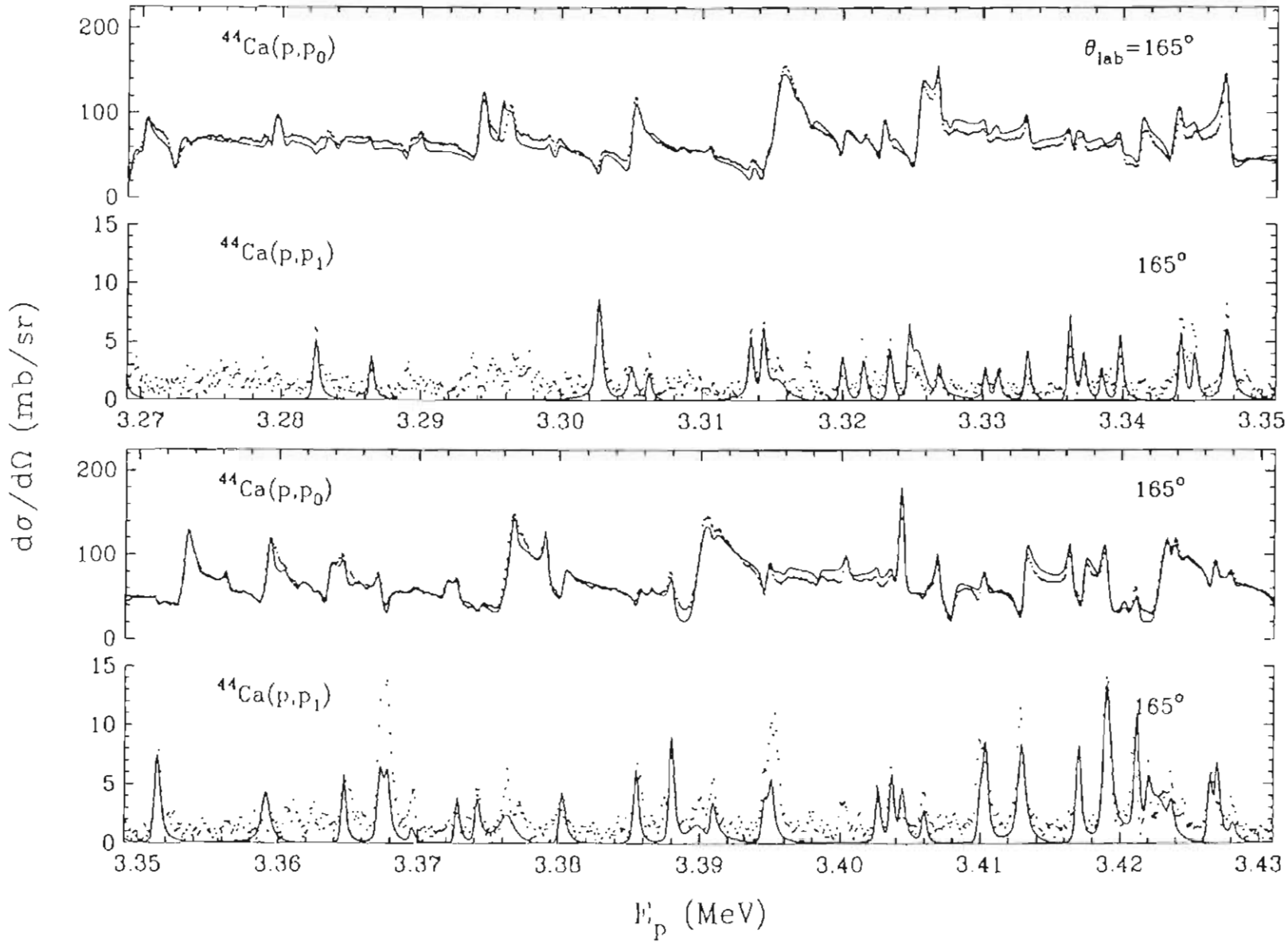
^{44}Ca(p,p$_0$)
θ_{lab}=165°
^{44}Ca(p,p$_1$)
165°
^{44}Ca(p,p$_0$)
165°
^{44}Ca(p,p$_1$)
165°
dσ/dΩ (mb/sr)
E$_p$ (MeV)

Figure 6.4: Data and fit for the ^{44}Ca(p,p) and ^{44}Ca(p,p$'$) reactions at 165° for incident proton energies of 3.43 to 3.59 MeV.

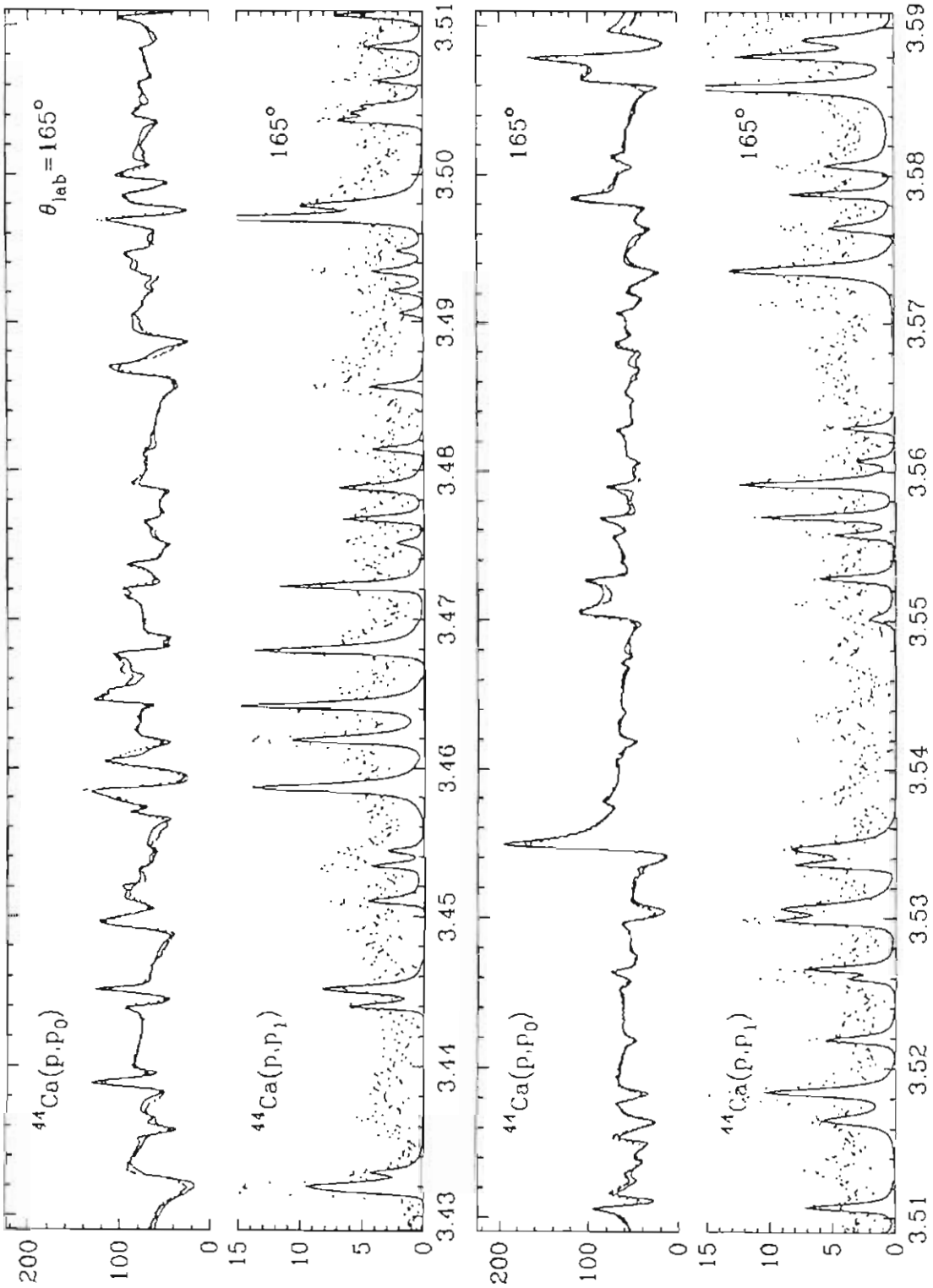
θ_{lab}=165°
^{44}Ca(p,p$_0$)
^{44}Ca(p,p$_1$)
165°
dσ/dΩ (mb/sr)
E$_p$ (MeV)

Figure 6.5: Data and fit for the ^{44}Ca(p,p) and ^{44}Ca(p,p$'$) reactions at 165° for incident proton energies of 3.59 to 3.75 MeV.

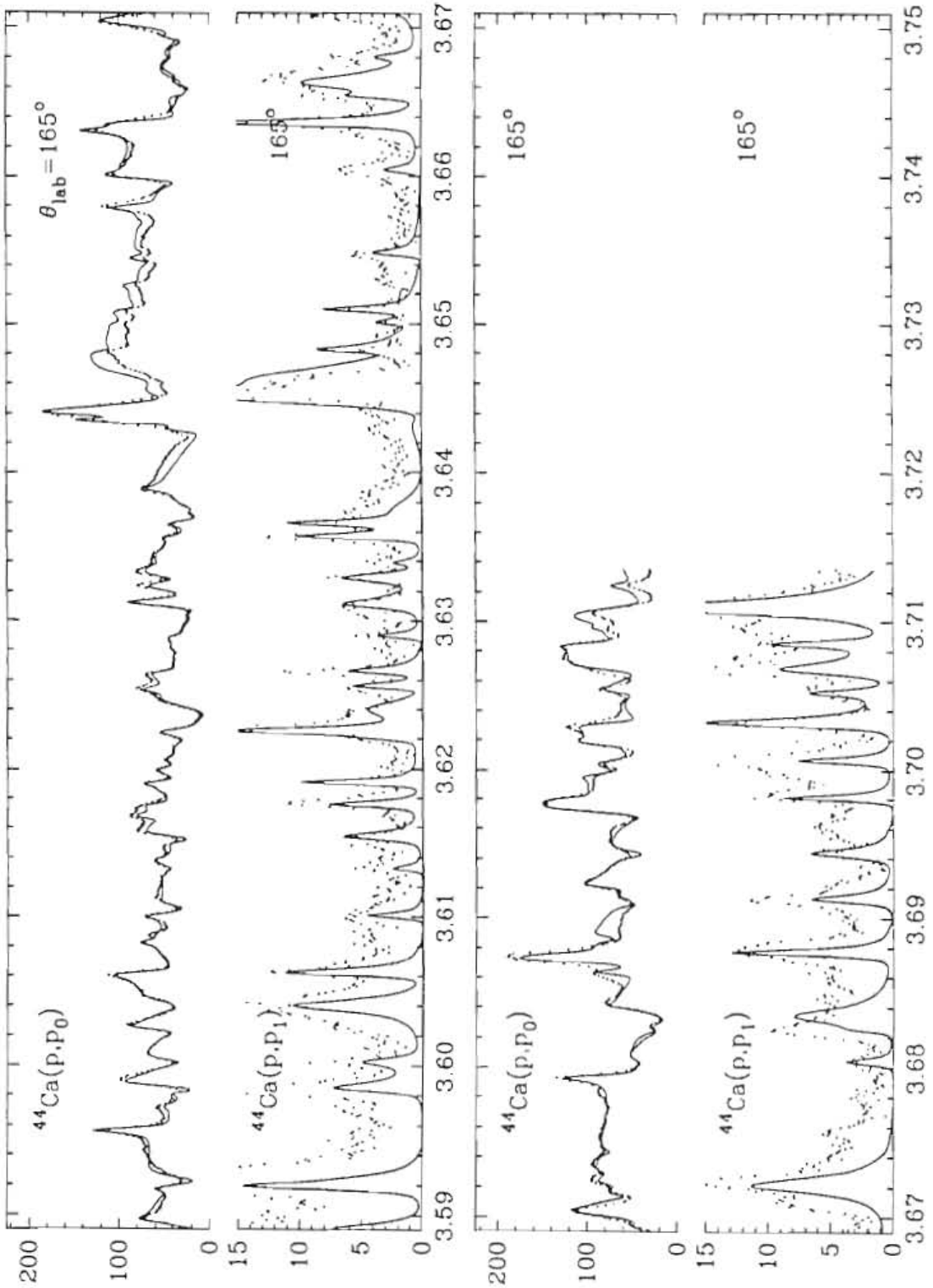
θ_{lab}=165°
^{44}Ca(p,p$_0$)
^{44}Ca(p,p$_1$)
165°
^{44}Ca(p,p$_0$)
^{44}Ca(p,p$_1$)
165°
165°
200
100
0
15
10
5
0
3.59
3.60
3.61
3.62
3.63
3.64
3.65
3.66
3.67
3.68
3.69
3.70
3.71
3.72
3.73
3.74
3.75
dσ/dΩ (mb/sr)
E$_p$ (MeV)

Figure 6.6: Interference effects on resonance shapes for $3/2^+$ and $1/2^+$ resonances as a function of energy separation. The values of the energy separation for the $3/2^+(\Gamma_{lab} = 25$ eV) resonance relative to the $1/2^+(\Gamma_{lab} = 100$ eV) resonance are: -400, -200, -100, 100, 200, 400 eV respectively from left to right.

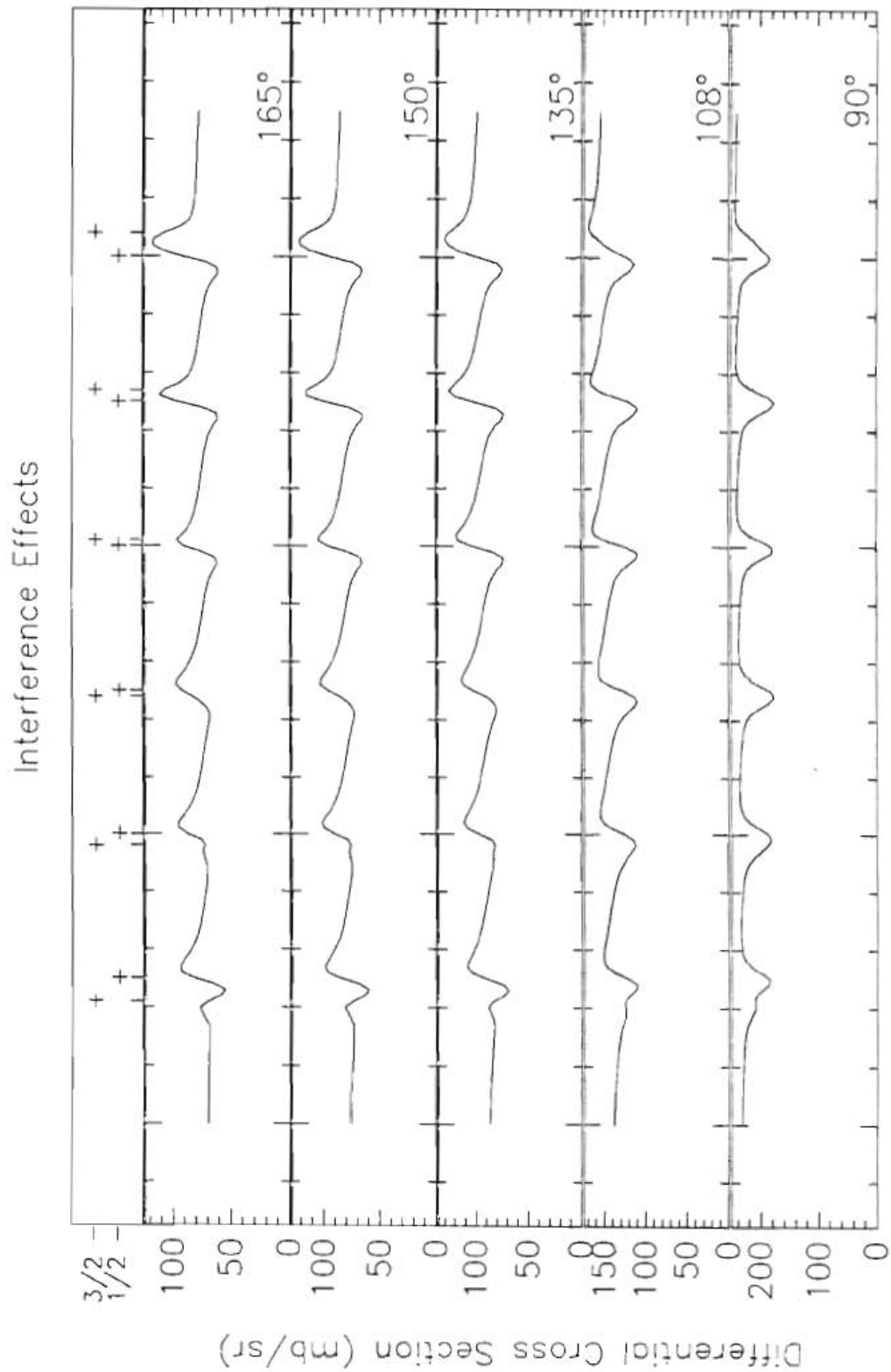
Interference Effects
3/2 −
1/2 −
165°
150°
135°
108°
90°
100
50
0
100
50
0
100
50
0
150
100
50
0
200
100
0
3.000
3.005
3.010
3.015
Incident Proton Energy (MeV)
Differential Cross Section (mb/sr)

In some cases, as was mentioned in chapter three, the anisotropy of the inelastic protons assisted in the J assignment. In general, however, the J assignment for the p- and d-wave resonances was inconclusive when the width of the resonance was small.

§6.3 Results: Level Sequences in ^{45}Sc.

From the resonance assignments one can construct level sequences. In figure 6.7 a plot of the various level sequences is presented. Based on the number of levels present in each sequence all five sequences seem to be good candidates for level density analysis. A more detailed look at each sequence is presented in figures 6.8-6.12 with reduced width sum and number plots. These plots give a general idea of the strength distribution for each sequence and are helpful in the identification of analog states.

§6.4 Identification of Analog States.

As is evident in figure 6.9 in the $1/2^-$ sequence there are two abnormally large increases in the reduced width sum plot; this indicates the presence of analog states. Two possible parent states are at excitation energies of 3.241 and 3.442 MeV in ^{45}Ca. These states were observed with the ^{44}Ca(d,p)^{45}Ca reaction and were determined to be $\ell=1$ states. The excitation energy in the ^{45}Ca system corresponds to incident proton energies of 2.9951 and 3.2200 MeV respectively; these values were determined using the energy relations shown in figure 4.5. From figure 6.9 these energies correspond to the location of the large strength observed in the $1/2^-$ sequence. Therefore it is likely that the analog identification is correct.

The analog state at ~3.0 MeV appears to be a single state, while the analog state at ~3.2 MeV is fragmented into at least six states. With the relation for the spectroscopic

Figure 6.7: Summary of level sequences observed in ^{45}Sc for incident proton energy ranges 2.95 to 3.72 MeV.

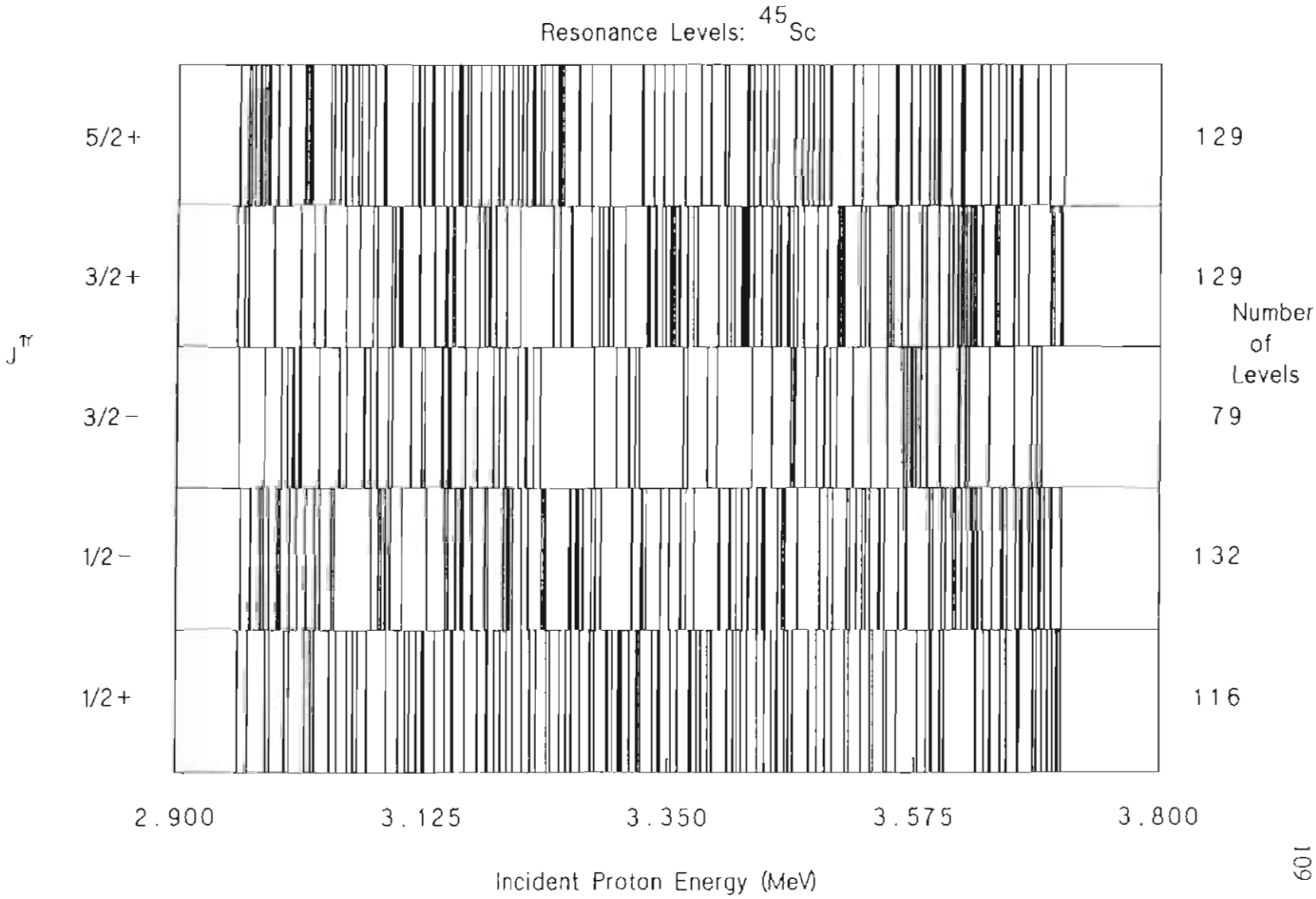
Resonance Levels: ^{45}Sc
5/2+
3/2+
3/2−
1/2−
1/2+
J^{π}
129
129
79
132
116
Number of Levels
2.900
3.125
3.350
3.575
3.800
Incident Proton Energy (MeV)

Figure 6.8: Sum of reduced widths plot and number plot for the $1/2^+$ level sequence in ^{45}Sc.

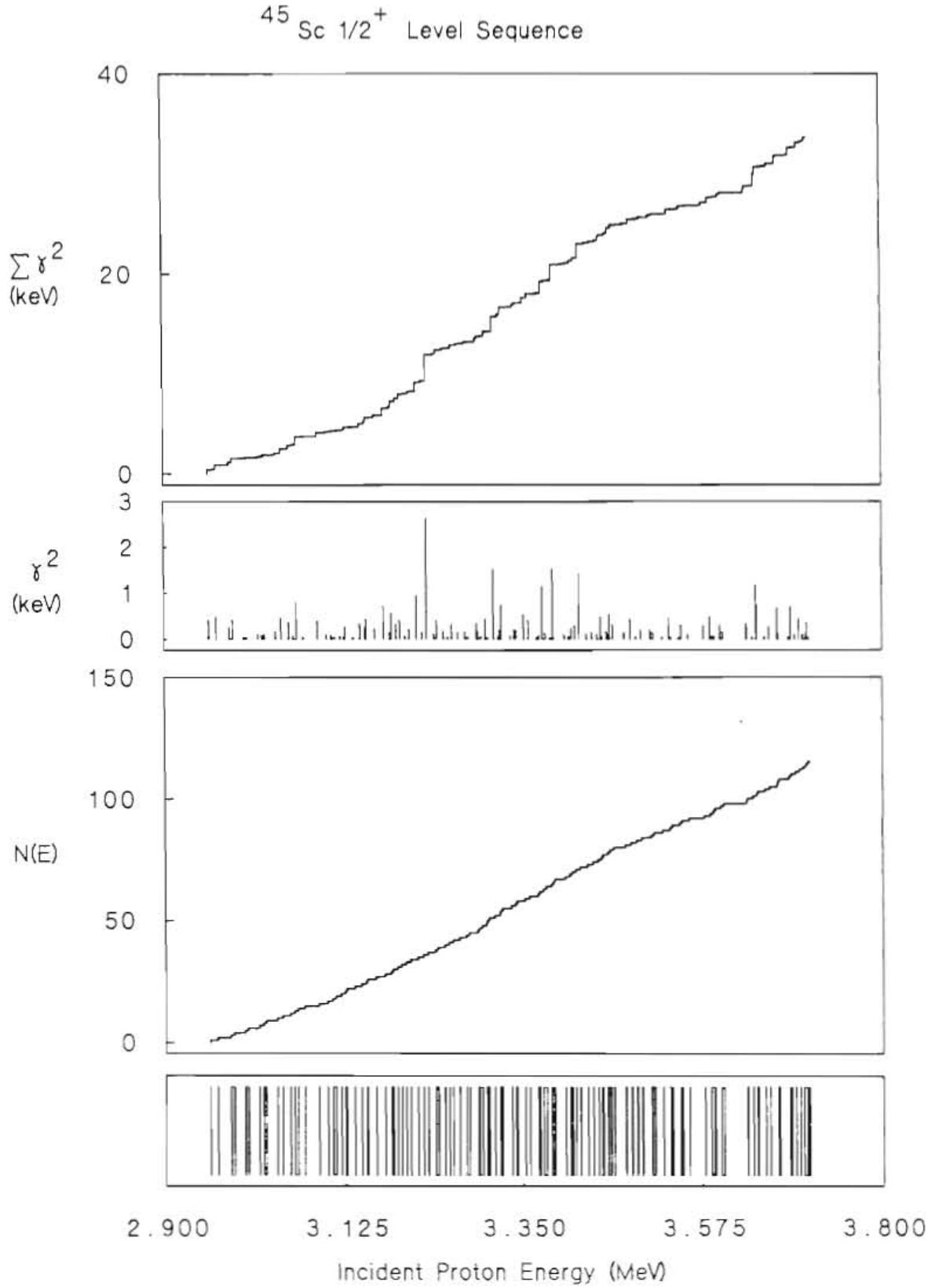
45 Sc 1/2+ Level Sequence
40
20
0
∑γ2 (keV)
3
2
1
0
γ2 (keV)
150
100
50
0
N(E)
2.900
3.125
3.350
3.575
3.800
Incident Proton Energy (MeV)

Figure 6.9: Sum of reduced widths plot and number plot for the $1/2^-$ level sequence in ^{45}Sc.

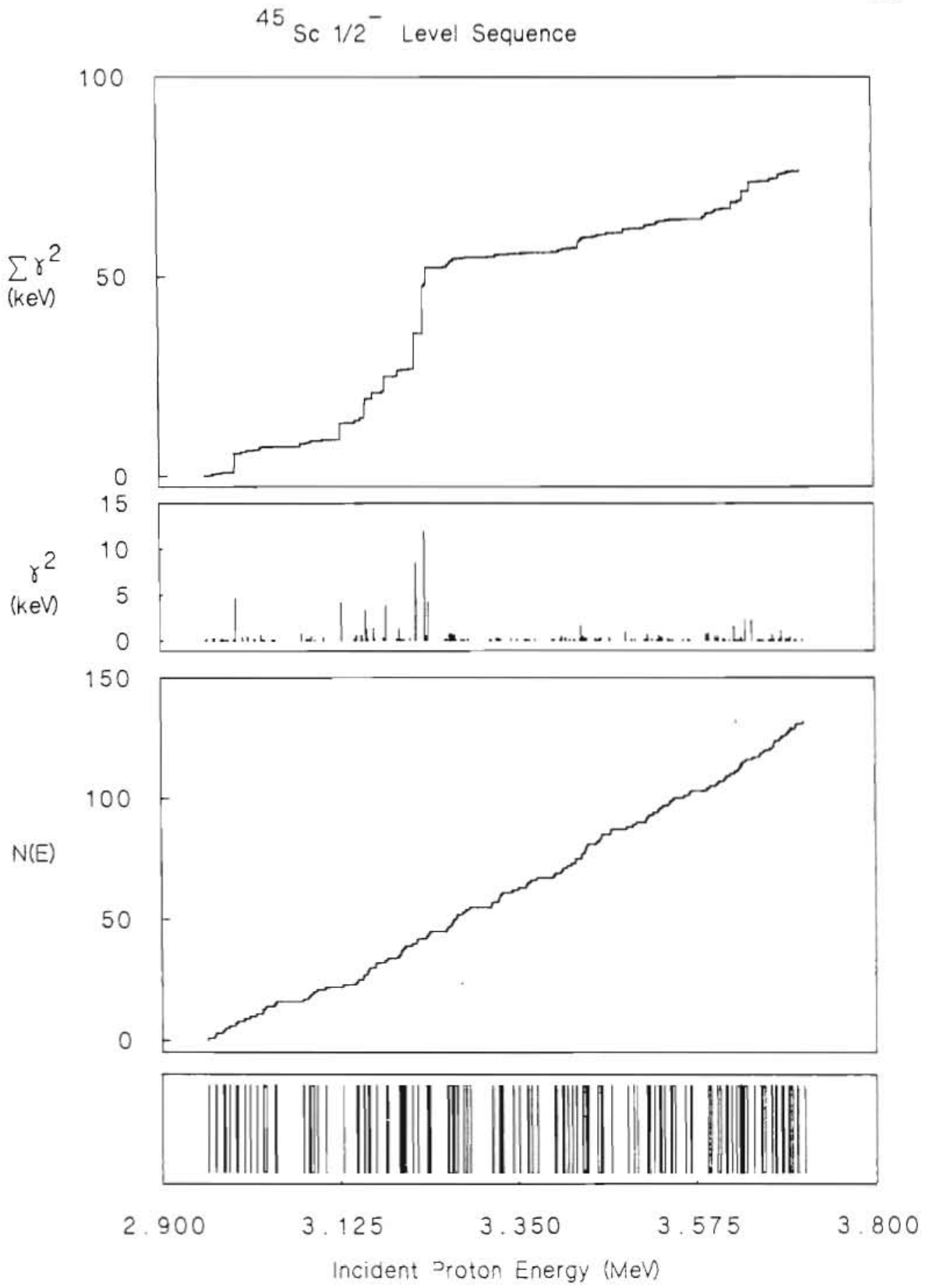
45 Sc 1/2⁻ Level Sequence
100
50
0
Σγ²
(keV)
15
10
5
0
γ²
(keV)
150
100
50
0
N(E)
2.900
3.125
3.350
3.575
3.800
Incident Proton Energy (MeV)

Figure 6.10: Sum of reduced widths plot and number plot for the $3/2^-$ level sequence in ^{45}Sc.

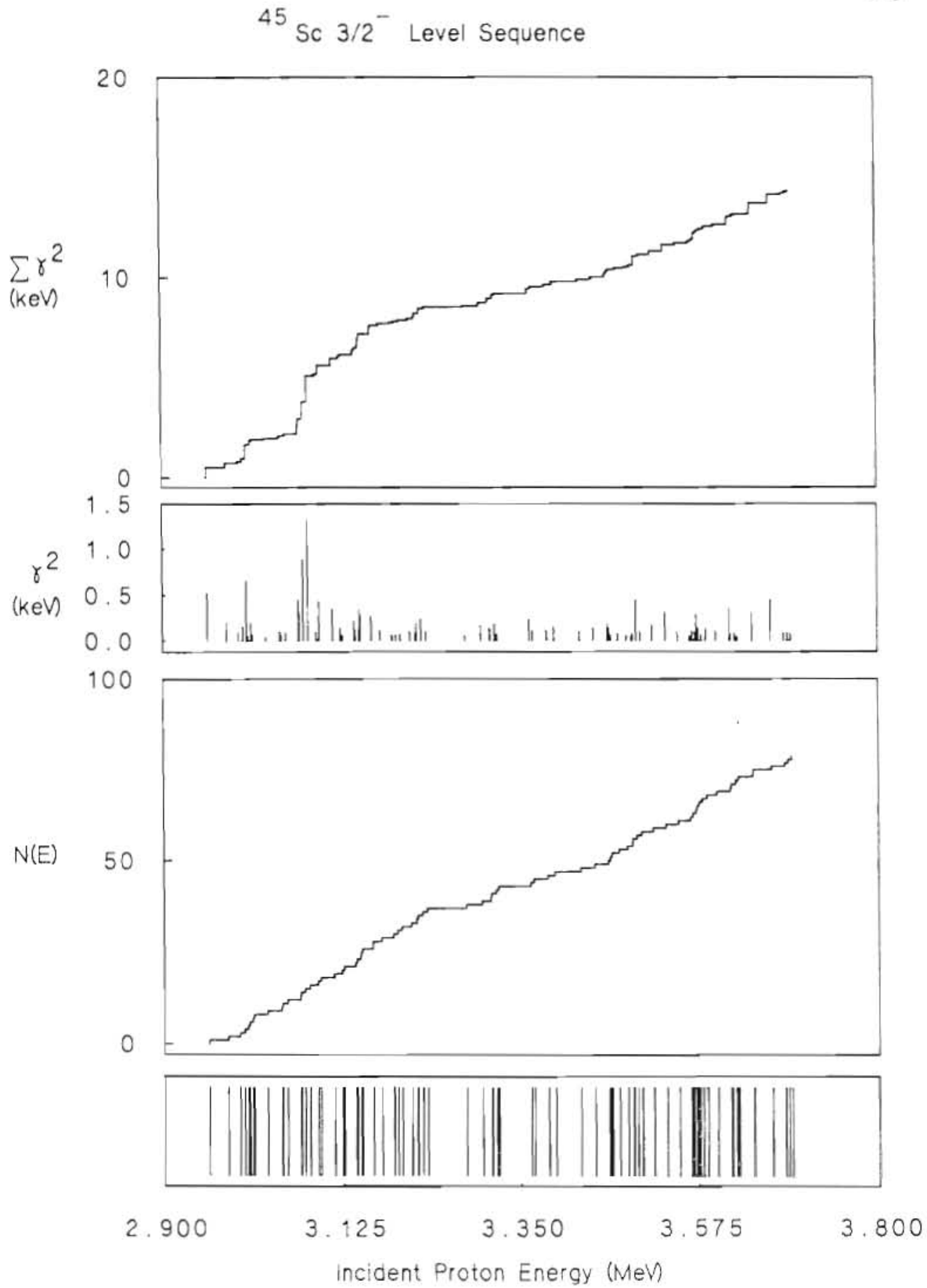
^{45}Sc 3/2$^-$ Level Sequence
20
10
0
$\sum\gamma^2$ (keV)
1.5
1.0
0.5
0.0
γ^2 (keV)
100
50
0
N(E)
2.900
3.125
3.350
3.575
3.800
Incident Proton Energy (MeV)

Figure 6.11: Sum of reduced widths plot and number plot for the $3/2^+$ level sequence in ^{45}Sc.

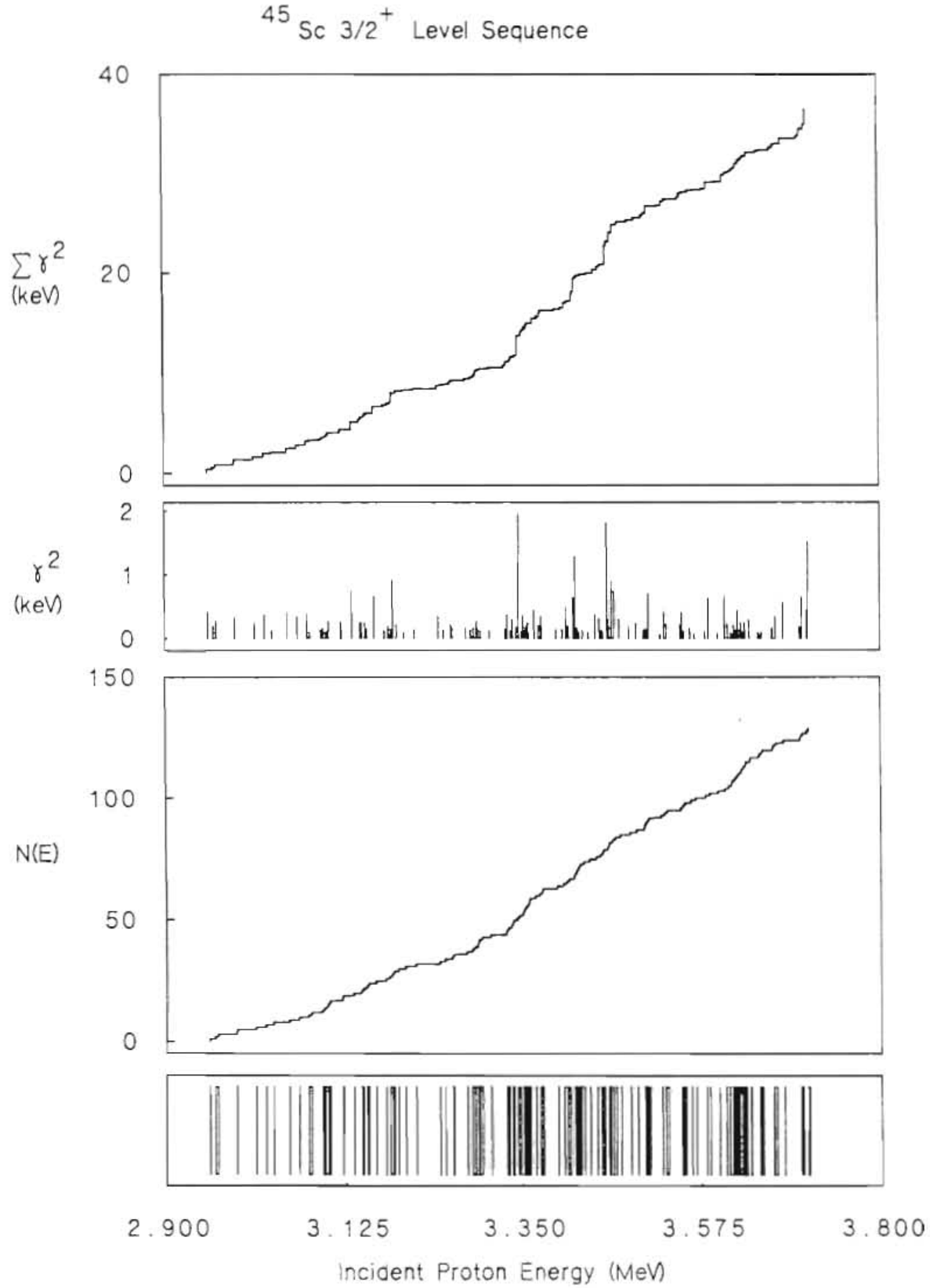
^{45}Sc 3/2^{+} Level Sequence
40
20
0
$\sum \gamma^2$ (keV)
2
1
0
γ^2 (keV)
150
100
50
0
N(E)
2.900
3.125
3.350
3.575
3.800
Incident Proton Energy (MeV)

Figure 6.12: Sum of reduced widths plot and number plot for the $5/2^+$ level sequence in ^{45}Sc.

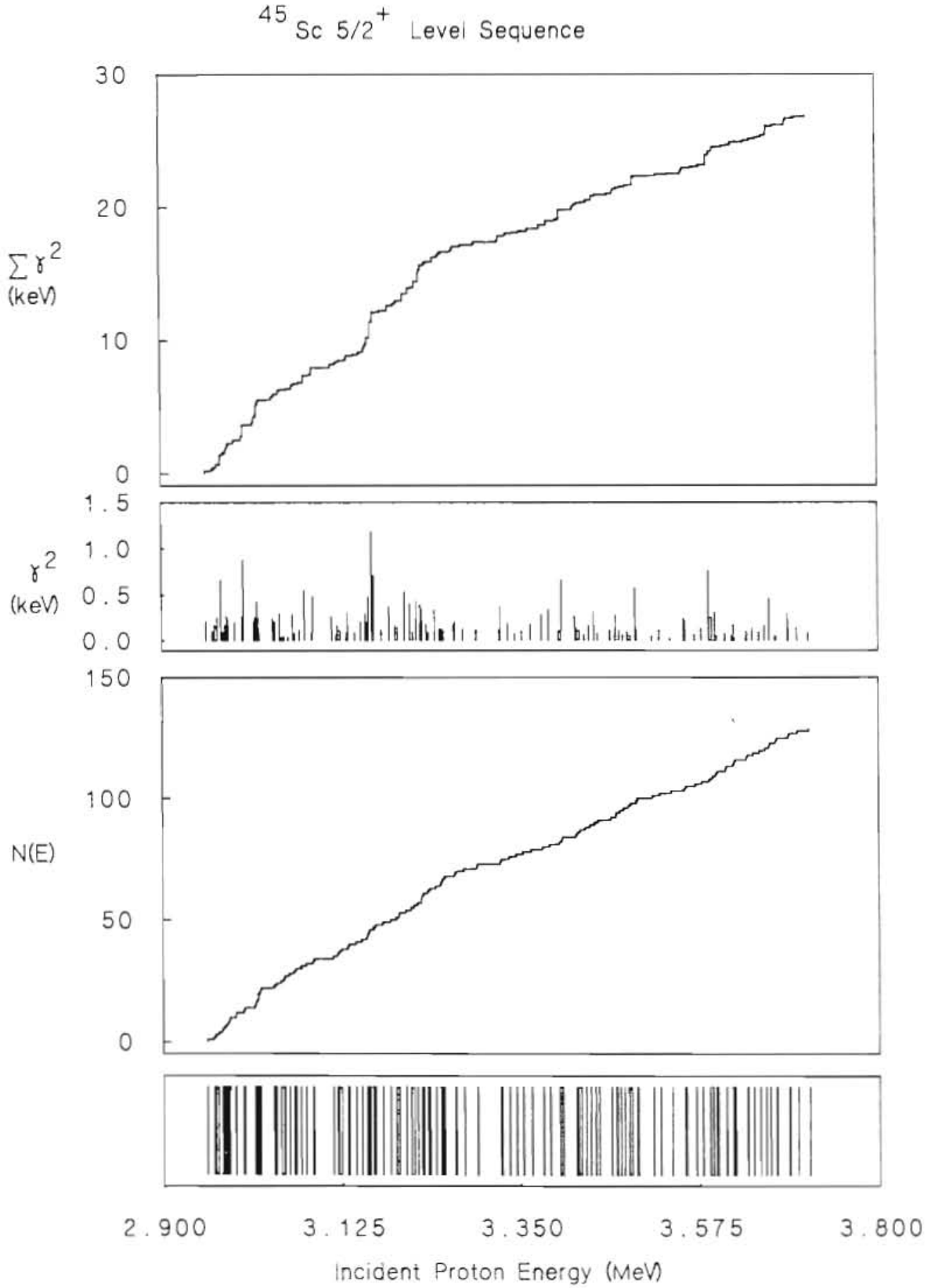
45 Sc 5/2+ Level Sequence
30
20
10
0
Σγ2 (keV)
1.5
1.0
0.5
0.0
γ2 (keV)
150
100
50
0
N(E)
2.900
3.125
3.350
3.575
3.800
Incident Proton Energy (MeV)

factor one can estimate the expected strength. From chapter three the relation between S_{dp} and Γ_{pp} is

$$S_{dp} = [\,2T + 1]\frac{\Gamma_{pp}}{\Gamma_{sp}} .$$

The values used are listed in table 6.1. Three models were used to calculate the single-particle widths; these are contained in the code HANS (Harney, 1968). The models used were: Zaidi, Darmodjo and Harney (ZDH) (Zaidi,1967) , MacDonald and Mekjian (MM) (Mekjian,1968) and Thompson, Adams and Robson (TAR) (Thompson,1968). From the information in table 6.1, one concludes that by removing the six levels representing the fragmented analog state at ~3.2 MeV, the effect of the analog state can be removed to first order. In figure 6.13 the $1/2^-$ sequence is presented with both analog states removed, that is, without the seven associated states.

With the analog states identified it is now possible to proceed to analyze the individual level sequences for level density determinations. This will be done in the following chapter.

Table 6.1: Analog State Parameters for $1/2^-$ States in ^{45}Sc

Resonance E_p (MeV)	$(2J+1)S_{dp}$	Γ_{sp} (keV)	Model	Γ_{pp} (Calc.)	Γ_{pp} (Obs.)	Fraction observed
2.9951	0.12	44.	ZDH	2.7	1.5	0.56
	0.12	54.	MM	3.3	1.5	0.46
	0.12	55.	TAR	3.3	1.5	0.46
3.1951*	0.79	60.	ZDH	24.	14.5*	0.61
	0.79	73.	MM	29.	14.5	0.50
	0.79	73.	TAR	29.	14.5	0.50

*This analog consists of the six resonances located at E_p = 3.1291, 3.1598, 3.1853, 3.2232, 3.2344 and 3.2389 MeV. Γ_{pp} (obs.) is the sum of the six states assumed to be fragments of the analog state at ~3.2 MeV.

Figure 6.13: Sum of reduced widths plot and number plot for the $1/2^-$ level sequence in ^{45}Sc. Analog states have been removed.

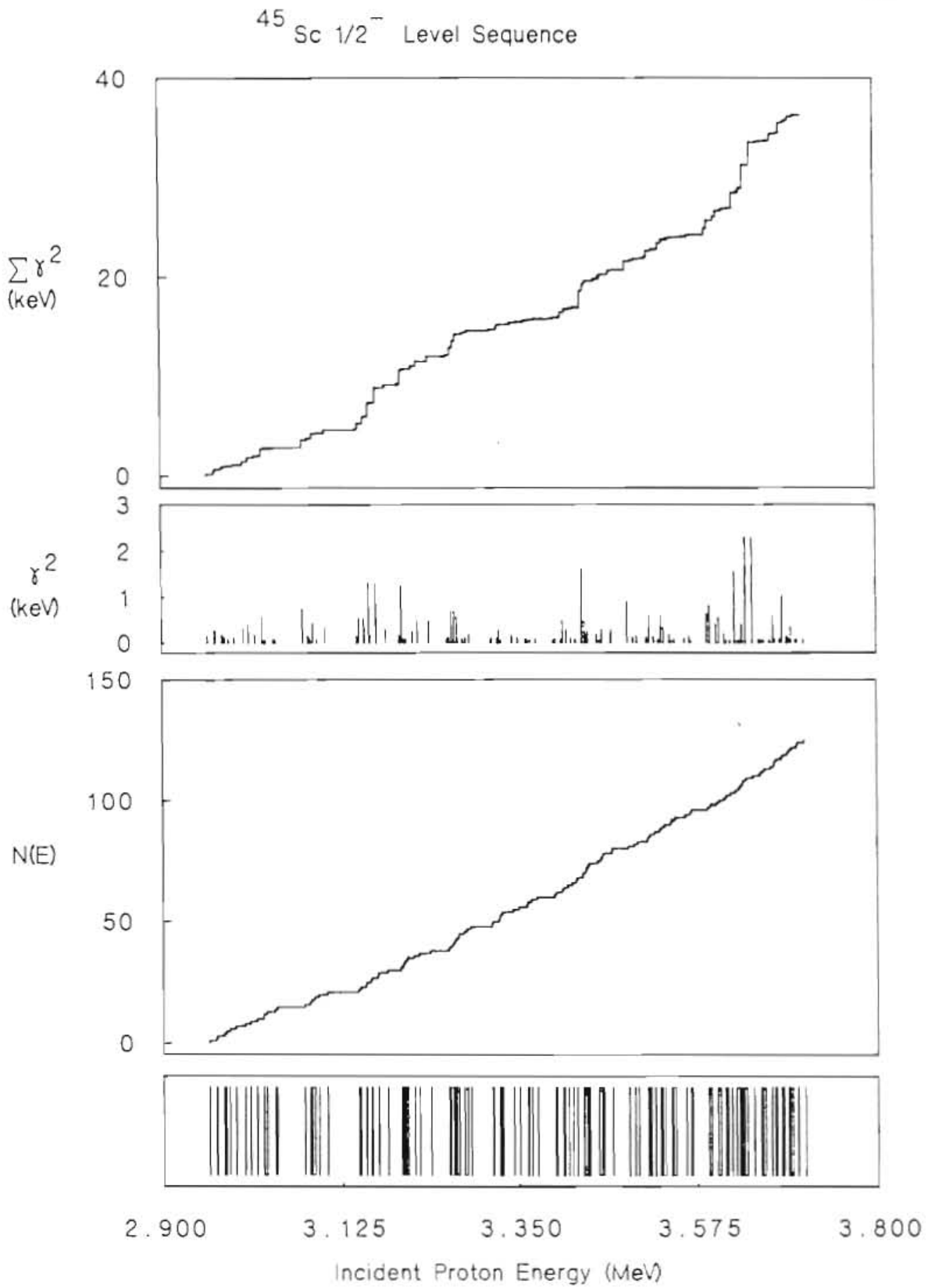
^{45}Sc 1/2$^-$ Level Sequence
40
20
0
$\sum\gamma^2$ (keV)
3
2
1
0
γ^2 (keV)
150
100
50
0
N(E)
2.900
3.125
3.350
3.575
3.800
Incident Proton Energy (MeV)

Chapter Seven

Level Sequence Analysis in ^{45}Sc

The level sequences obtained in chapter six will now be examined in more detail. The suitability of the level sequences for determination of the level density will be considered. In addition to considerations discussed in chapter four, the major emphasis will be on statistical tests using the Wigner and Porter-Thomas distributions. Then the level density will be determined using the iterative and bootstrap methods discussed in chapter four. Finally a discussion of the application of the results to tests of the parity and angular momentum dependence of the level density will be presented.

§7.1 Statistical Tests of ^{45}Sc Level Sequences

The first test for the level sequences is a comparison of the observed level spacings with the Wigner distribution. In figures 7.1 to 7.5 the observed spacings are plotted with a Wigner distribution superimposed; both binned and cumulative plots are presented. By visual comparison it is clear from the figures that the $1/2^+$ sequence agrees rather well with the expected Wigner distribution. However for the other sequences, $1/2^-$, $3/2^-$, $3/2^+$ and $5/2^+$ the results are not as encouraging. For these sequences there is an excess of observed small spacings, indicating impure sequences, that is level sequences which have levels of different J^π included. This misassignment

Figure 7.1: Wigner distribution overlay comparison for the $1/2^+$ level sequence in ^{45}Sc. Experimental level spacings are plotted (a) in 8 bins of equal probability and (b) as a cumulative distribution.

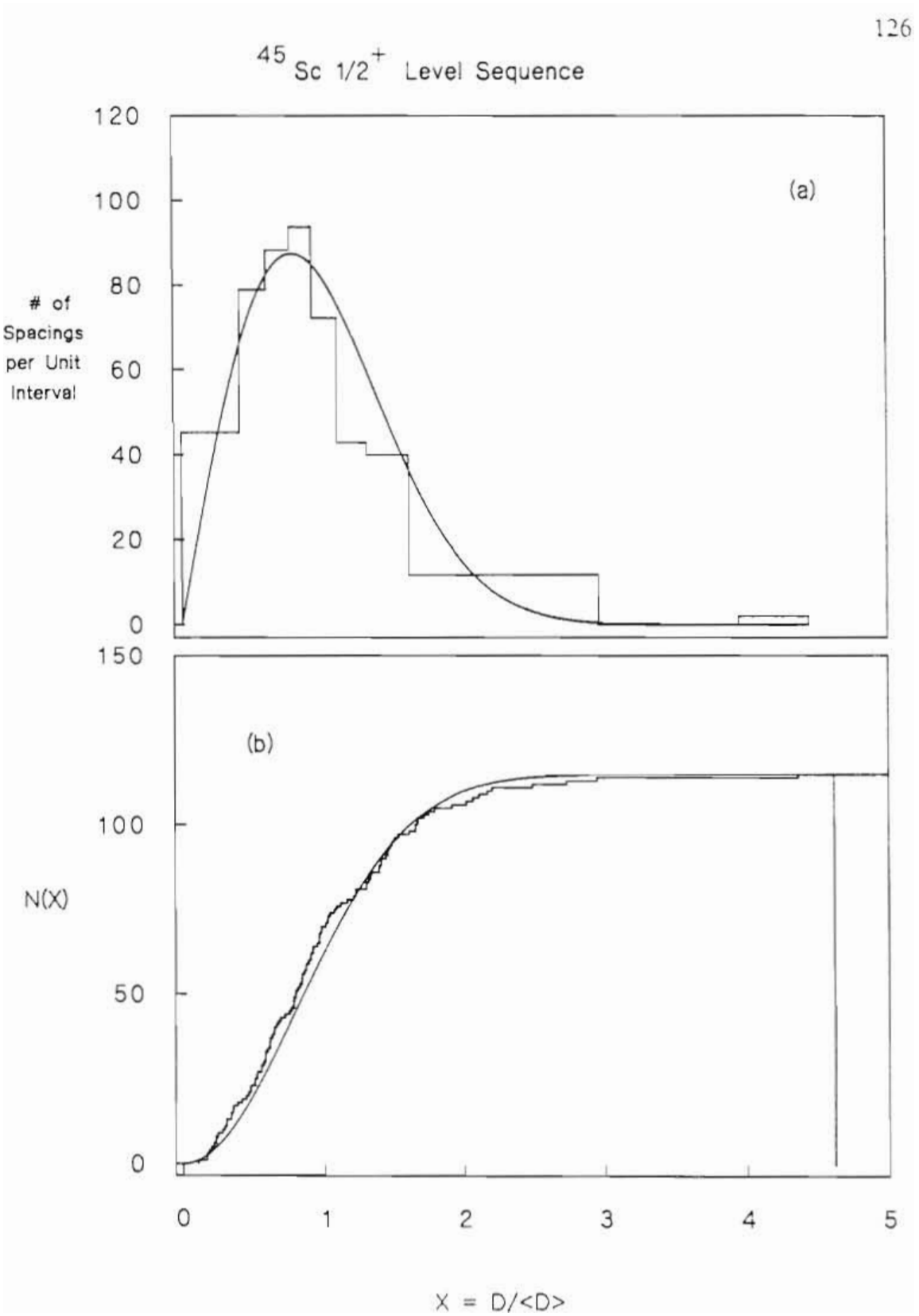
^{45}Sc 1/2^{+} Level Sequence
120
100
80
60
40
20
0
# of Spacings per Unit Interval
(a)
150
100
50
0
N(X)
(b)
0
1
2
3
4
5
X = D/<D>

Figure 7.2: Wigner distribution overlay comparison for the $1/2^-$ level sequence in ^{45}Sc. The analog states at 3.0 and 3.2 MeV have been removed. Experimental level spacings are plotted (a) in 8 bins of equal probability and (b) as a cumulative distribution.

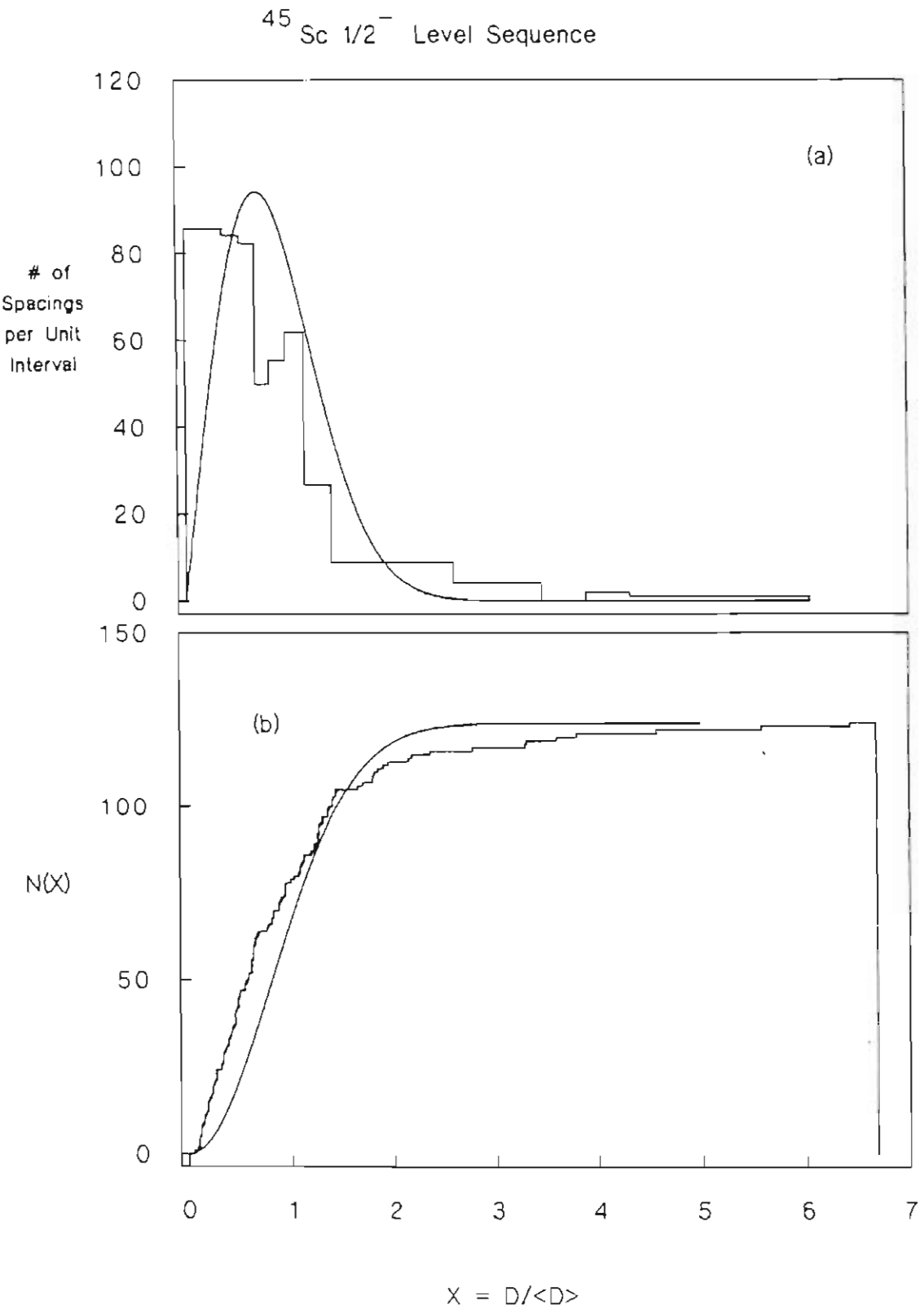
^{45}Sc 1/2$^-$ Level Sequence
120
100
80
60
40
20
0
(a)
# of Spacings per Unit Interval
150
100
50
0
(b)
N(X)
0
1
2
3
4
5
6
7
X = D/<D>

Figure 7.3: Wigner distribution overlay comparison for the $3/2^-$ level sequence in ^{45}Sc. Experimental level spacings are plotted (a) in 8 bins of equal probability and (b) as a cumulative distribution.

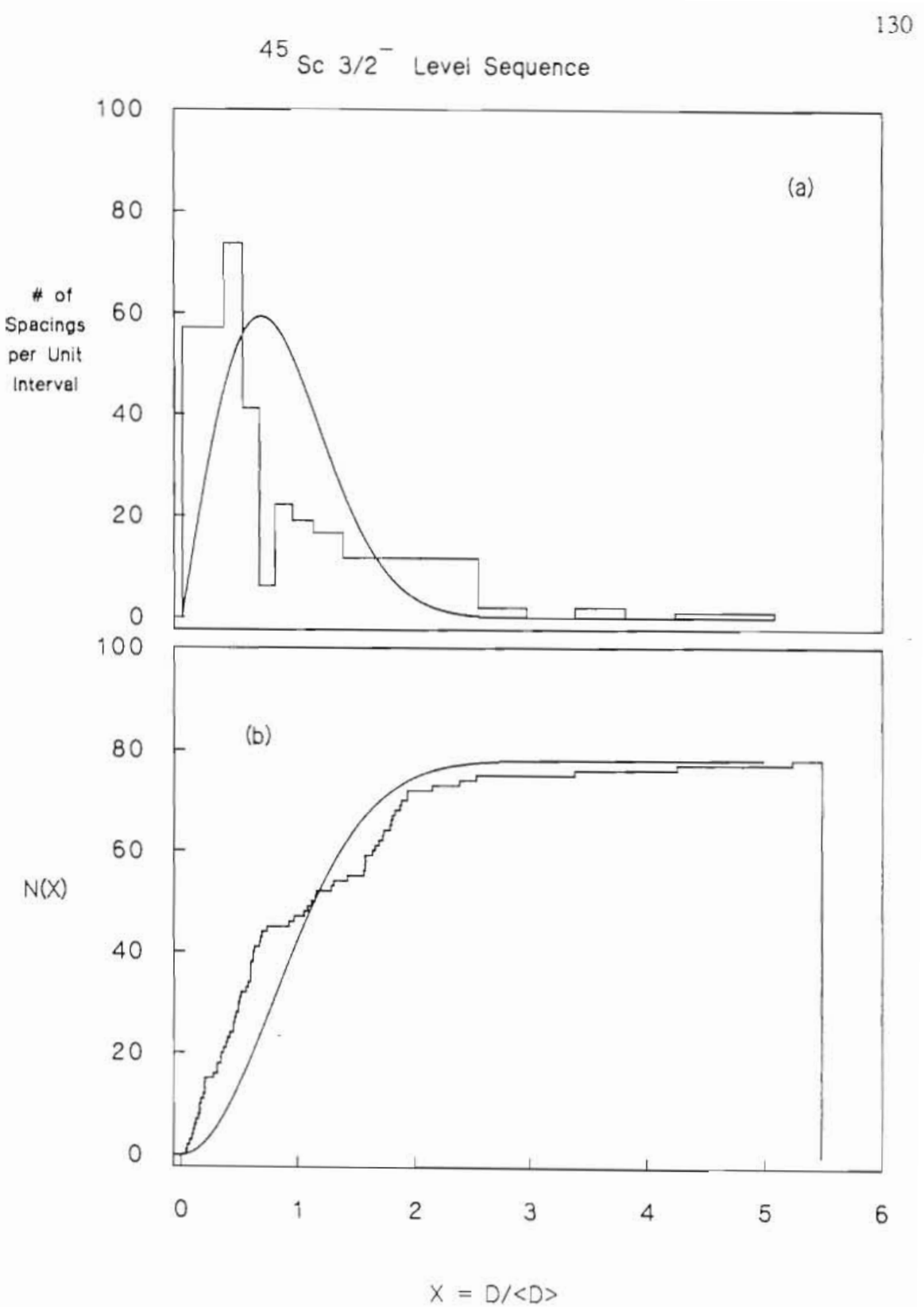
^{45}Sc 3/2$^-$ Level Sequence
(a)
(b)
# of Spacings per Unit Interval
N(X)
X = D/<D>
0
20
40
60
80
100
0
1
2
3
4
5
6

Figure 7.4: Wigner distribution overlay comparison for the $3/2^+$ level sequence in ^{45}Sc. Experimental level spacings are plotted (a) in 8 bins of equal probability and (b) as a cumulative distribution.

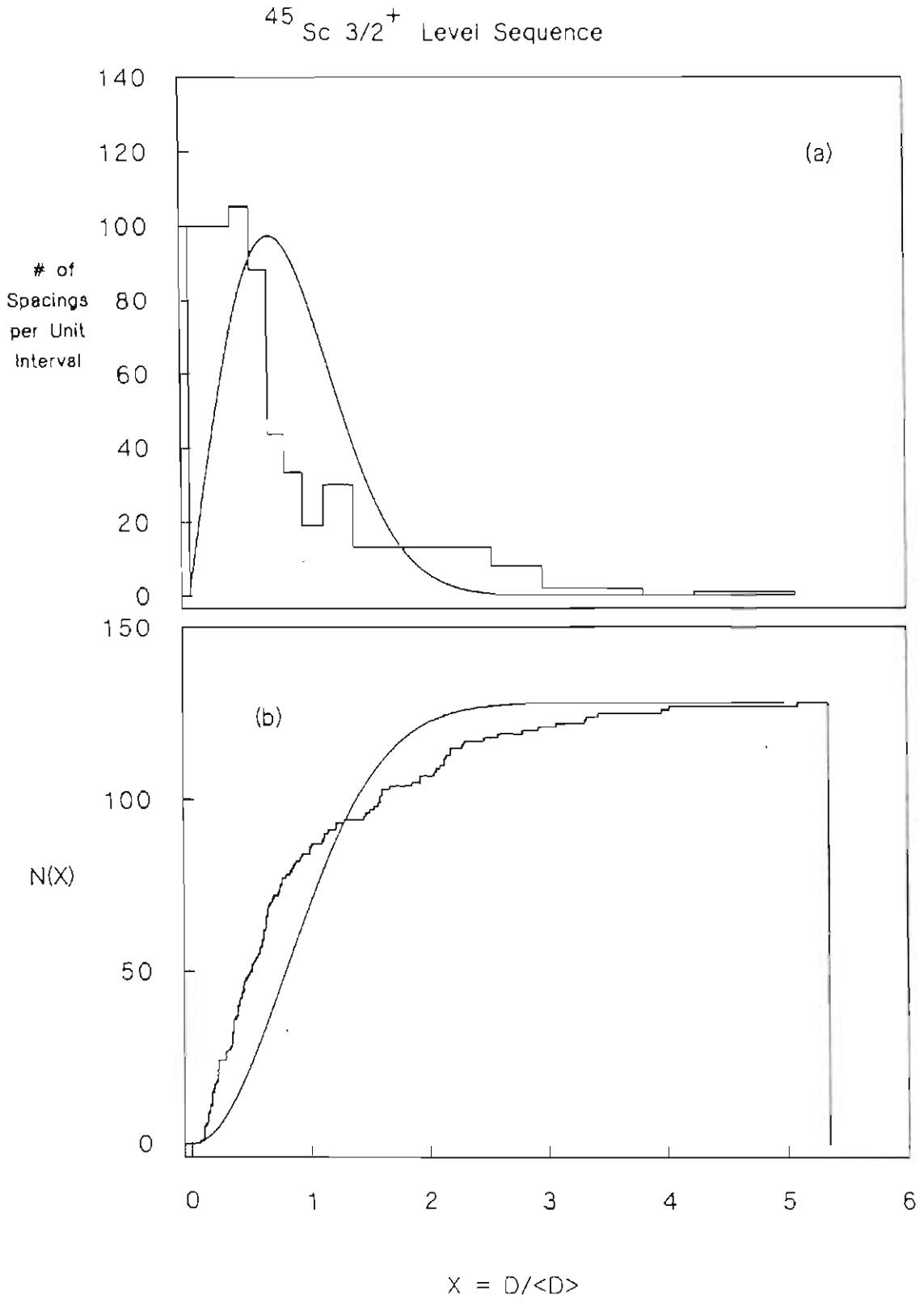
^{45}Sc 3/2^{+} Level Sequence
140
120
100
80
60
40
20
0
# of Spacings per Unit Interval
(a)
150
100
50
0
N(X)
(b)
0
1
2
3
4
5
6
X = D/<D>

Figure 7.5: Wigner distribution overlay comparison for the $5/2^+$ level sequence in ^{45}Sc. Experimental level spacings are plotted (a) in 8 bins of equal probability and (b) as a cumulative distribution.

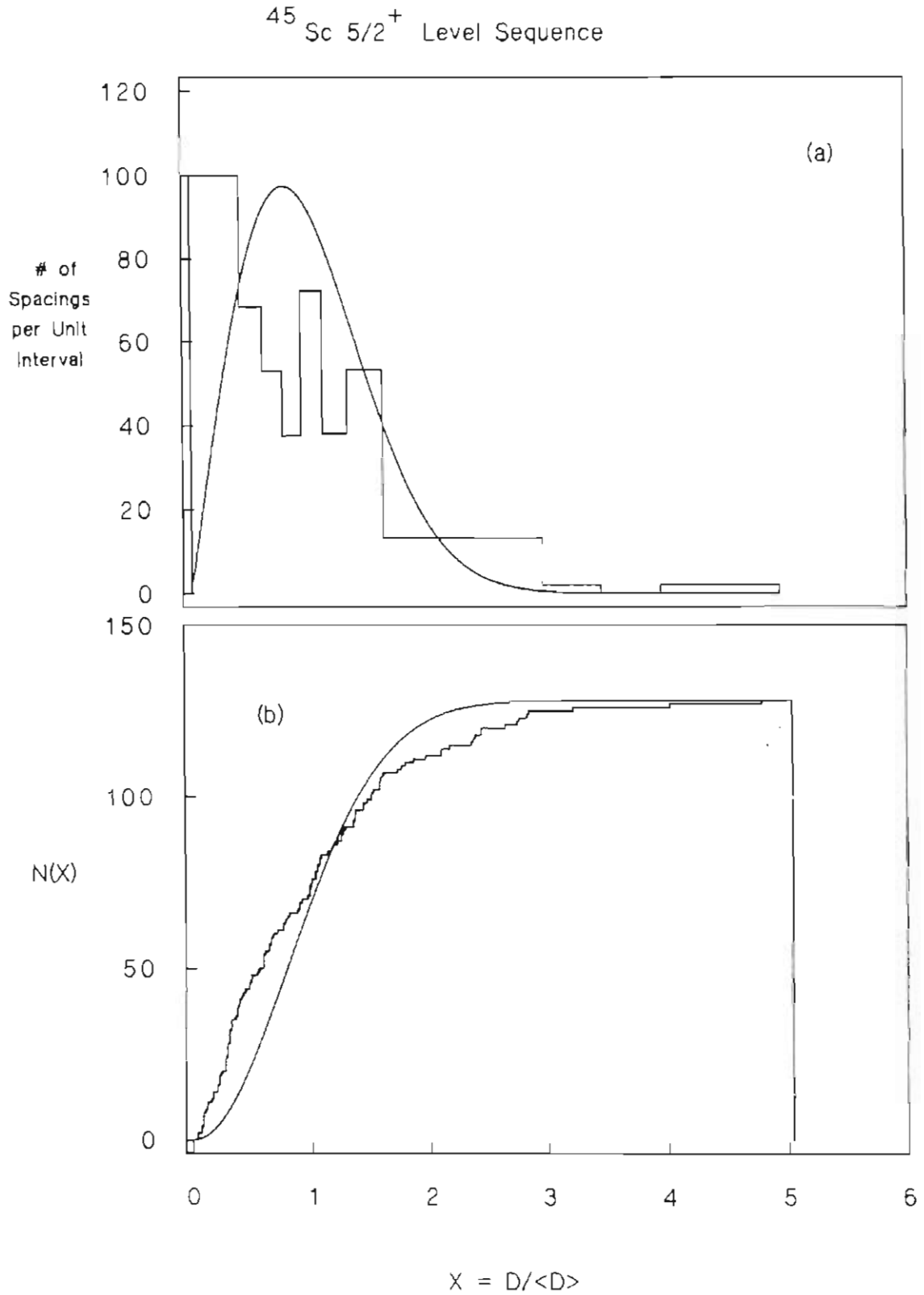
^{45}Sc 5/2^{+} Level Sequence
120
100
80
60
40
20
0
(a)
# of Spacings per Unit Interval
150
100
50
0
(b)
N(X)
0
1
2
3
4
5
6
X = D/<D>

is more prevalent in the p- and d-wave resonances. The ambiguity in the determination of the J value for p- and d-wave resonances was discussed in chapters three and four. Because of these extra levels, the $\ell = 1$ and 2 sequences do not seem to be good candidates for more detailed study until the J assignments are improved.

The other useful statistical test is the Porter-Thomas distribution. In figures 7.6 to 7.10 the observed level sequences for ^{45}Sc are presented in both binned and cumulative plots with an overlay of the PT distribution. The results are similar to the comparison with the Wigner distribution. The PT comparison indicates good agreement for the $1/2^+$ level sequence. However in figures 7.7 to 7.10 it is clear that the other sequences agree less well with the shape of the cumulative PT distribution.

§7.2 Determination of Level Densities in ^{45}Sc.

Using the iterative and bootstrap methods discussed in chapter four, the level densities and missing fractions were obtained for the five level sequences in ^{45}Sc. The results are summarized in Table 7.1.

§7.3 Analysis of Results.

Except for the $1/2^+$ level sequence, the level densities determined for the ^{45}Sc system can not be used for more detailed analysis. Comparisons with the Wigner and Porter-Thomas distributions indicate the the $\ell = 1$ and 2 sequences are impure and incomplete. The $1/2^+$ sequence appears to be reliable, but the other sequences need further experimental work to remove the ambiguity in the J assignment. This additional information would most effectively be obtained by measuring angular distributions for the inelastic channel ^{44}Ca(p,p$'$). These angular distributions would allow an

Figure 7.6: Porter-Thomas distribution overlay comparison for the $1/2^+$ level sequence in ^{45}Sc. Experimental level widths are plotted (a) in 8 bins of equal probability and (b) as a cumulative distribution.

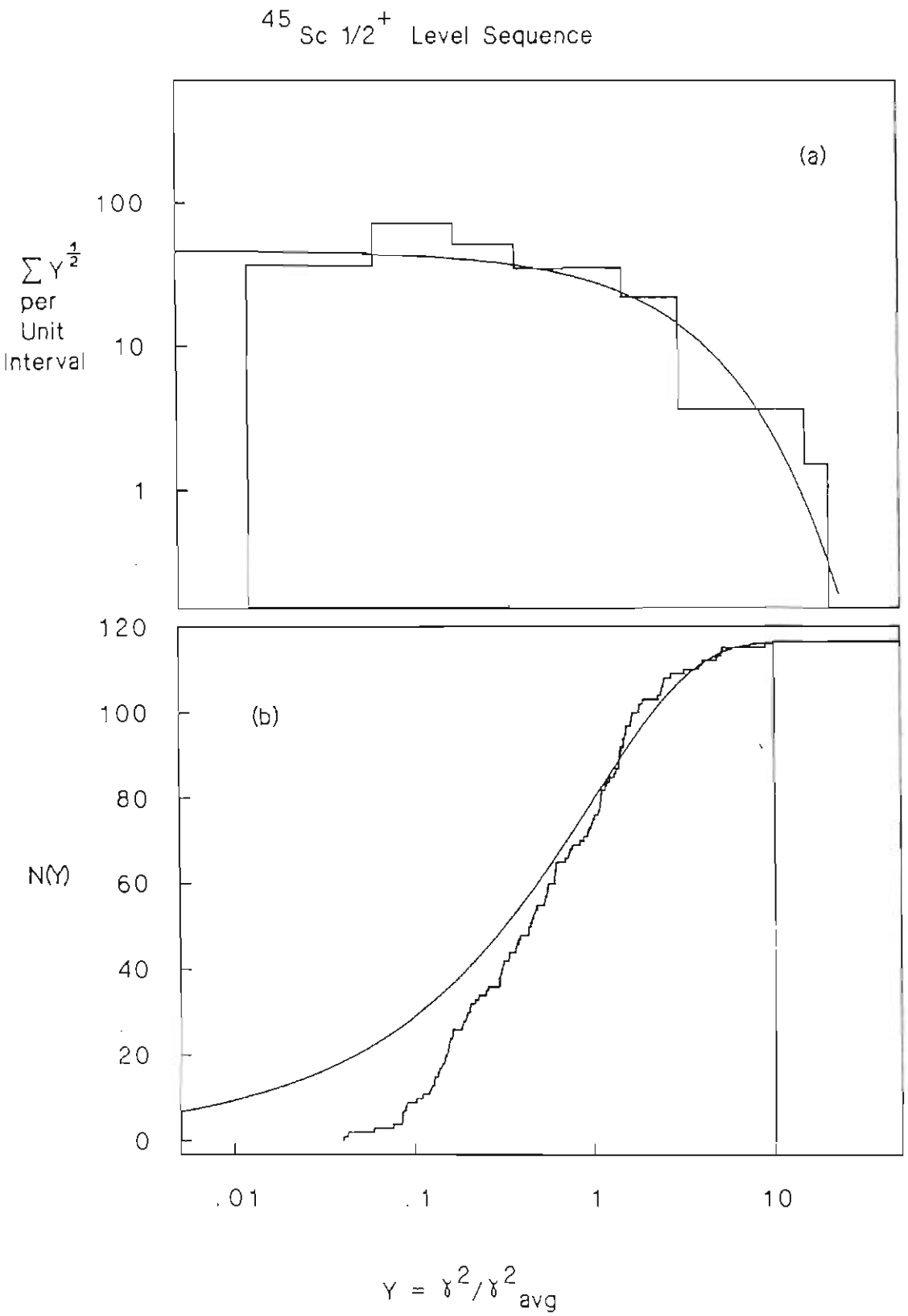
^{45}Sc 1/2^{+} Level Sequence
(a)
100
10
1
$\sum Y^{\frac{1}{2}}$ per Unit Interval
(b)
120
100
80
60
40
20
0
N(Y)
.01
.1
1
10
$Y = \gamma^2/\gamma^2_{avg}$

Figure 7.7: Porter-Thomas distribution overlay comparison for the $1/2^-$ level sequence in ^{45}Sc. The analog states at 3.0 and 3.2 MeV have been removed. Experimental level widths are plotted (a) in 8 bins of equal probability and (b) as a cumulative distribution.

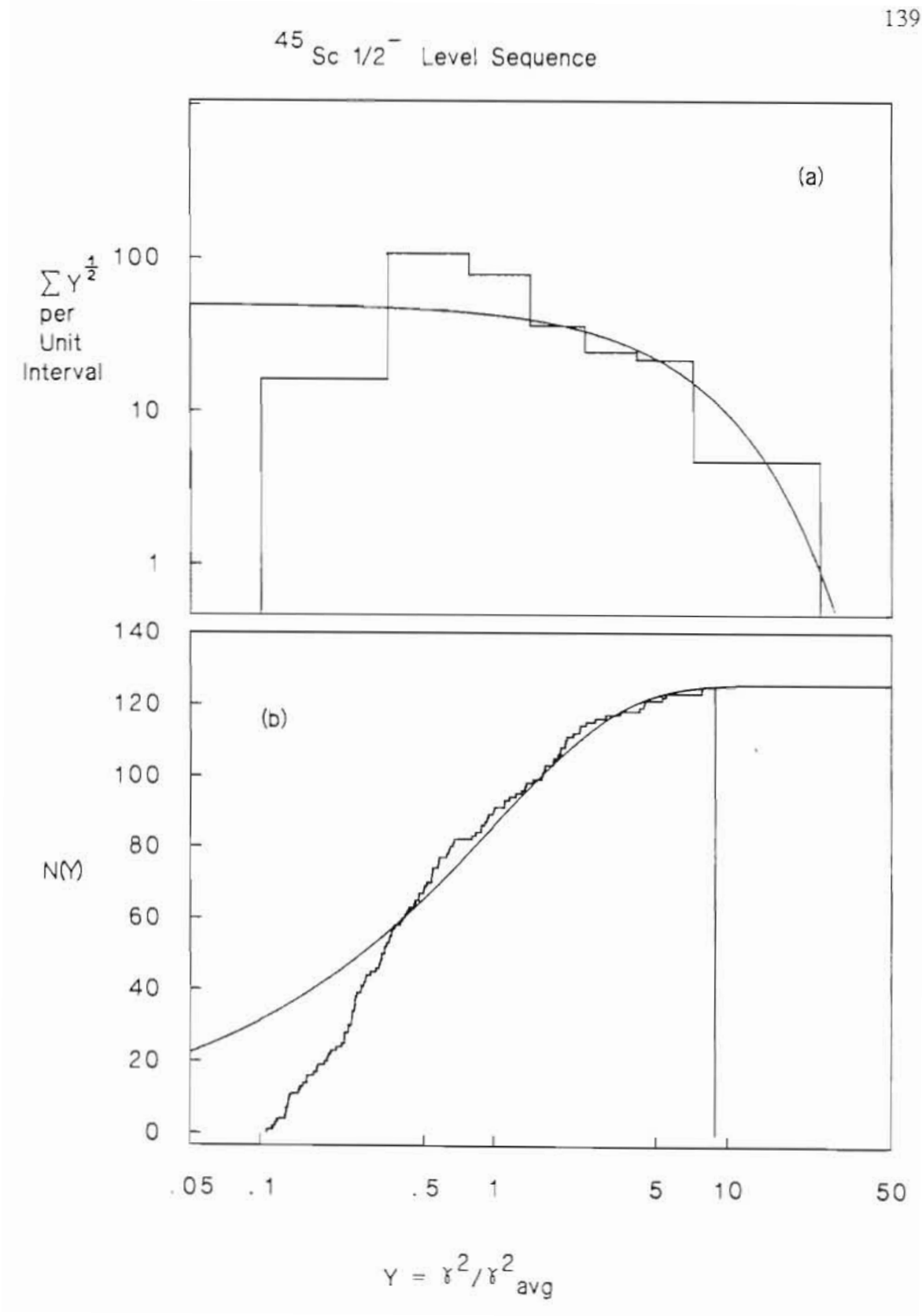
^{45}Sc 1/2$^-$ Level Sequence
(a)
$\sum Y^{\frac{1}{2}}$ per Unit Interval
100
10
1
(b)
N(Y)
140
120
100
80
60
40
20
0
.05
.1
.5
1
5
10
50
$Y = \gamma^2/\gamma^2_{avg}$

Figure 7.8: Porter-Thomas distribution overlay comparison for the $3/2^-$ level sequence in ^{45}Sc. Experimental level widths are plotted (a) in 8 bins of equal probability and (b) as a cumulative distribution.

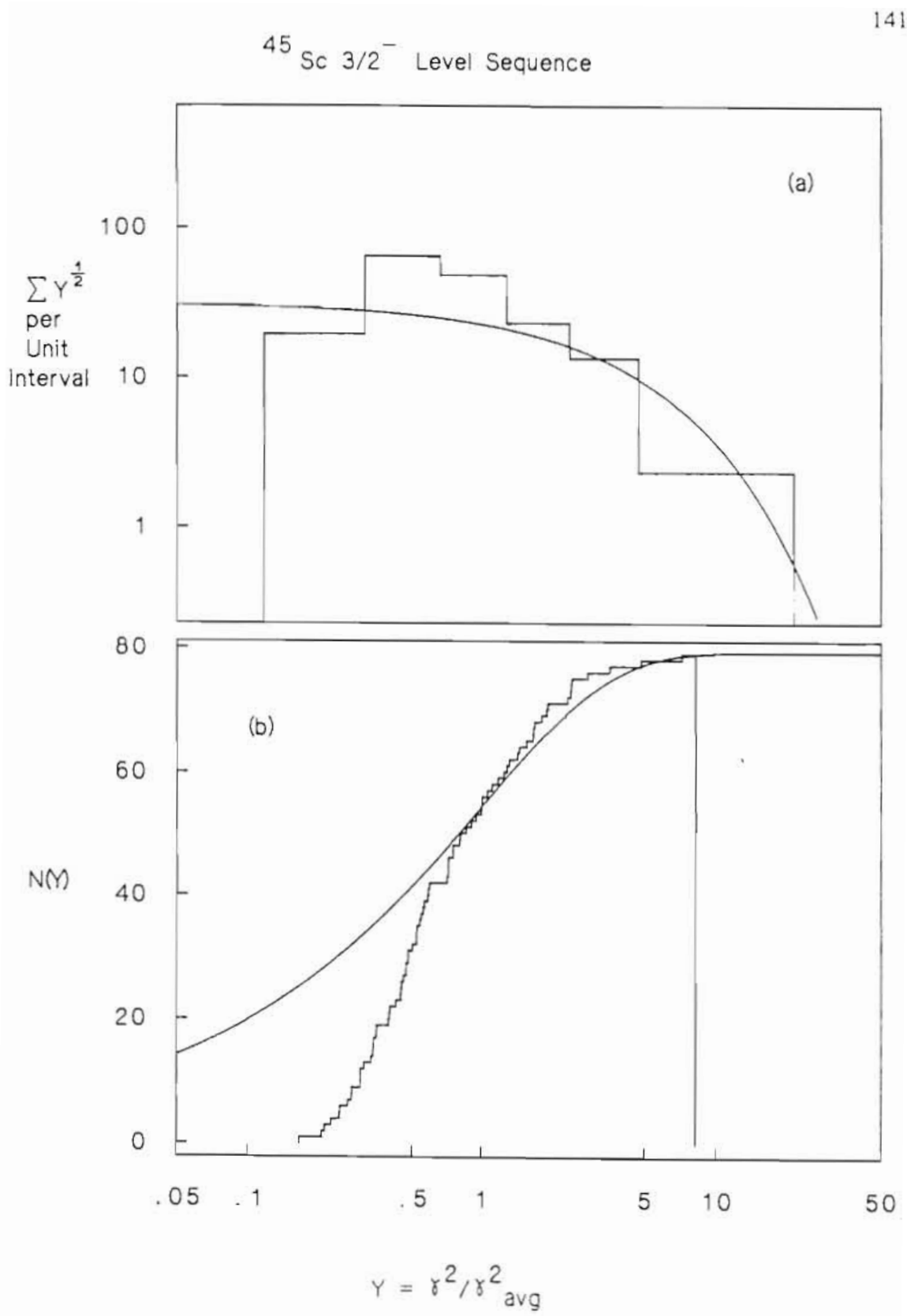
^{45}Sc 3/2$^-$ Level Sequence
(a)
100
10
1
$\sum Y^{\frac{1}{2}}$ per Unit Interval
(b)
80
60
40
20
0
N(Y)
.05
.1
.5
1
5
10
50
$Y = \gamma^2/\gamma^2_{avg}$

Figure 7.9: Porter-Thomas distribution overlay comparison for the $3/2^+$ level sequence in ^{45}Sc. Experimental level widths are plotted (a) in 8 bins of equal probability and (b) as a cumulative distribution.

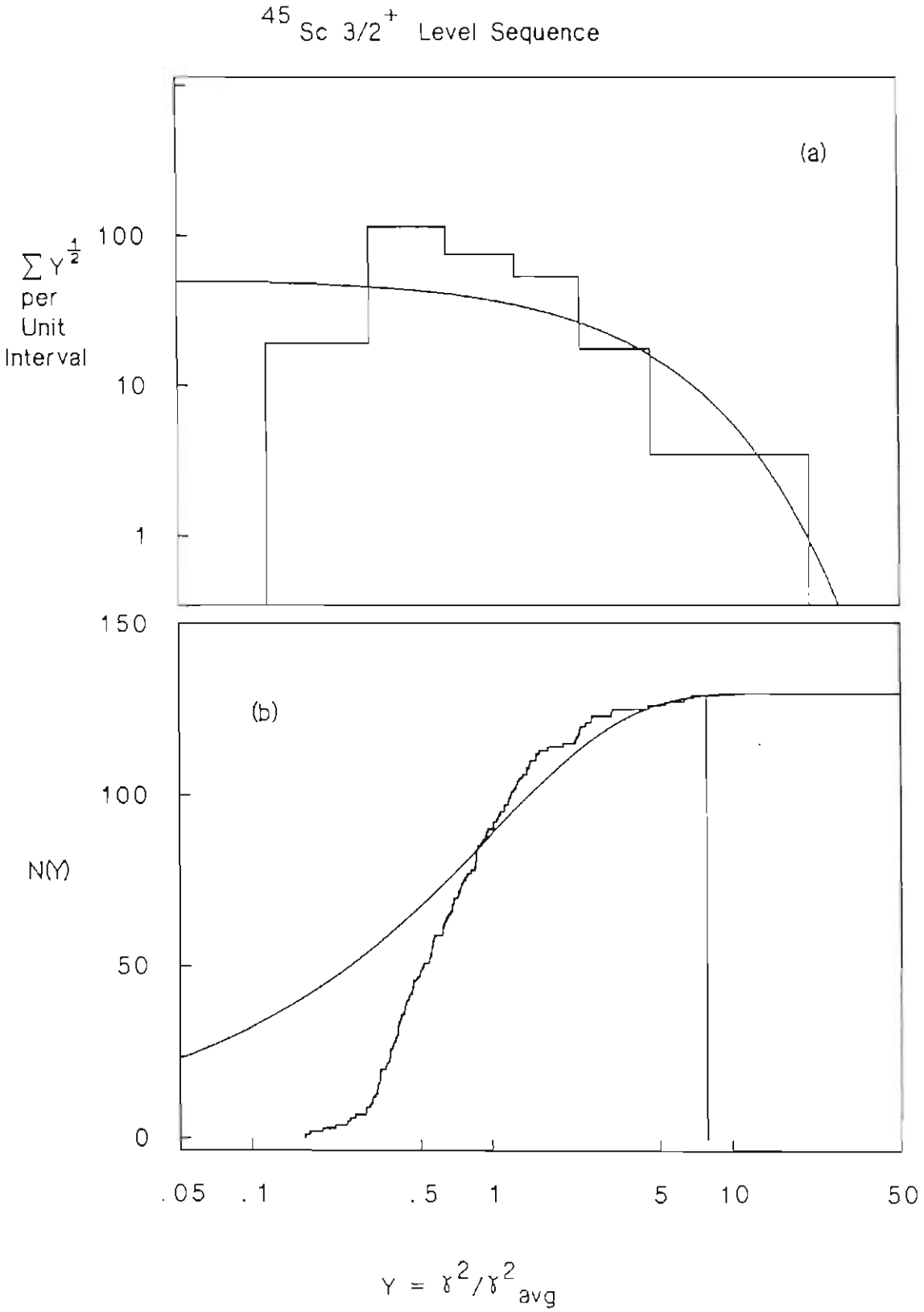
^{45}Sc 3/2^{+} Level Sequence
(a)
$\sum Y^{\frac{1}{2}}$ per Unit Interval
100
10
1
150
(b)
100
N(Y)
50
0
.05
.1
.5
1
5
10
50
$Y = \gamma^2/\gamma^2_{avg}$

Figure 7.10: Porter-Thomas distribution overlay comparison for the $5/2^+$ level sequence in ^{45}Sc. Experimental level widths are plotted (a) in 8 bins of equal probability and (b) as a cumulative distribution.

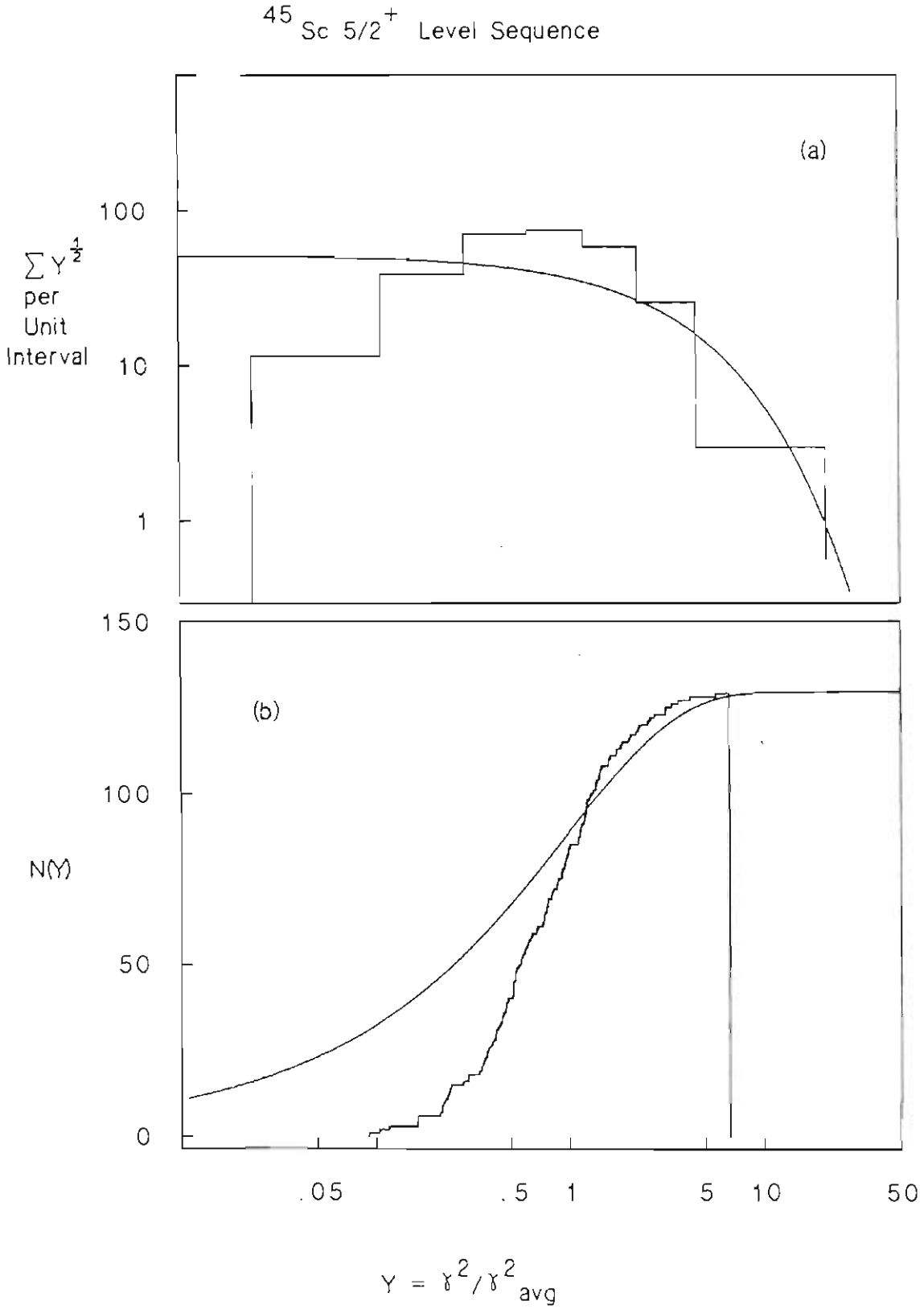
^{45}Sc 5/2^{+} Level Sequence
(a)
100
10
1
$\sum Y^{\frac{1}{2}}$ per Unit Interval
(b)
150
100
50
0
N(Y)
.05
.5
1
5
10
50
$Y = \gamma^2/\gamma^2_{avg}$

Table 7.1: Summary of level sequence parameters for ^{45}Sc

Sequence J^{π}	$N_{observed}$	$\langle\gamma^2\rangle_{observed}$ (eV)	ρ_O[a]	ρ_I[b] (MeV^{-1})	ρ_B[c]	Strength Function[d]
$1/2^+$	116	290.	154.	186.	185.	.054
$1/2^-$[e]	125	291.	166.	237.	225.	.066
$3/2^-$	79	182.	108.	176.	161.	.029
$3/2^+$	129	283.	171.	280.	253.	.072
$5/2^+$	105	226.	142.	192.	189.	.043

Notes:

Due to the inconclusive J assignments for small levels in the $1/2^-$, $3/2^-$, $3/2^+$, and $5/2^+$ level sequences the iterative and bootstrap determined level densities can not be considered reliable.

a: Level density observed, calculated directly from data.

b: Level density calculated using iterative method.

c: Level density calculated using bootstrap method.

d: Strength function calculated using $\langle\gamma^2\rangle_{observed}$ and level density determined from the bootstrap method.

e: Analog states at E_p = 3.0 and 3.2 MeV have been removed.

unambiguous determination of the J value using angular correlation methods (Mitchell,1985).

Chapter Eight

Summary

The s-wave resonance average level densities for eleven nuclides were determined from proton resonance data. These level densities were compared directly with s-wave neutron data; the two sets of level densities were in good agreement. These proton s-wave level densities were also compared with two phenomenological models with favorable results which parallel results from neutron data. These agreements indicate the usefulness of proton resonance data both in accurately determining level densities and in extending the data base for phenomenological level density models.

After these promising results an in depth study of ^{45}Sc was performed. In the ^{45}Sc system resonance parameters for 585 resonances were extracted from the observed reaction $^{44}Ca(p,p)$ for incident proton energies of 2.95 to 3.72 MeV. In this study two $1/2^-$ analog states were observed at energies of 3.0 and 3.2 MeV. The analog state at 3.2 MeV was fragmented into six resonances.

The resonances observed were used to determine the level densities for the various level sequences. Excellent results were obtained for the $1/2^+$ sequence, but the $1/2^-$, $3/2^-$, $3/2^+$ and $5/2^+$ sequences were impure and incomplete. The impurity problems arise from the ambiguity in the J assignment for p- and d-wave resonances. Because of this ambiguity accurate evaluation of the J and parity dependence of the level density is not possible with these data. Further study of the $^{44}Ca(p,p')$ reaction

could eliminate the ambiguity in the J assignments, and make possible more extensive analysis of the parity and J dependence of the average level density.

However the present results do provide the major first step towards the goal of obtaining pure and complete sets of data for large p- and d-wave level sequences.

Appendix A

^{45}Sc Resonance Parameters

Resonance parameters for levels in the ^{45}Sc compound nucleus system observed in the ^{44}Ca(p,p) and ^{44}Ca(p,p´) reactions. The incident proton energy range was 2.95 - 3.72 MeV.

All resonances were fit with the J^{π} that seemed to visually agree best with the data. Although in all cases the best fit was chosen, for some of the resonances there were ambiguities in the J assignment. This generally occurred for p-wave resonances with widths less than ~20eV and for d-wave resonances with widths less than ~10 eV. These lower limits were larger when the resonance had a strong inelastic width or if there was interference with a neighboring level.

The analysis for the inelastic widths is incomplete since there is only limited angular distribution information. In the analysis the lowest acceptable ℓ value was assigned. If there were two or more inelastic channels the widths were initially set equal and adjusted to improve the fit.

Absolute energy errors are ~ 3 keV with relative energy errors on the order of 50-100 eV. Errors for laboratory widths are ~10% increasing to ~20% for widths of many 100 eVs.

^{45}Sc Resonance Parameters

#	Energy (MeV)	J	π	s_p	ℓ_p	Γ_p (eV)	γ^2_p (eV)	$s_{p'}$	$\ell_{p'}$	$\Gamma_{p'}$ (eV)	$\gamma^2_{p'}$ (eV)
1	2.9545	1.5	1	0.5	2	30	408				
								1.5	0	10	240
2	2.9557	2.5	1	0.5	2	15	203				
								2.5	0	10	239
3	2.9561	0.5	1	0.5	0	225	405				
4	2.9565	1.5	-1	0.5	1	150	520				
								1.5	1	13	798
								2.5	1	15	921
5	2.9584	0.5	-1	0.5	1	40	138				
6	2.9610	1.5	1	0.5	2	14	188				
7	2.9637	2.5	1	0.5	2	7	93				
								2.5	0	10	232
8	2.9646	1.5	1	0.5	2	20	267				
								1.5	0	5	115
9	2.9656	0.5	1	0.5	0	265	471				
10	2.9662	2.5	1	0.5	2	12	159				
								2.5	0	7	161
11	2.9669	0.5	-1	0.5	1	75	256				
								1.5	1	20	1180
12	2.9683	0.5	-1	0.5	1	75	255				
13	2.9697	2.5	1	0.5	2	18	238				
14	2.9742	2.5	1	0.5	2	50	655				
								2.5	0	30	672
15	2.9759	2.5	1	0.5	2	7	91				
16	2.9768	0.5	-1	0.5	1	50	168				
17	2.9787	2.5	1	0.5	2	12	156				
								2.5	0	12	264
18	2.9797	0.5	-1	0.5	1	35	117				
								1.5	1	40	2249
19	2.9803	1.5	-1	0.5	1	60	201				
20	2.9813	2.5	1	0.5	2	20	258				
								2.5	0	40	874
21	2.9819	0.5	1	0.5	0	140	244				
22	2.9830	2.5	1	0.5	2	18	232				
								2.5	0	18	391

#	Energy (MeV)	J	π	s_p	ℓ_p	Γ_p (eV)	γ^2_p (eV)	$s_{p'}$	$\ell_{p'}$	$\Gamma_{p'}$ (eV)	$\gamma^2_{p'}$ (eV)
23	2.9842	2.5	1	0.5	2	12	154				
24	2.9847	0.5	-1	0.5	1	20	66				
25	2.9860	0.5	1	0.5	0	235	407				
26	2.9880	1.5	1	0.5	2	25	319				
								1.5	0	75	1601
27	2.9888	1.5	1	0.5	2	15	191				
28	2.9909	2.5	1	0.5	2	6	76				
								2.5	0	10	211
29	2.9914	2.5	1	0.5	2	15	190				
30	2.9926	0.5	-1	0.5	1	30	98				
								1.5	1	100	5359
31	2.9951	0.5	-1	0.5	1	1400	4590				
32	2.9957	1.5	-1	0.5	1	25	81				
								1.5	1	25	1324
								2.5	1	25	1324
33	2.9995	0.5	1	0.5	0	15	25				
34	3.0008	2.5	1	0.5	2	20	249				
								2.5	0	30	612
35	3.0013	1.5	-1	0.5	1	45	146				
								1.5	1	30	1556
								2.5	1	30	1556
36	3.0025	2.5	1	0.5	2	70	872				
								2.5	0	10	203
37	3.0035	0.5	1	0.5	0	25	42				
								1.5	2	15	4550
								2.5	2	15	4550
38	3.0038	0.5	-1	0.5	1	100	323				
39	3.0057	1.5	-1	0.5	1	200	645				
40	3.0076	1.5	-1	0.5	1	15	48				
								1.5	1	10	507
								2.5	1	10	507
41	3.0106	0.5	-1	0.5	1	125	400				
42	3.0115	1.5	-1	0.5	1	60	192				
43	3.0126	1.5	1	0.5	2	20	244				
44	3.0134	1.5	-1	0.5	1	20	63				
45	3.0149	2.5	1	0.5	2	15	182				

#	Energy (MeV)	J	π	s_p	ℓ_p	Γ_p (eV)	γ^2_p (eV)	$s_{p'}$	$\ell_{p'}$	$\Gamma_{p'}$ (eV)	$\gamma^2_{p'}$ (eV)
46	3.0162	2.5	1	0.5	2	17	206				
47	3.0171	2.5	1	0.5	2	20	242				
								2.5	0	10	193
48	3.0177	0.5	1	0.5	0	55	91				
49	3.0189	0.5	-1	0.5	1	50	158				
								1.5	1	20	973
50	3.0194	2.5	1	0.5	2	15	181				
51	3.0196	2.5	1	0.5	2	25	302				
								2.5	0	20	383
52	3.0198	2.5	1	0.5	2	35	422				
53	3.0216	2.5	1	0.5	2	20	240				
								2.5	0	20	380
54	3.0228	2.5	1	0.5	2	10	120				
55	3.0230	0.5	1	0.5	0	40	66				
56	3.0252	1.5	1	0.5	2	30	358				
								1.5	0	50	939
57	3.0263	0.5	1	0.5	0	60	99				
								1.5	2	40	11076
								2.5	2	40	11076
58	3.0271	0.5	-1	0.5	1	40	125				
								1.5	1	100	4724
59	3.0274	0.5	-1	0.5	1	180	563				
60	3.0302	1.5	-1	0.5	1	12	37				
								1.5	1	15	700
61	3.0313	0.5	-1	0.5	1	18	56				
62	3.0347	1.5	1	0.5	2	10	117				
63	3.0391	2.5	1	0.5	2	20	233				
								2.5	0	10	179
64	3.0401	0.5	1	0.5	0	100	162				
65	3.0416	0.5	-1	0.5	1	20	61				
66	3.0423	2.5	1	0.5	2	17	197				
								2.5	0	10	177
67	3.0443	0.5	-1	0.5	1	15	45				
68	3.0468	0.5	1	0.5	0	275	443				
								1.5	2	20	5109
								2.5	2	20	5109

#	Energy (MeV)	J	π	s_p	ℓ_p	Γ_p (eV)	γ^2_p (eV)	$s_{p'}$	$\ell_{p'}$	$\Gamma_{p'}$ (eV)	$\gamma^2_{p'}$ (eV)
69	3.0478	1.5	-1	0.5	1	30	91				
								1.5	1	20	877
								2.5	1	20	877
70	3.0481	2.5	1	0.5	2	25	287				
71	3.0493	1.5	-1	0.5	1	18	54				
								1.5	1	10	436
								2.5	1	10	436
72	3.0516	2.5	1	0.5	2	3	34				
73	3.0534	2.5	1	0.5	2	3	34				
74	3.0544	1.5	1	0.5	2	35	397				
75	3.0551	1.5	-1	0.5	1	27	81				
								1.5	1	40	1710
								2.5	1	40	1710
76	3.0566	0.5	1	0.5	0	225	358				
77	3.0587	2.5	1	0.5	2	3	33				
78	3.0620	0.5	1	0.5	0	40	63				
79	3.0645	2.5	1	0.5	2	25	279				
								2.5	0	10	165
80	3.0659	0.5	1	0.5	0	500	788				
								1.5	2	20	4745
								2.5	2	20	4745
81	3.0665	1.5	1	0.5	2	30	333				
82	3.0673	2.5	1	0.5	2	7	77				
83	3.0710	1.5	-1	0.5	1	150	441				
84	3.0721	1.5	-1	0.5	1	105	308				
								2.5	1	30	1209
85	3.0732	2.5	1	0.5	2	10	110				
86	3.0744	0.5	1	0.5	0	25	39				
87	3.0769	1.5	-1	0.5	1	300	875				
88	3.0781	0.5	-1	0.5	1	250	728				
89	3.0787	1.5	1	0.5	2	35	381				
90	3.0795	2.5	1	0.5	2	50	544				
								2.5	0	10	157
91	3.0824	1.5	1	0.5	2	8	86				
92	3.0832	1.5	-1	0.5	1	450	1302				
								1.5	1	150	5821

#	Energy (MeV)	J	π	s_p	ℓ_p	Γ_p (eV)	γ^2_p (eV)	$s_{p'}$	$\ell_{p'}$	$\Gamma_{p'}$ (eV)	$\gamma^2_{p'}$ (eV)
								2.5	1	75	2910
93	3.0847	0.5	-1	0.5	1	50	144				
94	3.0872	0.5	-1	0.5	1	25	71				
95	3.0880	2.5	1	0.5	2	7	75				
96	3.0899	2.5	1	0.5	2	45	481				
97	3.0909	0.5	-1	0.5	1	150	429				
98	3.0923	0.5	1	0.5	0	250	382				
99	3.0934	1.5	-1	0.5	1	30	85				
								1.5	1	15	562
								2.5	1	15	562
100	3.0956	0.5	-1	0.5	1	20	56				
101	3.0960	1.5	1	0.5	2	12	126				
102	3.0970	1.5	-1	0.5	1	150	426				
103	3.0990	1.5	1	0.5	2	15	157				
								1.5	0	20	295
104	3.1025	1.5	1	0.5	2	8	83				
105	3.1032	0.5	1	0.5	0	60	90				
106	3.1038	1.5	1	0.5	2	10	104				
107	3.1059	1.5	1	0.5	2	25	260				
108	3.1065	0.5	-1	0.5	1	115	322				
109	3.1095	0.5	1	0.5	0	50	74				
110	3.1135	0.5	1	0.5	0	25	37				
111	3.1137	2.5	1	0.5	2	25	256				
112	3.1140	1.5	-1	0.5	1	125	346				
								1.5	1	15	524
								2.5	1	25	874
113	3.1191	2.5	1	0.5	2	5	50				
114	3.1199	0.5	1	0.5	0	40	59				
115	3.1207	2.5	1	0.5	2	15	152				
								2.5	0	50	691
116	3.1212	1.5	1	0.5	2	25	253				
117	3.1223	1.5	1	0.5	2	10	101				
118	3.1239	1.5	-1	0.5	1	50	136				
119	3.1245	2.5	1	0.5	2	10	100				
								2.5	0	50	683
120	3.1250	0.5	1	0.5	0	20	29				

#	Energy (MeV)	J	π	s_p	ℓ_p	Γ_p (eV)	γ^2_p (eV)	$s_{p'}$	$\ell_{p'}$	$\Gamma_{p'}$ (eV)	$\gamma^2_{p'}$ (eV)
121	3.1268	1.5	-1	0.5	1	20	54				
122	3.1270	0.5	1	0.5	0	175	257				
123	3.1291	0.5	-1	0.5	1	1500	4080				
124	3.1321	2.5	1	0.5	2	8	79				
125	3.1339	2.5	1	0.5	2	30	297				
								2.5	0	5	66
126	3.1352	1.5	1	0.5	2	75	742				
								1.5	0	35	463
127	3.1370	0.5	1	0.5	0	15	21				
128	3.1416	1.5	-1	0.5	1	80	214				
								1.5	1	40	1278
								1.5	3	40	79556
129	3.1426	2.5	1	0.5	2	8	78				
								2.5	0	4	51
130	3.1434	1.5	-1	0.5	1	40	106				
								1.5	1	15	476
								2.5	1	10	317
131	3.1451	1.5	1	0.5	2	25	243				
								1.5	0	40	513
132	3.1455	0.5	-1	0.5	1	50	133				
133	3.1457	0.5	1	0.5	0	225	324				
134	3.1471	1.5	1	0.5	2	25	242				
135	3.1480	1.5	-1	0.5	1	40	106				
								1.5	1	70	2190
136	3.1482	0.5	-1	0.5	1	200	530				
137	3.1487	1.5	-1	0.5	1	125	331				
								1.5	1	100	3122
								2.5	1	40	1249
138	3.1500	2.5	1	0.5	2	20	193				
139	3.1501	1.5	-1	0.5	1	100	264				
								1.5	1	10	310
								2.5	1	15	466
140	3.1515	1.5	1	0.5	2	25	240				
141	3.1517	0.5	1	0.5	0	150	214				
142	3.1533	0.5	1	0.5	0	300	428				
143	3.1540	1.5	1	0.5	2	15	143				

#	Energy (MeV)	J	π	s_p	ℓ_p	Γ_p (eV)	γ^2_p (eV)	$s_{p'}$	$\ell_{p'}$	$\Gamma_{p'}$ (eV)	$\gamma^2_{p'}$ (eV)
144	3.1547	0.5	-1	0.5	1	200	525				
								1.5	1	150	4594
145	3.1554	0.5	-1	0.5	1	60	157				
								1.5	1	25	764
146	3.1561	2.5	1	0.5	2	30	286				
								2.5	0	30	373
147	3.1575	2.5	1	0.5	2	15	143				
								2.5	0	25	309
148	3.1585	2.5	1	0.5	2	20	190				
								2.5	0	40	493
149	3.1598	0.5	-1	0.5	1	1250	3265				
150	3.1604	2.5	1	0.5	2	50	474				
								2.5	0	25	306
151	3.1611	0.5	-1	0.5	1	500	1303				
152	3.1626	0.5	-1	0.5	1	60	156				
153	3.1631	1.5	1	0.5	2	70	661				
								1.5	0	50	609
154	3.1635	1.5	-1	0.5	1	100	259				
								2.5	1	15	446
155	3.1639	1.5	-1	0.5	1	60	155				
156	3.1641	0.5	1	0.5	0	150	211				
157	3.1644	2.5	1	0.5	2	125	1179				
								2.5	0	40	485
158	3.1673	2.5	1	0.5	2	75	704				
								2.5	0	40	481
159	3.1702	0.5	-1	0.5	1	500	1288				
160	3.1708	0.5	-1	0.5	1	75	193				
161	3.1748	1.5	-1	0.5	1	40	102				
162	3.1755	0.5	1	0.5	0	500	697				
163	3.1760	1.5	1	0.5	2	12	111				
164	3.1766	2.5	1	0.5	2	12	110				
								2.5	0	30	351
165	3.1809	1.5	1	0.5	2	20	183				
								1.5	0	40	462
166	3.1823	0.5	-1	0.5	1	115	291				
								1.5	1	25	701

#	Energy (MeV)	J	π	s_p	ℓ_p	Γ_p (eV)	γ^2_p (eV)	$s_{p'}$	$\ell_{p'}$	$\Gamma_{p'}$ (eV)	$\gamma^2_{p'}$ (eV)
167	3.1835	0.5	1	0.5	0	100	138				
168	3.1845	1.5	1	0.5	2	15	136				
169	3.1853	0.5	-1	0.5	1	1500	3791				
170	3.1857	0.5	1	0.5	0	400	551				
171	3.1861	2.5	1	0.5	2	40	364				
172	3.1866	1.5	1	0.5	2	100	909				
173	3.1896	1.5	-1	0.5	1	20	50				
								1.5	1	15	411
								1.5	3	35	57572
174	3.1913	0.5	1	0.5	0	225	308				
175	3.1917	1.5	1	0.5	2	23	207				
176	3.1935	2.5	1	0.5	2	18	161				
177	3.1948	1.5	-1	0.5	1	20	49				
								1.5	1	15	404
								1.5	3	30	48362
178	3.1964	0.5	1	0.5	0	300	409				
179	3.1970	2.5	1	0.5	2	15	134				
180	3.1974	2.5	1	0.5	2	10	89				
181	3.1991	0.5	-1	0.5	1	60	148				
182	3.2004	1.5	-1	0.5	1	25	61				
								1.5	1	15	397
								2.5	1	5	132
183	3.2011	1.5	1	0.5	2	10	88				
								1.5	0	20	218
184	3.2020	0.5	-1	0.5	1	500	1237				
185	3.2024	0.5	1	0.5	0	40	54				
								1.5	2	40	5778
								2.5	2	40	5778
186	3.2029	0.5	-1	0.5	1	40	98				
187	3.2049	0.5	-1	0.5	1	30	73				
188	3.2055	2.5	1	0.5	2	60	529				
								2.5	0	150	1617
189	3.2078	0.5	-1	0.5	1	30	73				
190	3.2082	0.5	1	0.5	0	150	202				
191	3.2118	2.5	1	0.5	2	45	393				
192	3.2125	1.5	-1	0.5	1	35	85				

#	Energy (MeV)	J	π	s_p	ℓ_p	Γ_p (eV)	γ^2_p (eV)	$s_{p'}$	$\ell_{p'}$	$\Gamma_{p'}$ (eV)	$\gamma^2_{p'}$ (eV)
193	3.2146	1.5	1	0.5	2	15	130				
194	3.2157	2.5	1	0.5	2	10	86				
195	3.2160	0.5	-1	0.5	1	100	243				
								1.5	1	100	2529
196	3.2173	0.5	1	0.5	0	700	933				
197	3.2194	1.5	-1	0.5	1	25	60				
198	3.2199	2.5	1	0.5	2	50	431				
								2.5	0	75	776
199	3.2209	1.5	-1	0.5	1	75	181				
								1.5	1	30	747
200	3.2226	0.5	-1	0.5	1	200	482				
201	3.2232	0.5	-1	0.5	1	3500	8431				
202	3.2246	0.5	1	0.5	0	100	132				
203	3.2252	2.5	1	0.5	2	45	384				
204	3.2256	2.5	1	0.5	2	30	256				
205	3.2261	2.5	1	0.5	2	30	256				
206	3.2268	1.5	-1	0.5	1	100	239				
207	3.2277	2.5	1	0.5	2	40	340				
								2.5	0	50	506
208	3.2301	0.5	1	0.5	0	2000	2632				
209	3.2325	2.5	1	0.5	2	20	169				
210	3.2332	1.5	-1	0.5	1	40	95				
211	3.2344	0.5	-1	0.5	1	5000	11877				
212	3.2354	2.5	1	0.5	2	10	84				
213	3.2369	0.5	-1	0.5	1	200	473				
214	3.2389	0.5	-1	0.5	1	1750	4133				
215	3.2396	0.5	1	0.5	0	75	97				
216	3.2429	2.5	1	0.5	2	40	332				
217	3.2430	0.5	1	0.5	0	300	389				
218	3.2447	1.5	1	0.5	2	40	331				
219	3.2487	2.5	1	0.5	2	15	123				
220	3.2500	2.5	1	0.5	2	10	82				
221	3.2513	1.5	1	0.5	2	15	123				
222	3.2515	0.5	1	0.5	0	125	160				
								1.5	2	15	1835
								2.5	2	15	1835

#	Energy (MeV)	J	π	s_p	ℓ_p	Γ_p (eV)	γ^2_p (eV)	$s_{p'}$	$\ell_{p'}$	$\Gamma_{p'}$ (eV)	$\gamma^2_{p'}$ (eV)
223	3.2518	2.5	1	0.5	2	15	123				
224	3.2541	2.5	1	0.5	2	13	106				
								2.5	0	30	282
225	3.2572	0.5	1	0.5	0	25	32				
226	3.2599	0.5	-1	0.5	1	30	69				
								1.5	1	15	332
227	3.2606	1.5	1	0.5	2	25	202				
								1.5	0	25	231
228	3.2618	0.5	-1	0.5	1	50	114				
								1.5	1	25	551
229	3.2622	0.5	1	0.5	0	250	318				
230	3.2626	1.5	1	0.5	2	20	161				
								1.5	0	30	276
231	3.2656	0.5	-1	0.5	1	300	685				
232	3.2669	2.5	1	0.5	2	20	160				
233	3.2676	0.5	-1	0.5	1	15	34				
234	3.2685	2.5	1	0.5	2	25	199				
								2.5	0	50	453
235	3.2692	0.5	-1	0.5	1	300	682				
236	3.2702	0.5	1	0.5	0	100	126				
237	3.2725	0.5	-1	0.5	1	250	566				
238	3.2736	0.5	-1	0.5	1	40	90				
239	3.2791	2.5	1	0.5	2	15	117				
240	3.2794	0.5	1	0.5	0	125	156				
241	3.2799	1.5	1	0.5	2	20	157				
242	3.2804	0.5	-1	0.5	1	35	78				
243	3.2825	1.5	-1	0.5	1	20	44				
								1.5	1	50	1039
								1.5	3	50	57986
244	3.2832	0.5	1	0.5	0	30	37				
245	3.2841	0.5	-1	0.5	1	45	100				
246	3.2865	1.5	1	0.5	2	15	116				
								1.5	0	30	259
247	3.2890	0.5	-1	0.5	1	75	166				
248	3.2901	1.5	1	0.5	2	20	154				
249	3.2939	1.5	1	0.5	2	25	192				

#	Energy (MeV)	J	π	s_p	ℓ_p	Γ_p (eV)	γ^2_p (eV)	$s_{p'}$	$\ell_{p'}$	$\Gamma_{p'}$ (eV)	$\gamma^2_{p'}$ (eV)
250	3.2941	0.5	1	0.5	0	275	339				
251	3.2946	1.5	1	0.5	2	35	268				
252	3.2958	2.5	1	0.5	2	14	107				
253	3.2958	1.5	1	0.5	2	20	153				
254	3.2960	0.5	1	0.5	0	125	153				
255	3.2965	2.5	1	0.5	2	14	107				
256	3.2992	1.5	1	0.5	2	15	114				
257	3.2998	0.5	1	0.5	0	35	42				
258	3.3027	1.5	-1	0.5	1	75	163				
								1.5	1	60	1177
								2.5	1	50	981
259	3.3050	0.5	1	0.5	0	350	427				
								1.5	2	15	1542
								2.5	2	15	1542
260	3.3062	0.5	1	0.5	0	20	24				
								1.5	2	15	1537
								2.5	2	15	1537
261	3.3084	0.5	1	0.5	0	10	12				
262	3.3106	1.5	1	0.5	2	15	112				
263	3.3135	1.5	-1	0.5	1	60	129				
								1.5	1	15	285
								2.5	1	15	285
264	3.3144	1.5	-1	0.5	1	50	107				
								1 5	1	20	379
								2.5	1	15	284
265	3.3152	0.5	1	0.5	0	1250	1510				
								1.5	2	20	1991
								2.5	2	20	1991
266	3.3167	0.5	-1	0.5	1	20	43				
267	3.3178	0.5	-1	0.5	1	40	85				
268	3.3200	1.5	-1	0.5	1	85	182				
								1.5	1	10	186
								2.5	1	10	186
269	3.3215	0.5	1	0.5	0	30	36				
								1.5	2	30	2928
								2.5	2	30	2928

#	Energy (MeV)	J	π	s_p	ℓ_p	Γ_p (eV)	γ^2_p (eV)	$s_{p'}$	$\ell_{p'}$	$\Gamma_{p'}$ (eV)	$\gamma^2_{p'}$ (eV)
270	3.3228	0.5	1	0.5	0	150	179				
271	3.3234	1.5	-1	0.5	1	30	64				
								1.5	1	30	555
								2.5	1	25	463
272	3.3248	2.5	1	0.5	2	15	109				
								2.5	0	20	156
273	3.3253	0.5	1	0.5	0	600	718				
								1.5	2	30	2894
								2.5	2	30	2894
274	3.3255	0.5	-1	0.5	1	45	95				
275	3.3269	2.5	1	0.5	2	50	365				
								2.5	0	5	39
276	3.3271	0.5	-1	0.5	1	125	265				
277	3.3277	0.5	-1	0.5	1	50	106				
278	3.3302	1.5	1	0.5	2	20	145				
								1.5	0	10	77
279	3.3305	0.5	-1	0.5	1	20	42				
280	3.3311	1.5	1	0.5	2	15	108				
								1.5	0	10	77
281	3.3332	1.5	1	0.5	2	50	362				
								1.5	0	15	115
282	3.3362	2.5	1	0.5	2	25	180				
								2.5	2	25	2331
283	3.3365	0.5	1	0.5	0	50	59				
284	3.3372	1.5	1	0.5	2	15	107				
								1.5	0	30	228
285	3.3385	1.5	1	0.5	2	10	71				
								1.5	0	15	113
286	3.3398	1.5	1	0.5	2	40	286				
								1.5	0	25	188
287	3.3412	0.5	1	0.5	0	150	176				
288	3.3435	0.5	1	0.5	0	150	176				
289	3.3437	0.5	-1	0.5	1	75	156				
290	3.3442	1.5	1	0.5	2	25	178				
								1.5	0	50	373
291	3.3452	2.5	1	0.5	2	10	71				

#	Energy (MeV)	J	π	s_p	ℓ_p	Γ_p (eV)	γ^2_p (eV)	$s_{p'}$	$\ell_{p'}$	$\Gamma_{p'}$ (eV)	$\gamma^2_{p'}$ (eV)
								2.5	0	20	149
292	3.3475	1.5	1	0.5	2	275	1949				
								1.5	2	20	1800
								2.5	2	40	3601
293	3.3513	1.5	1	0.5	2	15	105				
								2.5	2	15	1334
								2.5	4	15	0
294	3.3514	0.5	-1	0.5	1	50	103				
								1.5	1	100	1715
295	3.3530	1.5	1	0.5	2	50	351				
296	3.3532	0.5	1	0.5	0	450	524				
297	3.3537	2.5	1	0.5	2	14	98				
298	3.3541	1.5	1	0.5	2	15	105				
299	3.3563	1.5	1	0.5	2	25	174				
300	3.3589	1.5	1	0.5	2	30	209				
301	3.3591	0.5	1	0.5	0	350	405				
								1.5	2	25	2172
								2.5	2	25	2172
302	3.3595	1.5	1	0.5	2	35	243				
303	3.3605	1.5	1	0.5	2	10	69				
304	3.3614	0.5	-1	0.5	1	40	81				
305	3.3627	0.5	-1	0.5	1	35	71				
306	3.3635	1.5	-1	0.5	1	115	234				
307	3.3647	2.5	1	0.5	2	25	172				
								2.5	0	15	106
308	3.3668	0.5	-1	0.5	1	25	50				
309	3.3673	1.5	1	0.5	2	65	447				
								1.5	2	25	2118
								2.5	2	75	6355
310	3.3678	1.5	-1	0.5	1	50	101				
								1.5	1	80	1312
								2.5	1	20	328
311	3.3696	0.5	1	0.5	0	10	11				
								1.5	2	10	841
								2.5	2	10	841
312	3.3719	0.5	1	0.5	0	50	57				

#	Energy (MeV)	J	π	s_p	ℓ_p	Γ_p (eV)	γ^2_p (eV)	$s_{p'}$	$\ell_{p'}$	$\Gamma_{p'}$ (eV)	$\gamma^2_{p'}$ (eV)
313	3.3728	1.5	1	0.5	2	30	204				
								1.5	0	15	104
314	3.3742	0.5	-1	0.5	1	40	80				
								1.5	1	40	645
315	3.3760	1.5	1	0.5	2	50	339				
316	3.3763	0.5	1	0.5	0	1000	1140				
								1.5	2	25	2061
								2.5	2	25	2061
317	3.3769	1.5	1	0.5	2	40	271				
318	3.3791	2.5	1	0.5	2	40	270				
319	3.3803	0.5	1	0.5	0	100	113				
								1.5	2	20	1629
								2.5	2	20	1629
320	3.3855	1.5	-1	0.5	1	50	99				
								1.5	1	15	234
								2.5	1	25	391
321	3.3865	0.5	1	0.5	0	15	16				
322	3.3880	2.5	1	0.5	2	50	333				
								2.5	0	25	167
323	3.3898	0.5	1	0.5	0	1350	1520				
								1.5	2	20	1583
								2.5	2	20	1583
324	3.3909	0.5	1	0.5	0	50	56				
								1.5	2	20	1578
								2.5	2	20	1578
325	3.3946	1.5	-1	0.5	1	75	147				
								1.5	1	75	1146
326	3.3951	1.5	1	0.5	2	20	132				
								1.5	2	40	3117
								2.5	2	40	3117
327	3.3960	0.5	-1	0.5	1	25	49				
328	3.3984	0.5	-1	0.5	1	40	78				
329	3.4004	2.5	1	0.5	2	15	98				
330	3.4027	1.5	1	0.5	2	20	130				
								1.5	0	30	194
331	3.4037	2.5	1	0.5	2	15	97				

#	Energy (MeV)	J	π	s_p	ℓ_p	Γ_p (eV)	γ^2_p (eV)	$s_{p'}$	$\ell_{p'}$	$\Gamma_{p'}$ (eV)	$\gamma^2_{p'}$ (eV)
								2.5	0	30	194
332	3.4041	0.5	1	0.5	0	80	88				
333	3.4044	2.5	1	0.5	2	100	652				
								2.5	0	10	64
334	3.4060	0.5	-1	0.5	1	30	58				
								1.5	1	30	445
335	3.4070	1.5	1	0.5	2	75	487				
336	3.4080	0.5	-1	0.5	1	250	484				
337	3.4100	0.5	1	0.5	0	40	44				
								1.5	2	40	2982
								2.5	2	40	2982
338	3.4104	1.5	1	0.5	2	30	193				
								1.5	0	50	318
339	3.4129	0.5	-1	0.5	1	150	288				
								1.5	1	200	2915
340	3.4131	0.5	1	0.5	0	200	220				
341	3.4164	1.5	1	0.5	2	100	640				
342	3.4170	1.5	1	0.5	2	50	320				
								1.5	0	60	376
343	3.4173	0.5	1	0.5	0	250	274				
344	3.4184	0.5	-1	0.5	1	50	95				
345	3.4190	1.5	1	0.5	2	200	1277				
								1.5	0	30	187
								1.5	2	30	2178
								2.5	2	60	4357
346	3.4203	1.5	1	0.5	2	15	95				
347	3.4212	2.5	1	0.5	2	40	254				
								2.5	0	30	186
348	3.4220	1.5	1	0.5	2	25	158				
								1.5	0	25	155
349	3.4228	0.5	1	0.5	0	1300	1420				
								1.5	2	50	3591
								2.5	2	50	3591
350	3.4234	2.5	1	0.5	2	20	126				
351	3.4237	0.5	-1	0.5	1	35	66				
								1.5	1	35	496

#	Energy (MeV)	J	π	s_p	ℓ_p	Γ_p (eV)	γ^2_p (eV)	$s_{p'}$	$\ell_{p'}$	$\Gamma_{p'}$ (eV)	$\gamma^2_{p'}$ (eV)
352	3.4240	1.5	1	0.5	2	14	88				
353	3.4244	0.5	-1	0.5	1	20	38				
354	3.4265	1.5	-1	0.5	1	50	94				
								1.5	1	25	351
								2.5	1	25	351
355	3.4270	2.5	1	0.5	2	17	107				
								2.5	0	30	183
356	3.4281	1.5	1	0.5	2	20	126				
								2.5	2	40	2828
357	3.4316	0.5	-1	0.5	1	50	94				
								1.5	1	50	694
358	3.4320	0.5	1	0.5	0	100	108				
								1.5	2	100	6992
								2.5	2	100	6992
359	3.4324	0.5	-1	0.5	1	850	1602				
360	3.4329	2.5	1	0.5	2	10	62				
								2.5	0	10	60
361	3.4353	1.5	1	0.5	2	15	93				
362	3.4359	0.5	-1	0.5	1	250	469				
363	3.4366	0.5	-1	0.5	1	100	187				
364	3.4382	0.5	-1	0.5	1	50	93				
365	3.4386	0.5	1	0.5	0	125	134				
366	3.4390	2.5	1	0.5	2	25	155				
367	3.4396	0.5	-1	0.5	1	125	233				
368	3.4440	1.5	1	0.5	2	60	369				
								1.5	0	25	147
369	3.4447	1.5	-1	0.5	1	70	130				
370	3.4450	0.5	1	0.5	0	100	107				
								1.5	2	25	1683
								2.5	2	25	1683
371	3.4452	2.5	1	0.5	2	50	307				
								2.5	0	10	58
372	3.4490	1.5	1	0.5	2	50	305				
373	3.4492	0.5	1	0.5	0	450	480				
374	3.4498	2.5	1	0.5	2	12	73				
375	3.4506	0.5	-1	0.5	1	100	184				

#	Energy (MeV)	J	π	s_p	ℓ_p	Γ_p (eV)	γ^2_p (eV)	$s_{p'}$	$\ell_{p'}$	$\Gamma_{p'}$ (eV)	$\gamma^2_{p'}$ (eV)
376	3.4510	0.5	1	0.5	0	50	53				
								1.5	2	40	2647
								2.5	2	40	2647
377	3.4521	1.5	1	0.5	2	20	121				
378	3.4534	1.5	1	0.5	2	15	91				
								1.5	0	45	259
379	3.4544	0.5	-1	0.5	1	25	46				
								1.5	1	50	656
380	3.4567	0.5	1	0.5	0	150	159				
381	3.4569	0.5	-1	0.5	1	75	137				
382	3.4574	0.5	-1	0.5	1	150	275				
383	3.4586	1.5	1	0.5	2	300	1811				
								1.5	0	100	570
384	3.4599	1.5	1	0.5	2	50	301				
385	3.4601	0.5	1	0.5	0	500	528				
386	3.4607	1.5	1	0.5	2	30	180				
387	3.4619	1.5	-1	0.5	1	100	182				
								1.5	1	80	1030
								2.5	1	80	1030
388	3.4642	1.5	1	0.5	2	150	898				
								1.5	0	100	563
389	3.4644	0.5	1	0.5	0	300	315				
390	3.4645	1.5	-1	0.5	1	75	136				
391	3.4654	2.5	1	0.5	2	18	107				
392	3.4664	1.5	-1	0.5	1	30	54				
393	3.4679	1.5	1	0.5	2	125	744				
								1.5	0	100	559
394	3.4683	0.5	-1	0.5	1	100	181				
395	3.4689	0.5	-1	0.5	1	150	271				
396	3.4716	2.5	1	0.5	2	8	47				
397	3.4722	2.5	1	0.5	2	45	266				
								2.5	0	50	276
398	3.4738	1.5	1	0.5	2	50	295				
399	3.4751	1.5	-1	0.5	1	40	72				
								1.5	1	100	1246
400	3.4767	2.5	1	0.5	2	20	117				

#	Energy (MeV)	J	π	s_p	ℓ_p	Γ_p (eV)	γ^2_p (eV)	$s_{p'}$	$\ell_{p'}$	$\Gamma_{p'}$ (eV)	$\gamma^2_{p'}$ (eV)
								2.5	0	30	164
401	3.4788	0.5	1	0.5	0	125	130				
								1.5	2	50	3058
								2.5	2	50	3058
402	3.4814	2.5	1	0.5	2	10	58				
								2.5	0	30	162
403	3.4856	1.5	-1	0.5	1	25	44				
								1.5	1	50	607
								2.5	1	50	607
404	3.4862	1.5	1	0.5	2	30	174				
405	3.4864	0.5	1	0.5	0	400	413				
406	3.4871	2.5	1	0.5	2	15	87				
407	3.4888	0.5	-1	0.5	1	500	887				
408	3.4906	2.5	1	0.5	2	8	46				
								2.5	0	5	26
409	3.4921	1.5	-1	0.5	1	17	30				
								1.5	1	15	179
								2.5	1	15	179
410	3.4931	1.5	-1	0.5	1	35	61				
411	3.4934	0.5	1	0.5	0	40	41				
								1.5	2	60	3523
								2.5	2	60	3523
412	3.4948	1.5	1	0.5	2	40	229				
								2.5	2	25	1462
413	3.4962	0.5	-1	0.5	1	60	105				
414	3.4970	2.5	1	0.5	2	100	572				
								2.5	0	80	419
415	3.4978	1.5	-1	0.5	1	250	439				
								1.5	1	25	295
								2.5	1	25	295
416	3.4987	2.5	1	0.5	2	20	114				
417	3.4997	0.5	1	0.5	0	175	178				
418	3.5008	0.5	-1	0.5	1	75	131				
419	3.5036	1.5	-1	0.5	1	50	87				
								1.5	1	70	814
								2.5	1	50	581

#	Energy (MeV)	J	π	s_p	ℓ_p	Γ_p (eV)	γ^2_p (eV)	$s_{p'}$	$\ell_{p'}$	$\Gamma_{p'}$ (eV)	$\gamma^2_{p'}$ (eV)
420	3.5042	1.5	1	0.5	2	20	113				
								1.5	0	20	103
421	3.5046	1.5	1	0.5	2	20	113				
								1.5	0	20	103
422	3.5063	1.5	1	0.5	2	25	141				
								1.5	2	25	1416
								2.5	2	25	1416
423	3.5086	1.5	1	0.5	2	25	140				
								1.5	0	25	127
424	3.5107	1.5	1	0.5	2	125	702				
								1.5	0	30	152
425	3.5114	0.5	1	0.5	0	175	177				
426	3.5126	0.5	-1	0.5	1	40	69				
427	3.5138	0.5	-1	0.5	1	60	103				
428	3.5152	0.5	1	0.5	0	125	126				
429	3.5165	0.5	-1	0.5	1	350	603				
								1.5	1	75	846
430	3.5177	2.5	1	0.5	2	8	44				
431	3.5184	1.5	-1	0.5	1	100	172				
								1.5	1	100	1123
								2.5	1	100	1123
432	3.5219	0.5	-1	0.5	1	70	119				
								1.5	1	100	1114
433	3.5253	1.5	1	0.5	2	10	55				
434	3.5260	0.5	1	0.5	0	35	34				
								1.5	2	50	2684
								2.5	2	50	2684
435	3.5266	2.5	1	0.5	2	20	109				
								2.5	0	40	197
436	3.5276	0.5	-1	0.5	1	30	51				
437	3.5298	1.5	1	0.5	2	75	410				
								1.5	2	40	2125
								2.5	2	80	4251
438	3.5306	0.5	-1	0.5	1	350	594				
								1.5	1	100	1091
439	3.5335	1.5	1	0.5	2	40	217				

#	Energy (MeV)	J	π	s_p	ℓ_p	Γ_p (eV)	γ^2_p (eV)	$s_{p'}$	$\ell_{p'}$	$\Gamma_{p'}$ (eV)	$\gamma^2_{p'}$ (eV)
								1.5	0	75	364
440	3.5344	0.5	-1	0.5	1	200	338				
441	3.5346	0.5	1	0.5	0	450	446				
								1.5	2	75	3934
								2.5	2	75	3934
442	3.5347	1.5	-1	0.5	1	180	304				
443	3.5376	0.5	1	0.5	0	25	24				
444	3.5407	2.5	1	0.5	2	4	21				
445	3.5420	0.5	-1	0.5	1	100	167				
446	3.5439	0.5	-1	0.5	1	20	33				
447	3.5470	0.5	1	0.5	0	25	24				
448	3.5477	0.5	-1	0.5	1	40	66				
449	3.5500	1.5	1	0.5	2	40	213				
450	3.5501	0.5	1	0.5	0	300	293				
								1.5	2	10	503
								2.5	2	10	503
451	3.5503	1.5	-1	0.5	1	50	83				
452	3.5528	1.5	1	0.5	2	75	398				
								1.5	0	25	116
453	3.5557	1.5	1	0.5	2	20	105				
								1.5	0	40	185
454	3.5569	2.5	1	0.5	2	45	237				
								2.5	0	40	185
455	3.5588	0.5	1	0.5	0	75	72				
456	3.5591	2.5	1	0.5	2	40	210				
								2.5	0	150	690
457	3.5607	0.5	-1	0.5	1	50	82				
								1.5	1	25	254
458	3.5629	1.5	1	0.5	2	30	157				
								1.5	0	20	91
459	3.5650	1.5	-1	0.5	1	25	41				
460	3.5669	0.5	-1	0.5	1	75	122				
461	3.5682	1.5	-1	0.5	1	60	98				
462	3.5688	1.5	1	0.5	2	12	62				
463	3.5691	0.5	-1	0.5	1	20	32				
464	3.5707	2.5	1	0.5	2	12	62				

#	Energy (MeV)	J	π	s_p	ℓ_p	Γ_p (eV)	γ^2_p (eV)	$s_{p'}$	$\ell_{p'}$	$\Gamma_{p'}$ (eV)	$\gamma^2_{p'}$ (eV)
465	3.5719	1.5	-1	0.5	1	50	81				
466	3.5735	1.5	-1	0.5	1	175	284				
								1.5	1	125	1236
								2.5	1	125	1236
467	3.5764	1.5	-1	0.5	1	80	129				
								1.5	1	150	1473
								2.5	1	30	294
468	3.5781	0.5	1	0.5	0	300	287				
469	3.5787	2.5	1	0.5	2	25	128				
								2.5	0	50	221
470	3.5806	1.5	-1	0.5	1	35	56				
								1.5	1	75	729
								2.5	1	75	729
471	3.5814	1.5	1	0.5	2	20	102				
472	3.5859	1.5	1	0.5	2	125	635				
								1.5	0	200	872
473	3.5860	0.5	1	0.5	0	500	475				
474	3.5862	1.5	-1	0.5	1	80	128				
475	3.5880	2.5	1	0.5	2	150	760				
								2.5	0	40	173
476	3.5891	0.5	-1	0.5	1	400	640				
								1.5	1	100	954
477	3.5896	0.5	1	0.5	0	50	47				
478	3.5916	0.5	1	0.5	0	50	47				
479	3.5919	2.5	1	0.5	2	50	252				
								2.5	0	200	862
480	3.5924	0.5	-1	0.5	1	500	798				
								1.5	1	50	473
481	3.5957	2.5	1	0.5	2	60	300				
482	3.5973	1.5	1	0.5	2	15	75				
483	3.5981	2.5	1	0.5	2	10	50				
484	3.5985	1.5	-1	0.5	1	60	95				
								1.5	1	150	1402
								2.5	1	150	1402
485	3.5987	0.5	1	0.5	0	300	282				
486	3.6003	0.5	-1	0.5	1	250	395				

#	Energy (MeV)	J	π	s_p	ℓ_p	Γ_p (eV)	γ^2_p (eV)	$s_{p'}$	$\ell_{p'}$	$\Gamma_{p'}$ (eV)	$\gamma^2_{p'}$ (eV)
								1.5	1	50	465
487	3.6024	0.5	1	0.5	0	150	140				
488	3.6040	0.5	-1	0.5	1	350	552				
								1.5	1	350	3232
489	3.6062	1.5	1	0.5	2	135	667				
								1.5	0	75	314
490	3.6083	2.5	1	0.5	2	15	74				
491	3.6088	2.5	1	0.5	2	10	49				
492	3.6101	1.5	1	0.5	2	45	221				
								1.5	0	20	83
493	3.6107	0.5	-1	0.5	1	125	195				
494	3.6133	0.5	-1	0.5	1	35	54				
								1.5	1	25	226
495	3.6139	1.5	1	0.5	2	17	83				
496	3.6149	1.5	1	0.5	2	10	48				
497	3.6154	1.5	-1	0.5	1	225	351				
								1.5	1	25	225
								2.5	1	25	225
498	3.6166	1.5	-1	0.5	1	40	62				
499	3.6169	2.5	1	0.5	2	10	48				
500	3.6176	1.5	1	0.5	2	40	195				
								1.5	0	50	204
501	3.6183	0.5	-1	0.5	1	25	38				
502	3.6191	2.5	1	0.5	2	35	170				
								2.5	0	50	204
503	3.6200	1.5	1	0.5	2	25	121				
504	3.6207	2.5	1	0.5	2	5	24				
505	3.6220	1.5	-1	0.5	1	50	77				
								1.5	1	50	443
506	3.6226	1.5	1	0.5	2	90	435				
								1.5	0	80	324
507	3.6240	0.5	-1	0.5	1	1000	1547				
								1.5	1	100	883
508	3.6252	1.5	-1	0.5	1	25	38				
509	3.6256	1.5	1	0.5	2	25	120				
								1.5	0	75	302

#	Energy (MeV)	J	π	s_p	ℓ_p	Γ_p (eV)	γ^2_p (eV)	$s_{p'}$	$\ell_{p'}$	$\Gamma_{p'}$ (eV)	$\gamma^2_{p'}$ (eV)
510	3.6266	1.5	1	0.5	2	50	240				
								1.5	0	40	161
								2.5	2	40	1649
511	3.6279	0.5	-1	0.5	1	20	30				
512	3.6290	1.5	1	0.5	2	20	96				
								1.5	0	20	80
513	3.6302	0.5	-1	0.5	1	25	38				
514	3.6310	0.5	1	0.5	0	350	321				
								1.5	2	50	2038
								2.5	2	50	2038
515	3.6313	1.5	1	0.5	2	50	239				
516	3.6319	1.5	1	0.5	2	20	95				
517	3.6321	0.5	1	0.5	0	350	320				
518	3.6329	0.5	-1	0.5	1	250	383				
								1.5	1	100	866
519	3.6339	0.5	-1	0.5	1	25	38				
								1.5	1	25	216
520	3.6347	2.5	1	0.5	2	4	19				
521	3.6357	2.5	1	0.5	2	20	95				
								2.5	0	30	118
								2.5	2	30	1208
522	3.6366	1.5	1	0.5	2	60	285				
								1.5	0	40	158
523	3.6372	1.5	1	0.5	2	20	95				
524	3.6376	0.5	-1	0.5	1	1500	2290				
								1.5	1	50	429
525	3.6388	0.5	1	0.5	0	50	45				
526	3.6429	2.5	1	0.5	2	30	141				
527	3.6434	1.5	-1	0.5	1	200	303				
528	3.6437	0.5	1	0.5	0	1300	1181				
529	3.6439	1.5	-1	0.5	1	150	227				
530	3.6452	0.5	1	0.5	0	800	725				
								1.5	2	250	9834
531	3.6463	0.5	-1	0.5	1	1500	2271				
								1.5	1	250	2105
532	3.6482	1.5	1	0.5	2	20	93				

#	Energy (MeV)	J	π	s_p	ℓ_p	Γ_p (eV)	γ^2_p (eV)	$s_{p'}$	$\ell_{p'}$	$\Gamma_{p'}$ (eV)	$\gamma^2_{p'}$ (eV)
								1.5	0	50	193
533	3.6501	1.5	1	0.5	2	10	46				
								1.5	0	20	77
534	3.6510	2.5	1	0.5	2	20	93				
								2.5	0	40	153
535	3.6527	1.5	1	0.5	2	20	93				
536	3.6543	0.5	1	0.5	0	50	45				
537	3.6548	0.5	-1	0.5	1	50	75				
								1.5	1	50	413
538	3.6569	0.5	-1	0.5	1	25	37				
539	3.6579	2.5	1	0.5	2	35	162				
540	3.6598	0.5	1	0.5	0	300	269				
541	3.6604	0.5	-1	0.5	1	25	37				
								1.5	1	100	817
542	3.6631	2.5	1	0.5	2	45	207				
543	3.6636	2.5	1	0.5	2	100	459				
								2.5	0	75	281
544	3.6654	1.5	1	0.5	2	25	114				
								1.5	0	100	374
545	3.6662	1.5	1	0.5	2	35	160				
546	3.6663	1.5	-1	0.5	1	300	445				
								1.5	1	400	3228
								2.5	1	100	807
547	3.6681	0.5	-1	0.5	1	25	37				
								1.5	1	50	402
548	3.6694	0.5	1	0.5	0	50	44				
549	3.6699	1.5	1	0.5	2	75	342				
550	3.6701	0.5	1	0.5	0	750	667				
551	3.6706	2.5	1	0.5	2	10	45				
552	3.6715	0.5	1	0.5	0	125	111				
553	3.6721	0.5	-1	0.5	1	400	591				
								1.5	1	600	4784
554	3.6725	2.5	1	0.5	2	10	45				
555	3.6730	0.5	-1	0.5	1	30	44				
556	3.6744	0.5	-1	0.5	1	50	73				
557	3.6794	1.5	1	0.5	2	125	563				

#	Energy (MeV)	J	π	s_p	ℓ_p	Γ_p (eV)	γ^2_p (eV)	$s_{p'}$	$\ell_{p'}$	$\Gamma_{p'}$ (eV)	$\gamma^2_{p'}$ (eV)
558	3.6804	0.5	-1	0.5	1	50	73				
								1.5	1	50	391
559	3.6825	1.5	-1	0.5	1	50	73				
								1.5	1	75	585
560	3.6834	0.5	-1	0.5	1	700	1023				
								1.5	1	200	1557
561	3.6840	0.5	1	0.5	0	45	39				
562	3.6864	2.5	1	0.5	2	65	290				
563	3.6869	0.5	1	0.5	0	800	703				
564	3.6871	1.5	-1	0.5	1	60	87				
565	3.6877	2.5	1	0.5	2	45	200				
								2.5	0	100	359
566	3.6887	0.5	-1	0.5	1	100	145				
567	3.6910	0.5	-1	0.5	1	75	108				
568	3.6913	1.5	-1	0.5	1	50	72				
								1.5	1	100	766
								2.5	1	100	766
569	3.6921	0.5	1	0.5	0	100	87				
570	3.6944	0.5	-1	0.5	1	250	361				
								1.5	1	100	761
571	3.6972	0.5	1	0.5	0	500	436				
572	3.6981	2.5	1	0.5	2	30	132				
								2.5	0	50	176
573	3.6997	1.5	1	0.5	2	30	131				
574	3.7001	0.5	-1	0.5	1	45	64				
575	3.7007	1.5	1	0.5	2	40	175				
								1.5	0	80	280
576	3.7012	0.5	-1	0.5	1	50	71				
577	3.7017	0.5	1	0.5	0	100	86				
578	3.7032	1.5	1	0.5	2	150	656				
								1.5	0	150	523
579	3.7053	0.5	1	0.5	0	100	86				
								1.5	2	50	1696
								2.5	2	50	1696
580	3.7068	0.5	1	0.5	0	400	346				
								1.5	2	100	3381

#	Energy (MeV)	J	π	s_p	ℓ_p	Γ_p (eV)	γ^2_p (eV)	$s_{p'}$	$\ell_{p'}$	$\Gamma_{p'}$ (eV)	$\gamma^2_{p'}$ (eV)
								2.5	2	100	3381
581	3.7086	1.5	1	0.5	2	100	434				
								1.5	0	50	172
582	3.7095	0.5	1	0.5	0	30	25				
583	3.7099	0.5	-1	0.5	1	50	71				
584	3.7109	1.5	1	0.5	2	350	1517				
								1.5	0	500	1721
585	3.7125	2.5	1	0.5	2	20	86				

Bibliography

Agrawal, A. M., Garg, J. B. and Harvey, J. Phys. Rev. 30C, 1880 (1984).

Bethe, H.A. Phys. Rev. 50, 332 (1936).

Bethe, H. A. Rev. Mod. Phys. 9, 79 (1937).

Bilpuch, E. G., Lane, A. M., Mitchell, G. E., and Moses, J. D. Phys. Reports 28C, 147 (1976).

Brooks, W. K., Jr. "Proton Resonance Spectroscopy in ^{36}Ar." Ph.D. dissertation, Duke University, 1988.

Browne, J. C., Newson, H. W., Bilpuch, E. G. and Mitchell, G. E. Nucl. Phys. A153, 481 (1970).

Garg, J. B. Phys. Rev. 24C, 1922 (1981).

Gilbert, A. and Cameron, A. G. W. Can. J. Phys. 43, 1446 (1965).

Harney, H. L. Nucl. Phys. A119, 591 (1968).

Huizenga, J. R. and Moretto, L. G. Annu. Rev. Nucl. Sci. 22, 427 (1972).

Huizenga, J. R., Behkami, A. N., Svèntek, J. S. and Atcher, R. W. Nucl. Phys. A223, 577 (1973).

Ignatyuk, A. V., Smirenkin, G. N. and Tishin, A. S. Sov. J. Phys. 23, 255 (1975).

Jänecke, J. Isospin in Nuclear Physics, Wilkerson, D. H., ed. (North-Holland, Amsterdam 1969).

Kataria, S. K., Ramamurthy, V. S. and Kapoor, S. S. Phys. Rev. C 18, 549 (1978).

Kataria, S. K. and Ramamurthy, V. S. Nucl. Phys. A349, 10 (1980).

Keyworth, G. A., Kyker, G. C., Jr., Bilpuch, E. G. and Newson, H. W. Nucl. Phys. 89, 590 (1966).

King, S. E., Lau Y. C. and Gould C. R. IEEE Trans. Nucl. Sci. NS-28, 3822 (1981).

Lane, A. M. and Thomas, R. G. Rev. Mod. Phys. 30, 257 (1956).

Lindstrom, D. P., Newson, H. W., Bilpuch, E. G. and Mitchell, G. E. Nucl. Phys. A168, 37 (1971).

Lindstrom, D. P., Newson, H. W., Bilpuch, E. G. and Mitchell, G. E. Nucl. Phys. A187, 481 (1972).

Lynn, J. E. The Theory of Neutron Resonance Reactions (Clarendon, Oxford 1968).

Mekjian, A. and MacDonald, W. M. Nucl. Phys. A121, 385 (1968).

Mitchell, G. E., Bilpuch, E. G., Shriner, J. F., Jr. and Lane, A. M. Phys. Reports 117, 1 (1985).

Moses, J. D., Newson, H. W., Bilpuch, E. G. and Mitchell, G. E. Nucl. Phys. A175, 556 (1971).

Mughabghab, S. F., Divadeenam, M. and Holden, N. E. Neutron Cross-Sections (Academic, New York, 1981)

Nelson, R. O. "Proton Resonance Spectroscopy in ^{28}Si and ^{30}P." Ph.D. dissertation, Duke University, 1983.

Nelson, R. O., Bilpuch, E. G. and Mitchell, G. E. Nucl. Instrum. Methods A236, 128 (1985).

Newton, T. D. Can. J. Phys. 34, 804 (1956).

Nuclear Data Sheets 40, 149 (1983).

Parks, P. B., Newson, H. W., and Williamson, R. M. Rev. Sci. Instrum. 29, 834 (1958).

Perey, C. M. et al. Phys. Rev. 27C, 2556 (1983).

Perey, C. M. et al. Proc. Int. Conf. Nucl. Sci. Tech., Santa Fe, 1985, (Gordon and Breach, New York, 1986)

Porter, C. E. and Thomas, R. G. Phys. Rev. 104, 483 (1956).

Prochnow, N. H., Newson, H. W., Bilpuch, E. G. and Mitchell, G. E. Nucl. Phys. A194, 353 (1972).

Prochnow, N. H., Newson, H. W., Bilpuch, E. G. and Mitchell, G. E. Nucl. Phys. A213, 134 (1973).

Prochnow, N. H., Newson, H. W., Bilpuch, E. G. and Mitchell, G. E. Nucl. Phys. A199, 571 (1973).

Roberson, N. R. and Gould, C. R. IEEE Trans. Nucl. Sci. NS-32 1447 (1985).

Sales, K. B., Mitchell, G. E., Bilpuch, E. G. and Westerfeldt, C. R. J. Phys. G 7, 1405 (1981).

Schiff, L.I. Quantum Mechanics (McGraw-Hill, NewYork, 1968).

Sellin, D. L. "Excited States in ^{19}F." Ph.D. dissertation, Duke University, 1969.

Soderstrum, John P., Boyd, Mark A., Gould, C. R., and Roberson, N. R. XSYS Reference Manual, 6th ed. Triangle Universities Nuclear Laboratory, 1987.

Thompson, W. J., Adams, J. L. and Robson, D. Phys. Rev. 173, 975 (1968).

Vogt, E. Rev. Mod. Phys. 34, 723 (1962).

Vonach, H., Uhl, M., Strohmaier, B., Smith, B. W., Bilpuch, E. G. and Mitchell, G. E. Phys. Rev. 38C, 2541 (1988).

Watson, W. A., III, Bilpuch, E. G. and Mitchell, G. E. Phys. Rev. 24C, 1992 (1981).

Watson, W. A., III, Bilpuch, E. G. and Mitchell, G. E. Nucl. Instrum. Methods 188, 571 (1981).

Westerfeldt, C. R., Nelson, R. O., Bilpuch, E. G. and Mitchell, G. E. Nucl. Instrum. Methods A270, 467 (1988).

Wigner, E. P. and Eisenbud, L. Phys. Rev. 72, 29 (1947).

Wilson, W. M., Bilpuch, E. G. and Mitchell, G. E. Nucl. Phys. A245, 262 (1975).

Wilson, W. M., Bilpuch, E. G. and Mitchell, G. E. Nucl. Phys. A271, 49 (1976).

Zaidi, S. A. S. and Darmodjo, S. Phys. Rev. Lett. 19, 1446 (1967).

Biography

Bart Wayne Smith

Personal: Born September 14, 1962 Rolla, Missouri.
Married to Carol Paige Pickett, March 21, 1987.

Education: B. S. Physics, University of Missouri at Rolla
M. A. Physics, Duke University

Positions: Teaching Assistant, Duke University, 1984 - 1985
Research Assistant, Duke University, 1985 - present

Abstracts: "Comparison of average s-wave resonance spacings from proton and neutron resonances," B. W. Smith, E. G. Bilpuch, G. E. Mitchell, H. Vonach, M. Uhl, B. Strohmaier Bull. Am. Phys. Soc. 33, 2194 (1988).

Papers: "Comparison of average s-wave resonance spacings from proton and neutron resonances," H. Vonach, M. Uhl, B. Strohmaier, B. W. Smith, E. G. Bilpuch, G. E. Mitchell Phys. Rev. 38C, 2541 (1988).

Memberships: American Physical Society